

Institute of Biomaterial Science, Helmholtz Zentrum Geesthacht  
Director: Prof. Dr. Andreas Lendlein

# **Influence of surface topographic microstructure on behaviors of multipotent and pluripotent stem cells**



Inaugural-Dissertation  
to obtain the academic degree  
Doctor rerum naturalium (Dr. rer. nat.)  
submitted to the Department of Biology, Chemistry and Pharmacy  
of Freie Universität Berlin

by  
Zhengdong Li  
from Chengdu, Sichuan, P.R. China  
03. 2018, Berlin

This thesis was performed in the Institute of Biomaterial Science and Berlin-Brandenburg Center for Regenerative Therapies, Helmholtz Zentrum Geesthacht in Teltow during the period 1/10/2011 - 31/03/2018 under the supervision of Prof. Dr. Andreas Lendlein and Prof. Nan Ma. It is submitted to the Department of Biology, Chemistry and Pharmacy of Freie Universität Berlin.

1st Reviewer: Prof. Dr. Andreas Lendlein

2nd Reviewer: Prof. Dr. Anna Gorbushina

Date of defense: 21.09.2018

# Contents

Acknowledgement .....	1
Foreword .....	2
Summary/Zusammenfassung .....	3
Chapter I: General Introduction .....	6
Chapter II: Integrin $\beta 1$ activation by micro-scale curvature promotes pro-angiogenic secretion of human mesenchymal stem cells .....	14
Chapter III: Modulation of the mesenchymal stem cell migration capacity via preconditioning with topographic microstructure .....	54
Chapter IV: Influence of surface roughness on neural differentiation of human induced pluripotent stem cells.....	74
Chapter V: Conclusion and discussion.....	95
Contribution to publications .....	107
List of publications.....	110
Curriculum Vitae.....	111
Selbständigkeitserklärung .....	112

## **Acknowledgement**

I would like to express my heartfelt gratitude and sincere appreciation to all people who have helped and inspired me during my doctoral study.

First, I thank my supervisors Prof. Andreas Lendlein and Prof. Nan Ma for giving me the opportunity to conduct all the research in this thesis. I thank them for the directing of my research and the guiding of all my experiments.

I thank Dr. Weiwei Wang who has helped me a lot in the lab work and scientific writing to finish my manuscripts. I greatly appreciate his valuable suggestion and the patience for my questions and problems.

I acknowledge all the colleagues from BKP group for all kind help not only in the work but also in my personal life. I thank them for creating comfortable atmosphere and joyful time when I worked in the institute.

I thank Dr. Manfred Gossen who has mentored my work in BCRT, I thank him also for providing me the opportunity to learn lots of new knowledges and technics. I enjoyed the time talking with him for many scientific and non-scientific topics.

I thank all the people who directly and indirectly helped me with my works in the institute. I thank all of my friends in Berlin, their presence made this journey more pleasant and joyful.

At last, I give all my deepest gratitude to my family for the endless love and support, this thesis is simply impossible without them. I am indebted to my parents, my sisters for their love and understanding, especially making it possible for me to complete the doctoral work.

This thesis is dedicated to my dearest wife, Ms. Ya Xi, she and our children have accompanied me through all the joys and sorrows in the past. I believe this would be the beginning of our new life.

## Foreword

This thesis is a cumulative work of the following published manuscripts:

1. Zhengdong Li *et al.* Integrin  $\beta$ 1 activation by micro-scale curvature promotes pro-angiogenic secretion of human mesenchymal stem cells. *Journal of Materials Chemistry B*. 2017, 5, 7415—7425. <https://doi.org/10.1039/c7tb01232b>
2. Zhengdong Li *et al.* Modulation of the mesenchymal stem cell migration capacity via preconditioning with topographic microstructure. *Clinical Hemorheology and Microcirculation*. *Clinical Hemorheology and Microcirculation*. 2017;67(3-4):267-278. <https://doi.org/10.3233/CH-179208>
3. Zhengdong Li *et al.* Influence of surface roughness on neural differentiation of human induced pluripotent stem cells. *Clinical Hemorheology and Microcirculation* 64 (2016) 355–366. <https://doi.org/10.3233/CH-168121>

## Summary/Zusammenfassung

**Objective:** Using mechanical cues to control stem cells fate has attracted the widespread attention in the field of stem cell-based regenerative therapies. The aim of the present work was to determine the influence of surface microstructures (curvature level) on secretome, migration of human mesenchymal stem cells (MSCs) and to reveal the underlying mechanism. Furthermore, the efficiency of the neural differentiation of human induced pluripotent stem cells (iPSCs) on the surface with microstructures was evaluated.

**Methods:** Human adipose derived mesenchymal stem cells (ADSCs) were cultivated on polystyrene surfaces with different curvature levels. Conditioned medium from such cultures was collected and its VEGF levels were analyzed. Further, the cells preconditioned by the surface curvatures were collected and reseeded on regular tissue culture plates to examine their migration capacity. For the underlying mechanism, the activation level of integrin, focal adhesion kinase (FAK) and mitogen-activated protein kinase (MAPK/ERK) were measured. Using matrigel coated polystyrene surface with different curvature levels for cultivation, human induced pluripotent stem cells (iPSCs) were induced to differentiate into neural lineages. Expression level of neural genes and protein was analyzed to evaluate the differentiation efficiency.

**Results:** Appropriate surface topographic curvature promoted the VEGF secretion of human ADSCs. The conditioned medium increased tube formation and migration of human umbilical vein endothelial cells (HUVECs) *in vitro* and stimulated blood vessels formation in the hen's egg test - chorioallantoic membrane (HET-CAM) *ex vivo*. For the underlying mechanism, the integrin mediated FAK-MAPK/ERK pathway was involved in the surface curvatures stimulated ADSCs behavior. Furthermore, the curvature was found to increase the neural differentiation efficiency of human iPSCs.

**Conclusion:** Surface with microscale curvature increases VEGF secretion and migration capacity of MSCs via activating the integrin mediated FAK-MAPK/ERK signaling pathway, but this regulation effect is depended on the curvature level. Further, the similar surface can promote the neural differentiation of human iPSCs. Surface microscale curvature

might be a useful strategy to enhance the therapeutic potential of stem cells in regenerative medicine.

**Zielsetzung:** Die Möglichkeit zur Kontrolle des Stammzellverhaltens durch mechanische Reize hat im Bereich der regenerativen Therapien große Aufmerksamkeit erlangt. Ziel der vorliegenden Arbeit war es, den Einfluss der Mikroskalaskrümmung von Oberflächen auf die Sekretion des vaskulären endothelialen Wachstumsfaktors (VEGF) Sekretion durch humane mesenchymale Stammzellen (MSCs) zu bestimmen, deren Migration zu analysieren und die zugrundeliegenden Mechanismus aufzudecken. Darüber hinaus wurde die Effizienz der neuronalen Differenzierung von humanen induzierten pluripotenten Stammzellen (iPSCs) auf vergleichbaren Oberflächen ausgewertet.

**Methoden:** Auf Polystyrol-Oberflächen mit verschiedenen Mikroskalakrümmungsgraden wurden humane adipöse mesenchymale Stammzellen (ADSCs) kultiviert. Die konditionierten Medien wurden gesammelt und ihr VEGF Gehalt quantifiziert. Ferner wurden die durch die Oberflächenkrümmung vorkonditionierten Zellen gesammelt, auf der Gewebekulturplatten ausgesät, und ihr Migrationsverhalten untersucht. Die zugrundeliegenden Mechanismen wurden über Messung des Aktivierungsgrads von Integrin, fokaler Adhäsionskinase (FAK) und mitogenaktivierter Proteinkinase (MAPK/ERK) adressiert. Darüber hinaus wurden humane induzierte pluripotente Stammzellen (iPSCs) auf matrigelbeschichteten Polystyroloberfläche mit unterschiedlichen Krümmungsgraden kultiviert und in neuronale Zellen differenziert. Die Expression neuronaler Gene wurden analysiert, um die Differenzierungseffizienz zu bewerten.

**Ergebnisse:** Durch geeignete topographische Oberflächenkrümmung kann die VEGF-Sekretion von humanen ADSCs stimuliert werden. Das Krümmungskonditionierte Medium erhöhte die Ausbildung vaskulärer Strukturen (sogenannter *tube formation assay*) und die Migration von humanen Nabelschnurvenen-Endothelzellen (HUVECs) in vitro. Zudem verbesserte es die Blutgefäßbildung im Hühnereientest an der Chorion-Allantois-Membran (HET-CAM) ex vivo. Die Integrin-vermittelte FAK-MAPK / ERK Signaltransduktion war entscheidend in das Oberflächenkrümmung-stimulierte ADSC-

Verhalten involviert. Darüber hinaus wurde festgestellt, dass die Krümmung die neuronale Differenzierungseffizienz von menschlichen iPSCs beeinflusst.

**Schlussfolgerung:** Oberflächenkrümmung erhöht die VEGF Sekretion und Migrationskapazität von MSCs durch Aktivierung des Integrin-vermitteltes FAK-MAPK / ERK-Signalwegs. Die beobachteten Effekte sind von dem Krümmungsgrad abhängig. Ähnliche Krümmungsgrade können die neuronale Differenzierung von menschlichen iPSCs fördern. Der Einsatz solcher Oberflächenkrümmung könnten eine nützliche Strategie sein, um das therapeutische Potential von Stammzellen in der regenerativen Medizin zu verbessern.



# **Chapter I**

## **General Introduction**

## General Introduction

Over the past decade, Stem cells have attracted the enormous attention in the field of regenerative medicine for their ability to regenerate and repair the injured tissues [1, 2]. Stem cells are broadly classified into adult stem cells (ASCs) and embryonic stem cells (ESCs). ASCs are multipotent cells derived from adult somatic tissues with the potential to differentiate into many specific cell types. As the commonest type of ASCs, Mesenchymal stem cells (MSCs) are self-renewing clonal precursors of non-hematopoietic stromal tissues with multi-lineage differentiation potential, which can be found in almost all postnatal organs and tissues such as fat, skin and bone marrow [3]. MSCs have been considered as the promising cell source in regenerative medicine with the eventual clinical benefits such as abundance, homing ability, functional plasticity and immune-regulatory properties [4]. Recent studies indicated that the benefits of MSCs based therapy could be predominantly due to their paracrine activity rather than the direct differentiation [5]. Besides, the MSCs were also not able to preserve a long lifespan after transplantation [6, 7], the beneficial effects from transplanted MSCs may mainly attribute to the rapid targeting to the site of injury. Thus, cell rapidly migration to the lesion site remains the lingering problem in MSCs-based therapies. It is of great benefit to develop the MSCs migration and secretion capacity prior to their transplantation.

ESCs are derived from the inner cell mass of blastocysts and have the capacity to regenerate into cells types from all three germ layers (ectoderm, mesoderm and endoderm). Due to their capacities such as long term self-renewal, extended culturing and the pluripotency of differentiation, the ESCs are regarded as a very attractive cell resource in regenerative medicine. However, the ESCs always represent the ethical constraints because the embryo dies during the isolation from the blastocysts [8]. Until 2006, the induced pluripotent stem cells (iPSCs) were found by ectopic expression of four genes- *Oct4*, *Sox2*, *Klf4*, and *c-Myc* in both embryonic and adult murine fibroblasts [9]. Soon later, the human iPSCs were obtained with a somewhat altered gene set- *Oct4*, *Sox2*, *Nanog*, and *Lin28* [10]. Human iPSCs have been hailed as an ideal replacement for the ESCs and a prime candidate cell source for regenerative aims without many of the associated ethical concerns. In the past years, many remarkable progresses of iPSCs

based regenerative therapies have been made. For example, the dopaminergic neurons as the predominant cell type for treating Parkinson's disease (PD) has been effectively generated from iPSCs, and functionally integrated into cynomolgus monkey model [11]. Moreover, the first human clinical trial was performed in 2014, in which, iPSCs derived from skin cells from patients with wet age-related macular degeneration were reprogrammed to differentiate into retinal pigment epithelial (RPE) cells, then were transplanted back into the affected retina [12]. However, there are still some challenges needed to be overcome such as inefficient cell derivation, genetic abnormalities during in vitro expanding [13]. Most of all, it is of utmost importance to avoid the teratoma or tumor formation caused by inadequate differentiation [14]. It is only of benefit if there is a complete differentiation to generate the cell types of interest. Hence, controlled differentiation of iPSCs is critical for cell replacement based therapies.

Therefore, how to control the behaviors of stem cells remains the key role in their therapeutic application. It is an accepted knowledge that stem cell fate is regulated by the various stimuli dictated by the microenvironment including soluble factors and matrix-mediated signals, as well as cell-cell communication. However, soluble factor mediated signaling pathway can't completely elucidate many cellular behaviors [15]. Recently, the cues presented by the physical microenvironment are being thought to be important regulators of stem cell behaviors. Further understanding of these environmental instructions on stem cell behaviors is emerging, with the hope to better their therapeutic potential. The physical force and hemodynamic shear stress in a living organism surrounded mechanical environment are referred to mechanic transduction [16], such as the substrates stiffness, different stiffness level could conduct the MSCs to differentiate into neuronal, myogenic or osteogenic lineage [17]. As a natural topography of extracellular matrix, material surface topographic nanoscale roughness has been described as a strong modulator in regulating cell migration [18, 19] and the adhesion, proliferation and differentiation [20, 21]. However, there is very limited knowledge concerning the surface microscale microstructure on the stem cells fate. It is in a great need to figure out the potential effects and the undergoing mechanism.

Focusing on the interface between cell and material surface, the integrin as the cell transmembrane receptor and mechanotransducer, is responsible for sensing and translating external mechanical signal into cellular biochemical information [22]. On the one hand, intracellular activators such as talin and kindlin, can bind to the cytoplasmic tail of integrin to induce the conformational changes in the extracellular domain of integrin, which can increase the affinity of integrin to extracellular ligand [23]. On the other hand, surrounding environment regulates the conformation and clustering of integrin, which can lead to a series cellular response such as cell adhesion, cytoskeletal structure, migration, gene expression, cell survival, proliferation and differentiation [24, 25]. Intracellularly, integrin interacts with focal adhesion kinase (FAK) via the cytoskeletal protein talin [26]. FAK and Src activation upon integrin engagement can subsequently activate the downstream mitogen-activated protein kinase MAPK/ERK pathway [27, 28]. Further, the FAK-MAPK/ERK axis was reported to regulate the cellular behaviors such as proliferation, secretion, migration and differentiation [29, 30]. Thus, it is of great interest to study the effects of surface topographic microstructure (defined in surface curvature) on stem cell behaviors and the activity of FAK and MAPK, which may reveal the underlying mechanism and present a safe and robust approach to increase the therapeutic efficacy of MSCs in regenerative medicine.

## **Motivation**

Different topographical patterns and different cell types would have completely distinct interactions. It is necessary to broaden our study view to explore the underlying mechanisms. Curvature as one of the topographical cues in nano and micro scale size exist in our native body. Limited studies have been carried to explain their effects on the cell behaviors. It is demonstrated that the concave structure would enhance the cell migration and convex structure would promote the differentiation. Further, the secretion capacity of stem cells may be the predominant factor for their therapeutic efficiency. Therefore, it is in great need to know the effects of surface curvatures on stem cell secretion, migration and differentiation and the undergoing mechanisms; and if the effects of curvature are associated with the cell size. The results would help us to understand the

effects of curvature level on stem cells therapeutic efficiency and to design substrate surface for increasing their regenerative potential.

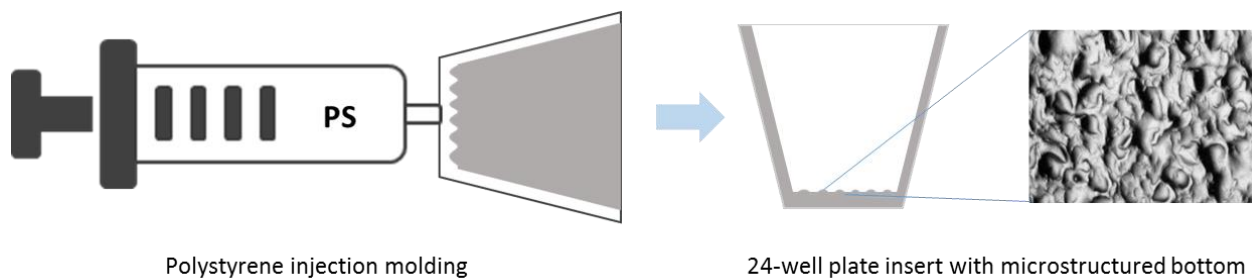
## Hypothesis

The surface microscale structures could influence the stem cells behaviors including secretion, migration and differentiation; the different microscale structure preconditioned cells would own the different levels in specific gene and protein expression and consequently own the distinct behaviors such as migration capacity. The curvature degree provided by surface microscale structures is the determining factor to influence stem cells behaviors. Further, curvature induced integrin gathering and activation would be the intermedium to transfer the signal from substrate surface into cells; the focal adhesion and downstream FAK-ERK signaling pathway would be activated by the integrin activation and consequently modulate the stem cells behaviors.

## Concept

Polystyrene was used to prepare the standard 24-well tissue culture plate fitting inserts via injection molding. Three differently structured cylinders were utilized to manufacture the inserts with different types of bottom microstructures: a cylinder with a polished contact surface (PS-000), and two cylinders with micro-structured surfaces according to the standard of German Institute for Standardization (DIN 16747: 1981-05), M30 (PS-160) and M45 (PS-320).(Figure.1) The prepared inserts were sterilized by gas sterilization (gas phase: 10% ethylene oxide, 54 °C, 65% relative humidity, 1.7 bar, 3 hours of gas exposure time and 21 hours of aeration phase).

Figure. 1. Manufacture of polystyrene 24 well inserts with microstructured bottom



The extracellular matrix was coated on the inserts to enhance the cell adhesion. As following, the behaviors including secretion, migration and differentiation of the multipotent or pluripotent stem cells on the microstructured bottom were evaluated. To assess the biological effects of secretion of mesenchymal stem cells, the conditioned media were collected and examined both *in vitro* using tube formation and migration assay of human umbilical vein endothelial cells (HUVECs) and *ex vivo* via the hen's egg test - chorioallantoic membrane (HET-CAM) assay. The migration capacity of microstructures conditioned mesenchymal stem cells was test in gap closure assay and time-laps microscope tracking. The neuronal differentiation efficiency is assessed by the gene and neuronal protein expression. To explore the underlying mechanism, the activation of integrin, FAK and MAPK/ERK is investigated using flow cytometry, ELISA and west blotting.

## Aims

This work is dedicated to investigate the modulation effects of surface with different microscale curvature levels on the secretion, migration capacities of human MSCs and the neural differentiation efficiency of iPSCs. The aim of the study is also trying to reveal the underlying mechanism of the surface curvature induced response of stem cells, such as the integrin activation, focal adhesion kinase activity and the consequent MAPK/ERK phosphorylation, which would improve our understanding of these influences of surface microscale structures on stem cell behaviors and the underlying molecular mechanisms.

## References

1. Stoltz, J.F., et al., *Stem Cells and Regenerative Medicine: Myth or Reality of the 21th Century*. Stem Cells Int, 2015. **2015**: p. 734731.
2. Mahla, R.S., *Stem Cells Applications in Regenerative Medicine and Disease Therapeutics*. Int J Cell Biol, 2016. **2016**: p. 6940283.
3. Meirelles, L.D.S., P.C. Chagastelles, and N.B. Nardi, *Mesenchymal stem cells reside in virtually all post-natal organs and tissues*. Journal of Cell Science, 2006. **119**(11): p. 2204-2213.
4. Liu, W.H., et al., *The multiple functional roles of mesenchymal stem cells in participating in treating liver diseases*. J Cell Mol Med, 2015. **19**(3): p. 511-20.

5. Chou, S.H., et al., *Mesenchymal stem cell insights: prospects in cardiovascular therapy*. Cell Transplant, 2014. **23**(4-5): p. 513-29.
6. Liu, X.B., et al., *Angiopoietin-1 preconditioning enhances survival and functional recovery of mesenchymal stem cell transplantation*. J Zhejiang Univ Sci B, 2012. **13**(8): p. 616-23.
7. Eggenhofer, E., et al., *Mesenchymal stem cells are short-lived and do not migrate beyond the lungs after intravenous infusion*. Front Immunol, 2012. **3**: p. 297.
8. Siep, L., *Ethical justification for human stem cell research. The view of the German Central Ethics Committee for Stem Cell Research*. Bundesgesundheitsblatt-Gesundheitsforschung-Gesundheitsschutz, 2008. **51**(9): p. 950-953.
9. Takahashi, K. and S. Yamanaka, *Induction of pluripotent stem cells from mouse embryonic and adult fibroblast cultures by defined factors*. Cell, 2006. **126**(4): p. 663-676.
10. Yu, J., et al., *Induced pluripotent stem cell lines derived from human somatic cells*. Science, 2007. **318**(5858): p. 1917-20.
11. Hallett, P.J., et al., *Successful function of autologous iPSC-derived dopamine neurons following transplantation in a non-human primate model of Parkinson's disease*. Cell Stem Cell, 2015. **16**(3): p. 269-74.
12. Ilic, D., et al., *Human embryonic and induced pluripotent stem cells in clinical trials*. Br Med Bull, 2015. **116**: p. 19-27.
13. Saha, K. and R. Jaenisch, *Technical Challenges in Using Human Induced Pluripotent Stem Cells to Model Disease*. Cell Stem Cell, 2009. **5**(6): p. 584-595.
14. Hong, S.G., et al., *Path to the Clinic: Assessment of iPSC-Based Cell Therapies In Vivo in a Nonhuman Primate Model*. Cell Reports, 2014. **7**(4): p. 1298-1309.
15. Kshitiz, et al., *Control of stem cell fate and function by engineering physical microenvironments*. Integrative Biology, 2012. **4**(9): p. 1008-1018.
16. Miller, C.J. and L.A. Davidson, *The interplay between cell signalling and mechanics in developmental processes*. Nature Reviews Genetics, 2013. **14**(10): p. 733-744.
17. Nava, M.M., M.T. Raimondi, and R. Pietrabissa, *Controlling self-renewal and differentiation of stem cells via mechanical cues*. J Biomed Biotechnol, 2012. **2012**: p. 797410.
18. Han, J.J., et al., *An in vitro study on the collective tumor cell migration on nanoroughened poly(dimethylsiloxane) surfaces*. Journal of Materials Chemistry B, 2015. **3**(8): p. 1565-1572.
19. Chen, W., Y. Sun, and J. Fu, *Microfabricated nanotopological surfaces for study of adhesion-dependent cell mechanosensitivity*. Small, 2013. **9**(1): p. 81-9.
20. Rosa, A.L. and M.M. Beloti, *Effect of cpTi surface roughness on human bone marrow cell attachment, proliferation, and differentiation*. Braz Dent J, 2003. **14**(1): p. 16-21.

21. Gittens, R.A., et al., *The effects of combined micron-/submicron-scale surface roughness and nanoscale features on cell proliferation and differentiation*. *Biomaterials*, 2011. **32**(13): p. 3395-403.
22. Ross, T.D., et al., *Integrins in mechanotransduction*. *Current Opinion in Cell Biology*, 2013. **25**(5): p. 613-618.
23. Calderwood, D.A., I.D. Campbell, and D.R. Critchley, *Talins and kindlins: partners in integrin-mediated adhesion*. *Nature Reviews Molecular Cell Biology*, 2013. **14**(8): p. 503-517.
24. Shattil, S.J., C. Kim, and M.H. Ginsberg, *The final steps of integrin activation: the end game*. *Nature Reviews Molecular Cell Biology*, 2010. **11**(4): p. 288-300.
25. Qin, J., O. Vinogradova, and E.F. Plow, *Integrin bidirectional signaling: a molecular view*. *Plos Biology*, 2004. **2**(6): p. 726-729.
26. Guan, J.L., *Role of focal adhesion kinase in integrin signaling*. *Int J Biochem Cell Biol*, 1997. **29**(8-9): p. 1085-96.
27. Mitra, S.K., D.A. Hanson, and D.D. Schlaepfer, *Focal adhesion kinase: In command and control of cell motility*. *Nature Reviews Molecular Cell Biology*, 2005. **6**(1): p. 56-68.
28. Guo, W.J. and F.G. Giancotti, *Integrin signalling during tumour progression*. *Nature Reviews Molecular Cell Biology*, 2004. **5**(10): p. 816-826.
29. Mitra, S.K., et al., *Intrinsic FAK activity and Y925 phosphorylation facilitate an angiogenic switch in tumors*. *Oncogene*, 2006. **25**(44): p. 5969-5984.
30. Tomakidi, P., et al., *Focal adhesion kinase (FAK) perspectives in mechanobiology: implications for cell behaviour*. *Cell Tissue Res*, 2014. **357**(3): p. 515-26.



## Chapter II

### **Integrin $\beta$ 1 activation by micro-scale curvature promotes pro-angiogenic secretion of human mesenchymal stem cells**

Journal of Materials Chemistry B. 2017, 5, 7415--7425.

<https://doi.org/10.1039/c7tb01232b>

# Integrin $\beta 1$ activation by micro-scale curvature promotes pro-angiogenic secretion of human mesenchymal stem cells

Zhengdong Li, ‡<sup>ab</sup> Weiwei Wang, ‡<sup>a</sup> Xun Xu, ‡<sup>ab</sup> Karl Kratz,<sup>ac</sup> Jie Zou,<sup>ab</sup> Liudmila Lysyakova,<sup>ac</sup> Matthias Heuchel,<sup>a</sup> Andreas Kurtz,<sup>d</sup> Manfred Gossen,<sup>a</sup> Nan Ma<sup>\*abc</sup> and Andreas Lendlein<sup>\*abc</sup>

<sup>a</sup> Institute of Biomaterial Science and Berlin-Brandenburg Center for Regenerative Therapies, Helmholtz-Zentrum Geesthacht, Kantstraße 55, 14513 Teltow, Germany; E-mail: nan.ma@hzg.de, [andreas.lendlein@hzg.de](mailto:andreas.lendlein@hzg.de)

<sup>b</sup> Institute of Chemistry and Biochemistry, Freie Universität Berlin, Takustraße 3, 14195 Berlin, Germany

<sup>c</sup> Helmholtz Virtual Institute „Multifunctional Biomaterials for Medicine“, Kantstraße 55, 14513 Teltow, Germany

<sup>d</sup> Charité – University Medicine Berlin, Augustenburger Platz 1, 13353 Berlin, Germany

‡ These authors contributed equally to this work.

## Abstract

Fine tuning of the substrate properties to modulate mesenchymal stem cell (MSC) function has emerged as an attractive strategy to optimize their therapeutic potential. In the context of mechanotransduction process, the conformational change of integrin (integrin activation) plays a critical role to perceive and transmit various signals. In this study, polymeric cell culture inserts with defined bottom roughness were fabricated as a model system for cell cultivation. We showed the conformational change of integrin and its downstream signaling cascade of human adipose-derived mesenchymal stem cells (hADSCs) could be modulated by the curvature of the cell-material interface. The

curvature of substrate surface with a roughness in the size range of a single cell could strongly increase high-affinity  $\beta 1$  integrin level of hADSCs without alteration of total  $\beta 1$  integrin level. Further, the integrin downstream FAK/ERK and Rho/ROCK pathways were activated and resulted in upregulated VEGF secretion of hADSCs. Conditioned medium on such a surface exhibited a strong pro-angiogenic effect, with an increased formation of tubular structure, a higher migration velocity of endothelial cells and an enhanced blood vessel density in *ex vivo* hen's egg test-chorioallantoic membrane (HET-CAM). These results highlighted the clinical potential to manipulate topographic features of cell culture substrate, whereby to regulate integrin affinity states and further control MSC functions.

Key words: micro-scale curvature, mesenchymal stem cells, integrin activation, FAK, angiogenesis

## 1 Introduction

Mesenchymal stem cells (MSCs) have demonstrated major advantages to meet the clinical requirements including abundance, homing ability, functional plasticity and immunoregulatory properties.<sup>1</sup> Accumulated evidences have proved that MSCs can transmit the cues from their micro-environment such as stiffness,<sup>2,3</sup> surface topography,<sup>4,8</sup> and external force<sup>9</sup> into biochemical activity, which is referred to mechanotransduction.<sup>10,11</sup> This opens a promising field of modulating and controlling MSC function simply through mechanical stimuli for improved therapeutic efficacy. Among these stimuli, surface topography/roughness is an effective approach to modulate MSCs. It has been demonstrated that bioceramic scaffolds with micro-nano-hybrid surface topographies could significantly enhance cell attachment and viability, osteogenic differentiation and pro-angiogenic effects of MSCs;<sup>7</sup> and poly( $\epsilon$ -caprolactone) surface with a roughness level similar to native bone induced the preferential osteogenic commitment of MSCs.<sup>12</sup> Hence, understanding the molecule mechanisms to further utilize these beneficial effects is of major clinical relevance.

Integrin, as a transmembrane receptor and primary mechanosensor of cells, plays a critical role to perceive various signals during the mechanotransduction process.<sup>13</sup> Integrin is a heterodimer of the non-covalently linked type I transmembrane  $\alpha$  and  $\beta$  subunits. A substantial proportion of integrins on cell surface are inactive. Upon extracellular stimulation, integrins undergo a change in conformation and affinity (integrin activation), which allows the recruitment of several cytoplasmic proteins.<sup>14</sup> High-affinity integrins are highly concentrated in the cell's contact points to ECM including focal adhesions and their variants (focal complexes, fibrillar adhesions and podosomes), mediating cell-ECM interaction. As integrins bind both extracellular and intracellular ligands, they regulate the bidirectional transmission of the mechanical and biochemical signals across the cell membrane.<sup>15</sup> On one hand, the 'inside-out' signaling leads to conformational changes in the extracellular domain of integrin, resulting in an increased affinity of integrin to extracellular ligands. This process is termed integrin activation and is regulated by different intracellular activators, such as talin or kindlin, which bind to the cytoplasmic tail of integrin.<sup>16</sup> Once activated, integrin mediates extracellularly the mechanical interaction of cells with ECM, connects to cytoskeletal actin intracellularly via a series of linker proteins and regulates several important signaling cascades by activating protein tyrosine kinases such as focal adhesion kinase (FAK) and Src-family kinases.<sup>17</sup> On the other hand, integrin can transmit the signals into the cells through the 'outside-in' signaling, providing extracellular information including its adhesive state and the surrounding environment. Both the conformational change and the clustering of integrin contribute to the 'outside-in' signaling and can lead to a series of cellular response to extracellular matrix such as cell adhesion, cytoskeletal structure, migration, gene expression, cell survival, proliferation and differentiation.<sup>15</sup> Therefore, understanding the integrin conformation/affinity change and its downstream pathways would be of great importance to clarify the mechanotransduction mechanism, providing valuable information for design and development of novel substrates potentially used as cell culture device or implants.

In this study, we hypothesized that tuning the curvature of cell-material interface might be an effective approach to regulate  $\beta$ 1 integrin affinity and its downstream signaling pathways, and further modulate MSC behavior and function. As a cell culture device,

polystyrene (PS)-based inserts with three roughness levels on the bottom were fabricated for culturing hADSCs (Fig. 1A-D). As the PS used here is an amorphous polymer, it can provide a homogeneous surface. A smooth surface (PS-000) was used here as a control. A surface (PS-160) with a roughness level comparable to hADSC dimension (~ 100  $\mu\text{m}$  in adhesion) was expected to regulate the MSCs at the single cell level via its local curvature, while a surface (PS-320) with a roughness surpassing hADSC size might be capable of modulating cell clusters. The cellular responses of hADSCs to the roughness including their morphology, surface markers and proliferation were evaluated. The VEGF secretion was quantified, and the effect of the conditioned media from the cell cultures on angiogenesis was examined both *in vitro* using human umbilical vein endothelial cells (HUVECs) and *ex vivo* via the hen's egg test - chorioallantoic membrane (HET-CAM) assay. In particular, we studied the underlying mechanism, through which the VEGF secretion of hADSCs was regulated by the micro-scale roughness. Our results demonstrated that the PS-160 surface with a roughness in the range of cell size could elevate high-affinity  $\beta 1$  integrin level without an alteration of total  $\beta 1$  integrin level, resulting in the significantly promoted VEGF secretion of hADSCs (as illustrated in Fig. 1E).

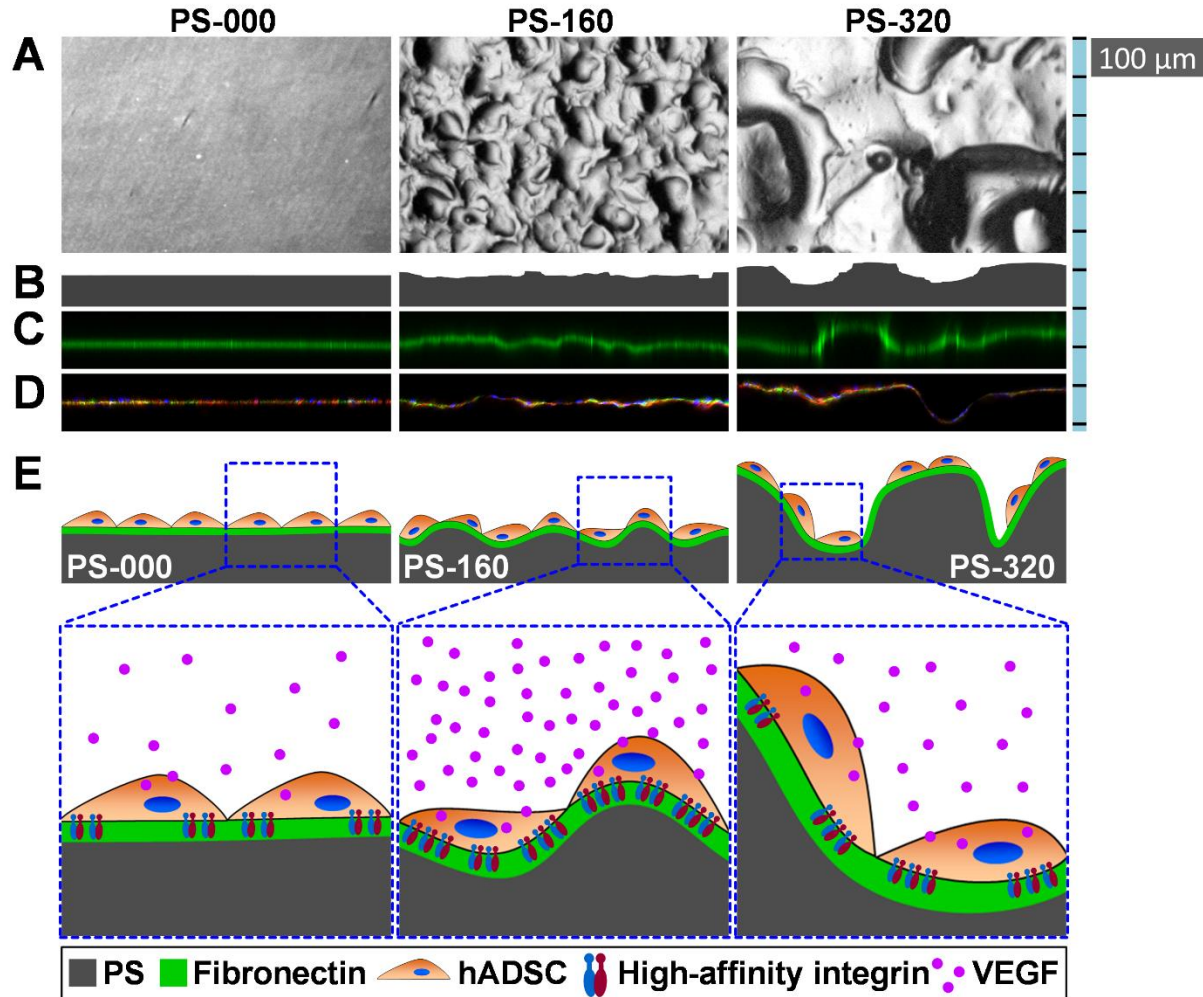


Fig. 1. Modulating VEGF secretion of hADSCs via micro-scale surface curvature. (A) Phase contrast microscope images showing the top-view of the insert bottoms with different roughness. (B) Side-view surface profiles of the insert bottoms determined by optical profilometry. (C) The inserts were coated with fibronectin to facilitate cell adhesion and the immunofluorescent staining images demonstrated the distribution of pre-coated fibronectin. The absorbed fibronectin formed the homogeneous layers (green) on all surfaces according to the cross-sectional view of the orthoimages. (D) The hADSCs were cultured on fibronectin-coated surfaces for 14 days followed by fluorescence staining to detect the actin cytoskeleton (red), nuclei (blue) and fibronectin (green) using a confocal laser scanning microscope. (E) Schematic diagram illustrating that the micro-scale curvature of the substrate surface could influence hADSC shape and morphology, and modulate VEGF secretion via integrin mediated mechanotransduction.

## 2 Experimental Section

### 2.1 Cell culture inserts

PS (Type 158K, BASF, Germany) with a number average molecular weight of  $M_n = 109.000 \text{ g}\cdot\text{mol}^{-1}$  was used without any further purification to prepare the inserts fitting standard 24-well tissue culture plates via injection molding as described before.<sup>18, 19</sup> The (micro)curvature of the injection molded polystyrene cell culture inserts was controlled by the utilization of metal cylinders having different micro surface roughness in a custom made mold. Three differently structured cylinders were utilized to manufacture the inserts with different types of bottom roughness: a cylinder with a polished contact surface (PS-000), and two cylinders with micro-structured surfaces according to the standard of German Institute for Standardization (DIN 16747: 1981-05), M30 (PS-160) and M45 (PS-320). The prepared inserts were sterilized by gas sterilization (gas phase: 10% ethylene oxide, 54 °C, 65% relative humidity, 1.7 bar, 3 h of gas exposure time and 21 h of aeration phase). Before using the prepared inserts for hADSC cultivation, the inserts were coated with human fibronectin (Sigma-Aldrich, St. Louis, MO, USA) to enhance the cell attachment. For each insert, 300  $\mu\text{l}$  of fibronectin solution (10  $\mu\text{g}/\text{ml}$  in PBS) was added and incubated at 37 °C for 1 h, followed by washing three times with PBS.

Optical profilometry and atomic force microscopy was employed for characterization of the PS surface structures. An optical profilometer type MicoProf 200 (FRT - Fries Research & Technologie GmbH, Bergisch Gladbach, Germany) equipped with a CWL 300 chromatic white-light sensor was utilized for determination of the arithmetic average roughness ( $R_a$ ) at micro scale and the mean spacing between the peaks ( $S_m$ ) of sterile PS substrates (details are given in Supporting method S1). Surface topography investigations and nanoindentation experiments were conducted with an atomic force microscope MFP-3D Bio-AFM (Asylum Research, Santa Barbara, CA, U S A) with PS substrates in the dry state at ambient conditions (for details see Supporting method S2).

## 2.2 Cell culture and conditioned medium collection

hADSCs were isolated from human adipose tissue as described previously<sup>4</sup>. The adipose tissue was obtained by abdominal liposuction from a female donor after informed consent (No.: EA2/127/07; Ethics Committee of the Charité - Universitätsmedizin Berlin, approval from 17.10.2008). The hADSCs were expanded in human adipose-derived stem cell medium (ADSC™ growth medium, Lonza, Walkersville, MD, USA) and then stored in liquid nitrogen. The cells were recovered and maintained in a cell culture incubator (37 °C, 5% CO<sub>2</sub>), and were used from passage three for all experiments. The HUVECs (Lonza, Walkersville, MD, USA) were cultured in the endothelial cell growth medium (EGM™, Lonza, Walkersville, MD, USA) in a cell culture incubator.

The conditioned media of hADSC cultures derived from different surfaces were collected at the indicated time points.  $1.0 \times 10^4$  cells were seeded per insert. 24 h before medium collection, the growth medium was replaced with 500 µl of fresh ADSC™ medium. Collected conditioned media were stored at -20 °C for further experiments.

## 2.3 Cell size and contact area to the substrate

To study the cell size and contact area to the material surface, hADSCs were seeded with the number of  $1.0 \times 10^4$  cells for each insert and were fixed after 3 days of culture to perform the fluorescence staining. Four fluorescent images in each group were then analyzed using ImageJ software (National Institutes of Health, USA) to calculate the cell size (2D spreading area). First, the total cell covered area was calculated, and the cell number was determined by counting the nuclei. Then the 2D spreading area of single cells was calculated by dividing the total cell covered area with the cell number. However, it should be noted that such an analysis becomes difficult at a higher cell density, due to the proximity of the cells.

The true cell size or contact area to the rough surfaces (3D spreading area) was further calculated based on the result of 2D spreading area. The ratio of surface area ( $S_{AR}$ ) between the rough surfaces and smooth surface was calculated via the model-based analysis ( $S_{AR}$ , PS-160/PS-000 = 1.18;  $S_{AR}$ , PS-320/PS-000 = 3.24; see supporting method



S4 and Fig. S6). Assuming that the cells were distributed randomly on the rough surfaces, the following equation was applied: 3D spreading area = 2D spreading area  $\times$   $S_{AR}$ . However, randomly distributed hADSCs were only observed on PS-160, but not on PS-320.

## 2.4 Fluorescence staining and laser scanning microscopy

$1.0 \times 10^4$  hADSCs were seeded into each insert. At the indicated time points for staining, the cells were fixed with 4% paraformaldehyde for 20 minutes, permeabilized with 0.1% Triton X-100 for 10 minutes and blocked with 1% BSA for 30 minutes. Vinculin was stained with mouse anti-human vinculin monoclonal antibody (Merck Millipore, Darmstadt, Germany) and Alexa Fluor® 488 labeled IgG antibody (Life Technologies, Darmstadt, Germany). F-actin was stained with Alexa Fluor® 555 Phalloidin (Life Technologies, Darmstadt, Germany). The cell nuclei were stained with Hoechst 33342 (NucBlue® Live Reagent, Life Technologies, Darmstadt, Germany). To detect the pre-coated fibronectin on different surfaces and study its organization during cell culture, fibronectin was stained with Anti-Fibronectin antibody-Alexa Fluor® 488 (Abcam, Cambridge, United Kingdom). After staining, the samples were scanned with a confocal laser scanning microscope (LSM 780, Carl Zeiss, Jena, Germany) using the mode of z-stack multilayer scanning, and the images were processed using ZEN 2012 software (Carl Zeiss, Jena, Germany). The cross-sectional view of the orthographic images was used to study the distribution of the pre-coated fibronectin, and the fluorescence intensity was analyzed using ImageJ software (National Institutes of Health, USA) to compare the adsorption density of fibronectin on different surfaces and in different areas. The top-view images of the samples were processed by Maximum Intensity Projection to study the cell morphology, fibronectin organization and focal adhesions, and further analyzed to study the cell size and contact area to the material surfaces.

In addition, to observe the cell-material interface, the tilted-view images were taken by tilting the samples to make a 25° angle between the objective and the material surface (Fig. S3A). A confocal laser scanning microscope (LSM 780, Carl Zeiss, Jena, Germany) was applied to scan the samples using the mode of z-stack multilayer scanning. The 3D

images were then reconstructed based on the single layer scanning images using the ZEN 2012 software (Carl Zeiss, Jena, Germany).

## 2.5 Flow cytometry

$1.0 \times 10^4$  hADSCs were seeded into each insert. After 14 days of culture, the cells were harvested and stained with a Human MSC Analysis Kit (Stemflow™, BD Biosciences, Heidelberg, Germany) according to the manufacturer's instruction to examine the cell surface markers. To quantify the  $\beta 1$  integrin, hADSCs were cultured in the inserts for 4 days. Then the cells were harvested using StemPro Accutase® (Thermo Fisher Scientific, Bonn, Germany) for 2 minutes at 37 °C, fixed with 4% (w/v) paraformaldehyde for 15 minutes. To detect  $\beta 1$  integrin in the whole cells (surface and cytoplasm), the cells were permeabilized with 0.1 % (w/v) Triton X-100 in PBS for 10 minutes. To detect  $\beta 1$  integrin on the cell surface, no permeabilization step was applied. After blocking with 1% (w/v) BSA for 30 minutes, the activated or total  $\beta 1$  integrin was stained using monoclonal mouse anti-human integrin beta-1 antibody (HUTS-4, Millipore, Darmstadt, Germany) or total integrin beta-1 antibody (Abcam, Cambridge, UK), and Alexa Fluor® 488 labeled IgG antibody (Life Technologies, Darmstadt, Germany). A flow cytometer (MACSQuant®, Miltenyi Biotec, Bergisch Gladbach, Germany) was used to analyze the cells, and the data were processed using Flowjo software (Tree Star Inc., Ashland OR, USA).

## 2.6 Enzyme-linked immunosorbent assay (ELISA)

The expression levels of VEGF, phosphorylated FAK (pFAK), total FAK (tFAK) and phosphorylated extracellular signal-regulated kinase (pERK) of hADSCs growing on different surfaces were quantified by ELISA. The VEGF concentration in the conditioned medium was determined using a human VEGF-A ELISA kit (Thermo Fisher Scientific, Bonn, Germany). The concentration of pFAK, tFAK and pERK in the cell extract were measured using the pFAK (pY397), tFAK and pERK (ERK1[pTpY202/204] and ERK2[pTpY185/187]) ELISA kits (Life Technologies, Darmstadt, Germany). The amount of total protein in the cell extract was determined using a BCA protein assay kit (Thermo

Fisher Scientific, Bonn, Germany) to normalize the expression levels of the proteins of interest.

## 2.7 Tube formation and migration of HUVECs

The tube formation and migration of HUVECs were tested using the conditioned media collected from the hADSC cultures on different surfaces. To assess the tube formation of HUVECs, a 24-well tissue culture plate was first coated with Geltrex® Matrix solution (Life Technologies, Darmstadt, Germany; 200 µl per well) according to the given protocol. Thereafter  $6.0 \times 10^4$  HUVEC cells per well were seeded on the matrix. For each well, 500 µl of conditioned medium collected at day 14 was applied for cell culture. The cells were stained with calcein (Life Technologies, Darmstadt, Germany) after 24 h of incubation, and the formed tubes were visualized using a fluorescence microscope (AxioSkop, Carl Zeiss, Jena, Germany). In each well, the images were taken in randomly selected observation fields and the number of the complete rings was counted.

The migration of HUVECs was tracked using a time-lapse imaging microscope (IX81 motorized inverted microscope, Olympus, Hamburg, Germany) equipped with a bold line cage incubator to maintain cell growth in a humidified atmosphere (37 °C, 5% CO<sub>2</sub>). HUVECs were seeded in a 24-well tissue culture plate with the number of  $2.0 \times 10^4$  cells per well. After 24 h of culture, the medium was replaced with the conditioned medium collected at day 14 (500 µl per well), and the cell migration was recorded up to 24 h. The migration trajectories and velocity were analyzed using ImageJ software (National Institutes of Health, USA) combined with the software plug-ins “manual tracking” and “chemotaxis and migration tool” (ibidi GmbH, Martinsried, Germany).

## 2.8 HET-CAM assay

HET-CAM assay was performed to assess the effect of the conditioned medium on angiogenesis. The fertile VALO SPF eggs of white Leghorn species (Lohmann Tierzucht GmbH, Cuxhaven, Germany) were bred at 37°C and 65% humidity for 8 days in the breeding incubator (BSS 300 MP GTFS, Grumbach GmbH, Asslar, Germany). Before the test, the position of the air bubbles was marked under a shell lamp, and the marked upper

part of the egg shell was removed. Then the exposed inner membrane was moistened with 0.9% NaCl and carefully removed. After that, 500 µl of conditioned medium collected at day 14 was dropped on the chorioallantoic membrane. Images were taken at the starting point, 24 h and 48 h later, respectively, using a stereomicroscope (MZ16A, Leica, Wetzlar, Germany). The vessels crossing the middle line of the image were counted, and the fold increase of the vessel density was calculated (fold increase = vessel density after 24 or 48 h / vessel density at starting point).

## 2.9 Inhibition experiment

FAK inhibitor PF-573228 and rho-associated coiled-coil-containing protein kinase (ROCK) inhibitor Y-27632 (both are from Sigma-Aldrich, St. Louis, MO, USA) were used in the inhibition experiment.  $1.0 \times 10^4$  hADSCs were seeded per insert. After 10 days of culture PF-573228, Y-27632 or both were added at a final concentration of 10 µM each. The inhibitor-containing medium was changed once at day 12. The conditioned medium was collected at day 14 and the cells were lysed to extract the proteins.

## 2.10 Statistics

The number of replication for experiments was larger than three as indicated respectively in figure legend for each assay, and data are expressed as mean  $\pm$  standard deviation. Statistical analysis was performed using two-tailed independent samples t-test, and a significant level (Sig.)  $< 0.05$  was considered to be statistically significant.

# 3 Results and discussion

## 3.1 Surface characterization

Three substrates were designed and prepared: PS-000 smooth surface, PS-160 with a surface roughness in the range of cell size, PS-320 with a roughness surpassing hADSC size. The insert bottom was analyzed by optical profilometry measurements and the obtained results are listed in Table S1. PS-000 exhibited a  $R_a$  value of  $0.13 \pm 0.07$  µm,

while higher  $R_a$  values of  $4.17 \pm 0.17 \mu\text{m}$  and  $25.4 \pm 3.8 \mu\text{m}$  were obtained for the micro-rough surfaces PS-160 and PS-320. The  $S_m$  value of PS-160 was  $164 \pm 16 \mu\text{m}$ , comparable to the dimension of single hADSC, while for PS-320 a higher  $S_m$  of  $316 \pm 36 \mu\text{m}$  was found. The nanoscale roughness obtained by atomic force microscopy exploring a scan size of  $2 \times 2 \mu\text{m}^2$  revealed average  $R_a$  values less than 15 nm for the different surfaces. As the surfaces were coated with human fibronectin prior to cell seeding, the fibronectin adsorption and distribution were evaluated. The coated fibronectin formed a homogenous layer on the insert bottom (Fig. 1C). The fibronectin density was at a similar level on different surfaces and in different areas according to the fluorescence intensity analysis. AFM investigations utilizing nanoindentation technique showed almost similar local mechanical properties of the different substrates. Here, a Young's modulus of  $31 \pm 2 \text{ GPa}$  was found for PS-000, while values of  $30 \pm 5$  and  $29 \pm 2 \text{ GPa}$  were obtained from nano-indenting the top of the hills of the rough samples PS-160 and PS-320 (Table S1).

### 3.2 hADSC proliferation, surface markers and morphology

We found the initial cell attachment after 24 h was similar on all surfaces (Fig. S1A), which was different to the result reported by Bigerelle *et al.* In their study, the bone marrow MSCs showed a lower attachment on the surface with the roughness relevant to the cell size.<sup>20</sup> The possible reasons for this discrepancy might be the surface chemistry of the cell culture materials employed, as we used fibronectin-coated PS compared to the titanium surfaces used in their study. Similarly, no effect of surface roughness on the proliferation rate of hADSCs was observed. The proliferation activity of the cells on different surfaces was similar during 2 weeks of cultivation (Fig. S1A). After 14 days of culture, no change of surface marker expression was observed, independent of the roughness of the culture surface. MSC markers were well preserved and non-MSC markers were not detected, demonstrating that the surface curvature has no influence on hADSC surface markers (Fig. S1B).

Immunofluorescent staining was performed to investigate the cell morphology. After 3 days of cell culture, analysis based on fluorescent images showed that hADSCs presented a smaller 2D projection size but a similar effective spreading area in 3D on PS-

160, as compared to the cells on smooth surface (Fig. 2), suggesting PS-160 surface could effectively modulate hADSC size and shape. In addition, distinct difference was observed in cells on different surfaces with respect to their orientation, distribution, F-actin arrangement and fibronectin organization (Fig. S2). The cells on PS-000 surface showed a highly aligned cell orientation and actin cytoskeleton. In contrast, cells and their stress fibers on PS-160 and PS-320 were less orientated. The fibronectin organization by the cells was affected by the surface curvature. Most fibronectin localized beneath the cells, and an increase in fibronectin fibrils around the cell periphery was observed. Notably, the cells on PS-320 were less homogeneously distributed, as compared to those on PS-000 and PS-160.

To further study the interaction of cells and materials, the stained samples were observed from a tilt angle (Fig. S3A). This approach could overcome the limitations of normal top-view method, as the images of cell-material interface could be generated with high resolution. The single layer scanning images indicated that the cells formed a monolayer on all surfaces (Fig. 1D). Accordingly, a smooth cell layer was observed on PS-000, whereas the rougher cell layers were found on PS-160 and PS-320 (Fig. S3B).

Moreover, our model-based analysis indicated that the cells on PS-160 and PS-320 surfaces might perceive the different cues of local curvature (Fig. S6 and Supporting method S4). Compared to PS-320, the PS-160 surface with a roughness in the range of cell size has apparently a larger portion of surface with optimal curvature properties for *in situ* regulation of hADSC properties. Accordingly, when hADSCs attached on PS-160 a large fraction of cells could be affected by the local curvature. In contrast, the larger portion of relatively smoother surface in the range of cell size on PS-320, for example the broad valleys, flat peaks or gentle slopes, may in average reduce the effect of local curvature experienced by the given hADSCs.

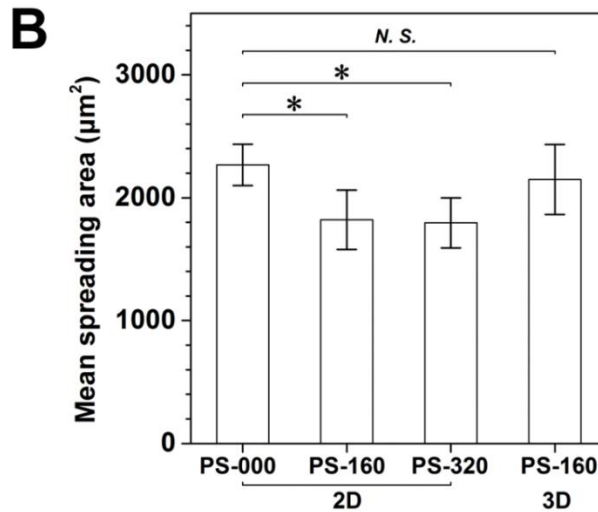
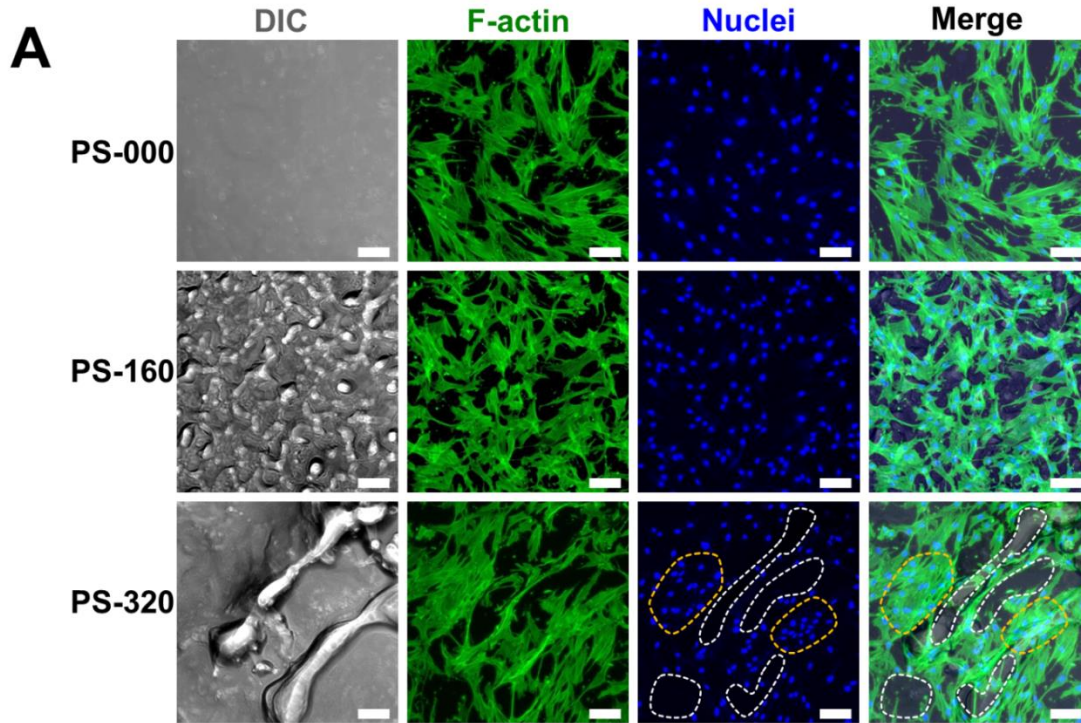


Fig. 2. hADSC size and contact area to the material surfaces. (A) Representative images of fluorescently stained hADSCs on different substrates (bar = 100 µm). Inhomogeneous cell distribution was observed on PS-320 surface, as indicated by the areas enclosed by the dash-lines (white: low cell density; yellow: high cell density). (B) 2D and 3D spreading area of single hADSCs on different surfaces. The quantification was based on 4 randomly selected images (\*Sig < 0.05).

### 3.3 Enhancement of integrin mediated FAK signaling by micro-scale curvature

Cells receive various mechanical signals via their transmembrane receptors (such as integrin) from their micro-environment, assemble focal adhesions accordingly and launch a series of intracellular biochemical signaling events.<sup>21</sup> To study the cell-material interaction and to determine the potential mechanism, the focal adhesion-related protein components were investigated. Flow cytometry analysis was performed to quantify activated and total  $\beta 1$  integrin in hADSCs cultured on different substrates. The significantly higher levels of activated  $\beta 1$  integrin on cell surface and in the whole cells were observed in PS-160 group at day 4, as compared to the cells on PS-000 and PS-320. The total  $\beta 1$  integrin was at the similar level for these three groups (Fig. 3A). These results were further confirmed by immunofluorescence staining and western blot analysis (Fig. S4). The focal adhesion complex formation was examined by immunofluorescent staining of vinculin. After 4 days of culture, hADSCs on PS-160 surface formed more focal adhesions than on PS-000 and PS-320 (Fig. 3B). These results suggested that PS-160 substrate could enhance the  $\beta 1$  integrin activation of hADSCs without alteration of the total  $\beta 1$  integrin level. Given that the surface chemistry of these substrates was identical, the enhanced  $\beta 1$  integrin activation might be predominantly due to the physical features of PS-160 surface. We speculated that the PS-160 roughness with a comparable scale to cell size might provide appropriate topographic cues such as the local curvature, which could be perceived by cells to modulate the integrin mediated adhesion. This observation is consistent with the previous findings that the focal adhesion complexes of MSCs were primarily formed at the regions of local curvature when they grew on 2D micro-patterns or in 3D micro-wells.<sup>4, 22</sup> Notably, the difference in fibronectin remodeling by hADSCs on different surfaces was observed here (Fig. S2). Fibronectin remodeling is dynamically related with integrin activation. On the one hand, extracellular fibronectin assembly requires the participation of integrin that recognize the RGD and synergy sequences in fibronectin.<sup>23</sup> On the other hand, the fibronectin density can affect the activation of cell surface integrin.<sup>24</sup>



The engagement of integrin with its extracellular ligand can activate various intracellular signaling components. Multiple structural and signaling proteins are recruited to focal adhesions upon cell adhesion to ECM. Among these proteins, FAK is one of the most prominent signaling molecules, which is composed of a central kinase domain flanked by an N-terminal FERM domain and a C-terminal FAT domain.<sup>25, 26</sup> Intracellularly, the autophosphorylation of FAK at Y397 can be initiated by the binding of integrins to ECM and their clustering. Y397 is the most important phosphorylation site since the kinase activity of FAK can be fully activated via its phosphorylation. Phosphorylation at Y397 creates a high-affinity binding site for the Src-homology 2 (SH2) domain of Src family kinases. The recruitment of Src by FAK leads to a conformational activation of Src, which consequently promotes the Src-dependent phosphorylation of FAK at other tyrosines.<sup>27</sup> In this study, at day 4 the ratio of phosphorylated to total FAK (pY397FAK/tFAK) was significantly higher in the PS-160 group as demonstrated by ELISA result, and this elevated FAK phosphorylation was maintained at least 14 days (Fig. 3C). Further, a higher FAK phosphorylation level in cells on PS-160 than on PS-000 and PS-320 was evidenced by the immunostaining and western blot results (Fig. S5).

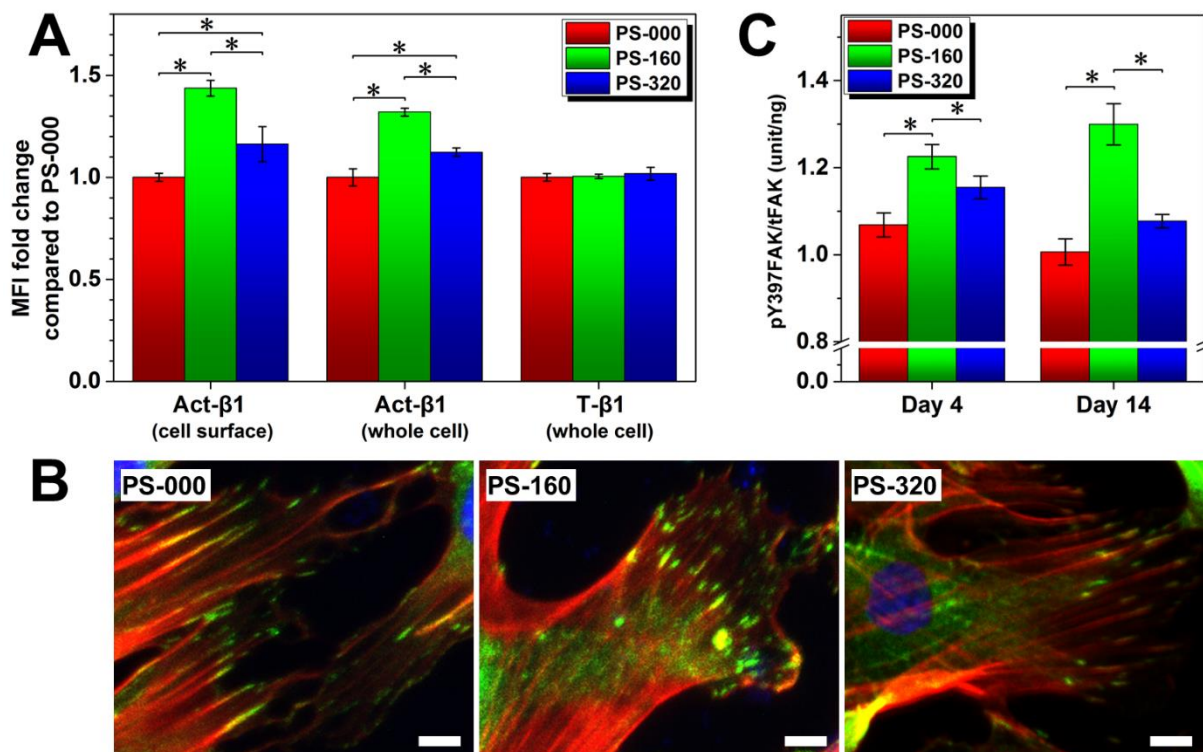


Fig. 3. PS-160 substrate enhanced  $\beta 1$  integrin activation, focal adhesion formation and FAK phosphorylation. (A) Activated  $\beta 1$  integrin (Act- $\beta 1$ ) and total  $\beta 1$  integrin (T- $\beta 1$ ) were quantified using flow cytometry, and the result was expressed as the fold change of mean fluorescence intensity (MFI) compared to PS-000 group. hADSCs on PS-160 showed the higher levels of activated  $\beta 1$  integrin on cell surface and in the whole cells compared to cells on PS-000 and PS-320. (B) Representative laser scanning microscopic images showed the formation of a higher number of focal adhesions on PS-160 than on PS-000 and PS-320 (red: F-actin; green: vinculin; blue: nuclei; bar = 10  $\mu\text{m}$ ). (C) FAK phosphorylation was induced by PS-160 surface to a significantly higher level than by PS-000 and PS-320. Cells cultured in 3 independent inserts of each group were analyzed (\*Sig < 0.05).

### 3.4 Promotion of VEGF secretion by micro-scale curvature

Upon integrin engagement, the activation of FAK and Src can subsequently activate the downstream mitogen-activated protein kinase (MAPK)/ERK pathway. The phosphorylation of FAK at Y925 facilitates the SH2-mediated binding of Grb2 adaptor protein, which can activate the Ras-Raf-MEK-ERK signaling and promote VEGF expression in tumor cells.<sup>28</sup> Here, the VEGF secretion of hADSCs on different surfaces was quantified and the pro-angiogenic effect of cell secretome was assessed.

First, the VEGF concentration in the conditioned media of hADSCs cultured on different surfaces was quantified at day 4, 7 and 14. Markedly, hADSCs cultured on PS-160 surface secreted more VEGF than those on PS-000 and PS-320 at all of the time points of measurement. At day 4, the VEGF concentration in the medium of PS-160 culture was around 40% and 50% higher than that in PS-000 and PS-320 cultures, respectively. After 2 weeks, the VEGF concentration in the medium of PS-160 culture still remained highest, around 80% and 20% increase over that in PS-000 and PS-320 groups, respectively (Fig. 4A). Further, to challenge the possible biological relevance of elevated VEGF in the hADSC secretome as a result of culturing cells on surfaces with micro-scale curvature, the pro-angiogenic effect of the conditioned media was assessed by an *in vitro* assay. The conditioned medium derived from hADSCs cultured on PS-160 surface could

significantly enhance the tube formation of HUVECs compared to accordingly conditioned media from PS-000 and PS-320 surfaces (Fig. 4B). To evaluate the HUVEC migration driven by the conditioned media, the cells were cultured in the conditioned media and their migration track was recorded using a time-lapse microscope. The HUVEC migration velocity was significantly elevated when grown in conditioned medium derived from PS-160 surface. The cells in PS-160 medium moved around 1.4 and 1.3 times as fast as the cells in PS-000- and PS-320 media, respectively (Fig. 4C). A HET-CAM assay was performed to further evaluate the pro-angiogenic capacity of conditioned media under *ex vivo* condition. A higher number of newly formed vessels was observed on the chorioallantoic membrane treated by PS-160 medium than by PS-000 and PS-320 media (Fig. 4D). Compared to the initial state, the PS-160 medium resulted in the highest fold increase of vessel density after 24 h, as compared to the PS-000 and PS-320 media. After 48 h of treatment, there was still a significant higher increase of the vessel density in the PS-160 medium treated group, consistent with the finding in the *in vitro* tubulogenesis assay. Our findings on the modulation of angiogenic capacity of freely migrating MSCs by local curvature are in part supported by the latest report using discrete adhesive micropatterns, with varying aspect ratio and local curvature, to stimulate immobilized MSCs the angiogenic factor secretion.<sup>29</sup> It should be noted that the enhanced pro-angiogenic effect of the conditioned medium from PS-160 might be due to not only the VEGF upregulation but also a synergistic effect with other growth factors. Further studies are necessary to clarify the secretion profile of angiogenic factors at different interface curvatures.

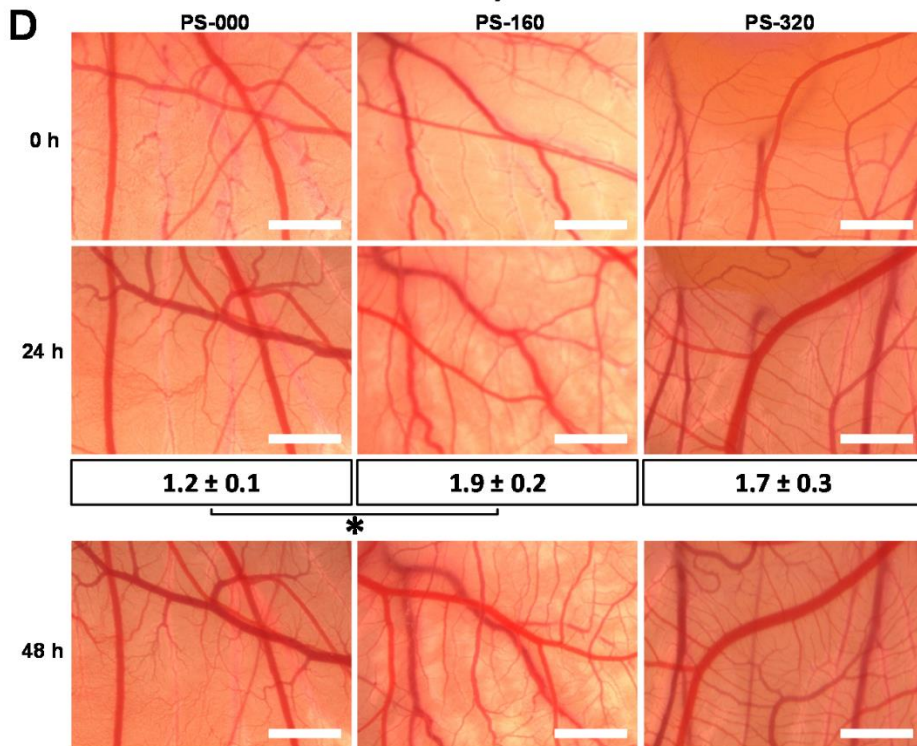
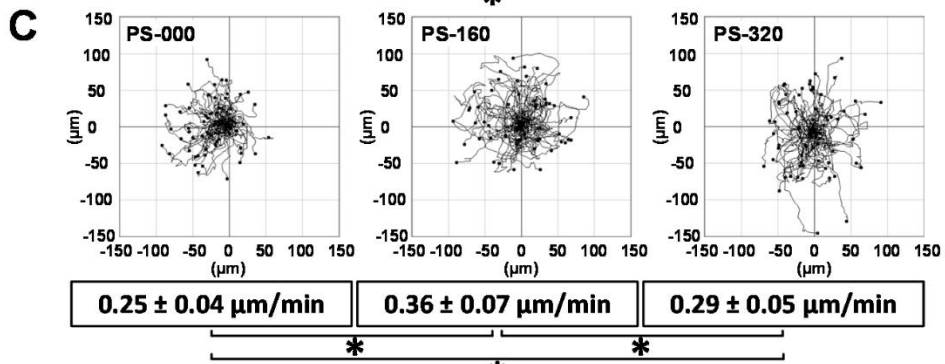
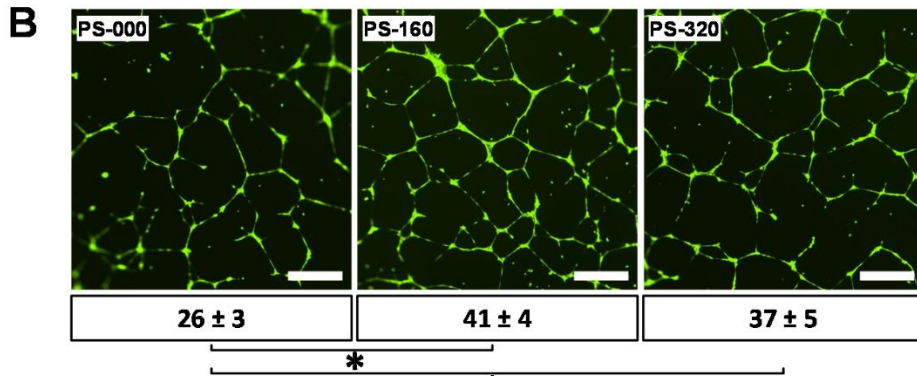
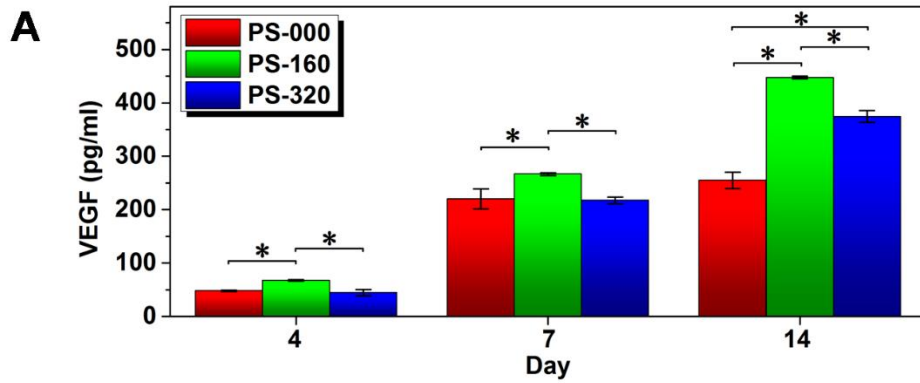


Fig. 4. PS-160 substrate promoted VEGF secretion of hADSCs, and enhanced pro-angiogenic effect of conditioned medium. (A) VEGF secretion of hADSCs on PS-160 surface was induced to a higher degree than on PS-000 and PS-320 surfaces. Cells cultured in 3 independent inserts of each group were analyzed (\*Sig < 0.05). (B) Representative images showed the tube formation of HUVECs in conditioned media derived from different surfaces. The HUVECs were stained by calcein. The number of the complete rings was counted in 7 randomly selected images to quantify the formed tubes. (C) For cell migration assay, HUVECs cultured in different conditioned media were tracked up to 24 h to generate the migration trajectories and to calculate the migration velocity. For each group, the migration velocity of 60 cells was analyzed. (D) Representative images showed the vessels on the chorioallantoic membrane at the starting point (0 h) and after incubation for 24 and 48 h with the conditioned media. The vessels were accounted based on 5 randomly selected images and the values indicated the fold increase of vessel density as compared to the starting point. (bar = 500  $\mu$ m; \*Sig < 0.05)

### 3.5 VEGF expression regulated by FAK signaling pathway

Small molecule inhibitors related to FAK and ROCK signaling pathways were applied to elucidate the underlying mechanism of micro-scale curvature induced enhancement of VEGF secretion. Without inhibition, the expression levels of both pY397FAK and VEGF were significantly higher in the cells growing on PS-160, as compared to the cells on PS-000 and PS-320 (Fig. 5A, B). When treated with FAK inhibitor, ROCK inhibitor or both for 4 days, pY397FAK expression was significantly inhibited (Fig. 5A). Accordingly, VEGF levels in the conditioned media were decreased by the inhibitors, as compared to the untreated group (Fig. 5B). In addition, the relative expression levels of related proteins in the untreated hADSCs on PS-160 were determined at different time points. The VEGF expression increased at the earlier stage and reached the peak at day 10. Notably, VEGF amounts determined in the cell culture supernatants largely followed the expression levels of pY397FAK and pERK1/2, and a significant correlation between the expression levels of these three proteins was observed (Fig. 5C). These results indicated the key regulatory

function of FAK signaling on VEGF expression of hADSCs in response to surface curvature.

MSCs sense and response to the mechanical environment through the interaction of a signaling network components including FAK, cytoskeletal dynamics and RhoA/ROCK.<sup>9</sup> In the current study, the participation of RhoA/ROCK pathway in VEGF secretion was observed. The regulation of VEGF secretion by RhoA/ROCK might be through different pathways. First, RhoA/ROCK could stimulate FAK phosphorylation and then activate the ERK signaling. Second, RhoA/ROCK could phosphorylate and activate the downstream target PTEN,<sup>30</sup> which in turn inactivates Akt.<sup>31</sup> This would promote ERK activation as phosphorylation of Raf by Akt can inhibit the activation of the Raf-MEK-ERK cascade.<sup>32</sup> Further studies focusing on the exact function of RhoA/ROCK for mediating VEGF secretion of MSCs will be interesting.

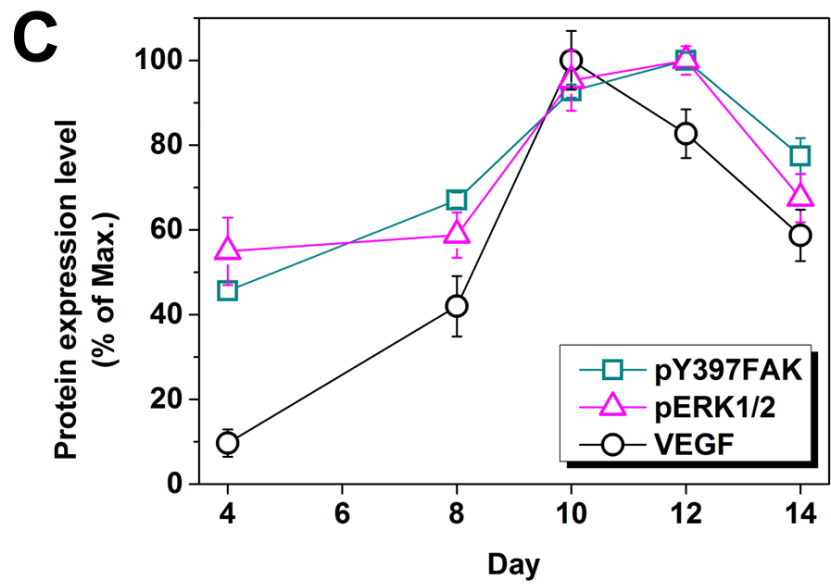
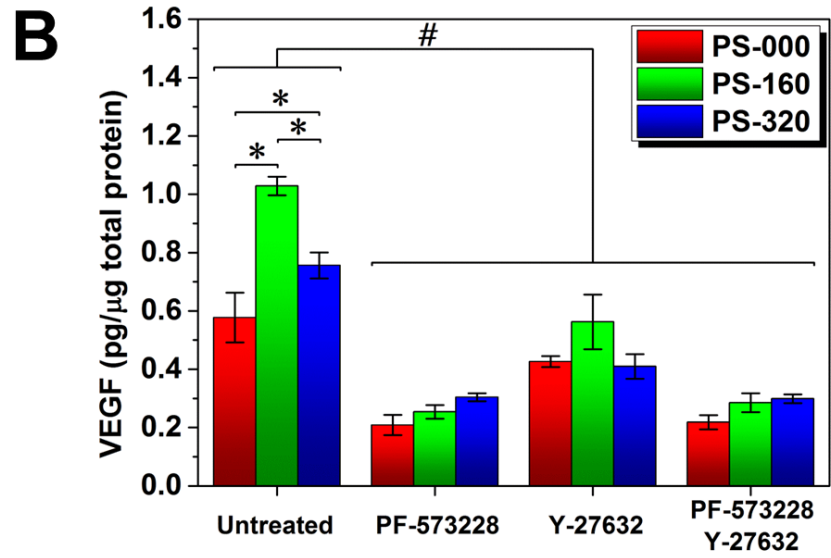
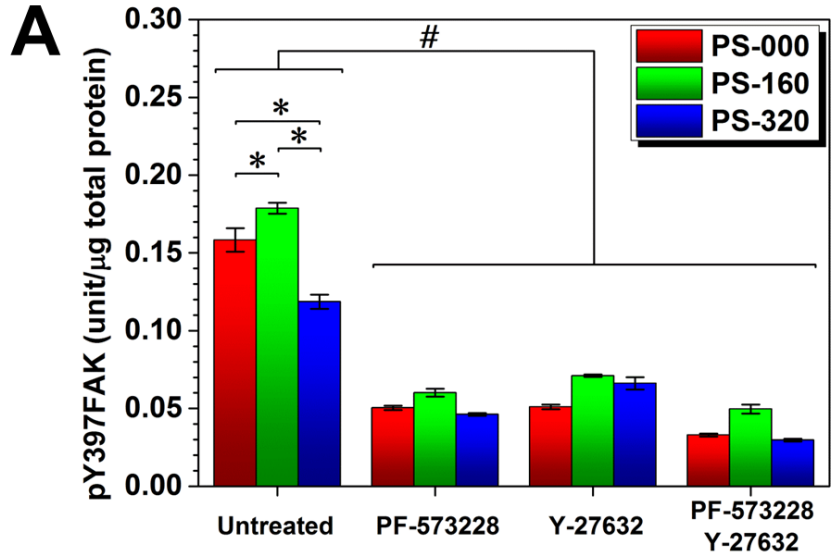


Fig. 5. Modulation of VEGF expression in hADSCs via FAK/ERK signaling. Both pY397FAK (A) and VEGF (B) levels were downregulated when the cells were treated with FAK inhibitor (PF-573228) or/and ROCK inhibitor (Y-27632). Cells cultured in 3 independent inserts of each group were analyzed (\*Sig < 0.05 in the untreated group; # Sig < 0.05 for inhibitor treated groups vs untreated group). (C) The expression levels of VEGF, pY397FAK and pERK1/2 exhibited the similar pattern in hADSCs on PS-160 surface and showed a significant correlation according to the analysis of Spearman's rank correlation coefficient (*rs*) and Pearson correlation coefficient (*rp*) (VEGF vs pY397FAK: *rs* = 0.9, *rp* = 0.957; VEGF vs pERK1/2: *rs* = 0.9, *rp* = 0.911; pY397FAK vs pERK1/2: *rs* = 1, *rp* = 0.931). The conditioned media or cell extract samples from 3 independent PS-160 inserts were collected to perform the ELISA analysis. The expression levels of proteins of interest were normalized against the amount of total protein of the cells.

In summary, these results demonstrated that integrin activation and its downstream signaling network were critically involved in hADSC modulation by micro-scale curvature (Fig. 6). When hADSCs attached on the surface with a roughness comparable to the cell dimension, complex changes in the micro-environment will be sensed by the cells. Parameters to consider such as the topography-dependent spectrum of local curvatures, alone or in conjunction with the contacted polymer area, could result in the alteration of cell shape, morphology, cytoskeleton organization and the distribution of adhesion points. Activation of the integrin can be enhanced under these conditions, where their extracellular domains undergo conformation/affinity changes and transmit signals across the cytoplasmic membrane. FAK, as a key component of the integrin triggered signaling pathway, was subsequently activated. The signaling network including FAK and Rho/ROCK may exert the regulatory effect on cell morphology and actin cytoskeleton organization, and activate downstream ERK signaling to enhance VEGF expression. This study pointed at a gateway to control parameters of MSCs critical for their therapeutic potential by specifying cell-material interactions. As a promising cell source in regenerative medicine, MSCs can accelerate tissue regeneration predominantly due to their paracrine activity rather than their direct differentiation,<sup>1, 33-36</sup> due to their low engraftment level and marginal survival rate at the injury site<sup>37, 38</sup>. The regulatory and trophic factors in MSC secretome can exert multiple functions to achieve therapeutic



effects in tissue regeneration. Hence, regulating MSC secretion is of great relevance to their clinical applications. Our results suggested that fine-tuning the surface roughness might be an effective and safe approach to improve the therapeutic functions of MSCs. These results shed light on design and developing biomaterials for both *in vitro* and *in vivo* applications. For instance, *in vitro* preconditioning of MSCs on the surface with such a well-defined topography may improve their therapeutic efficacy after transplantation; or surface topography treatment as a preconditioning approach could be used for producing cell-free therapeutics. The MSC pre-seeded implant materials with an appropriate surface topography may accelerate tissue regeneration *in vivo*, which might be attributed to elevated level of predominant pro-angiogenic factors in MSC secretome<sup>39-41</sup>.

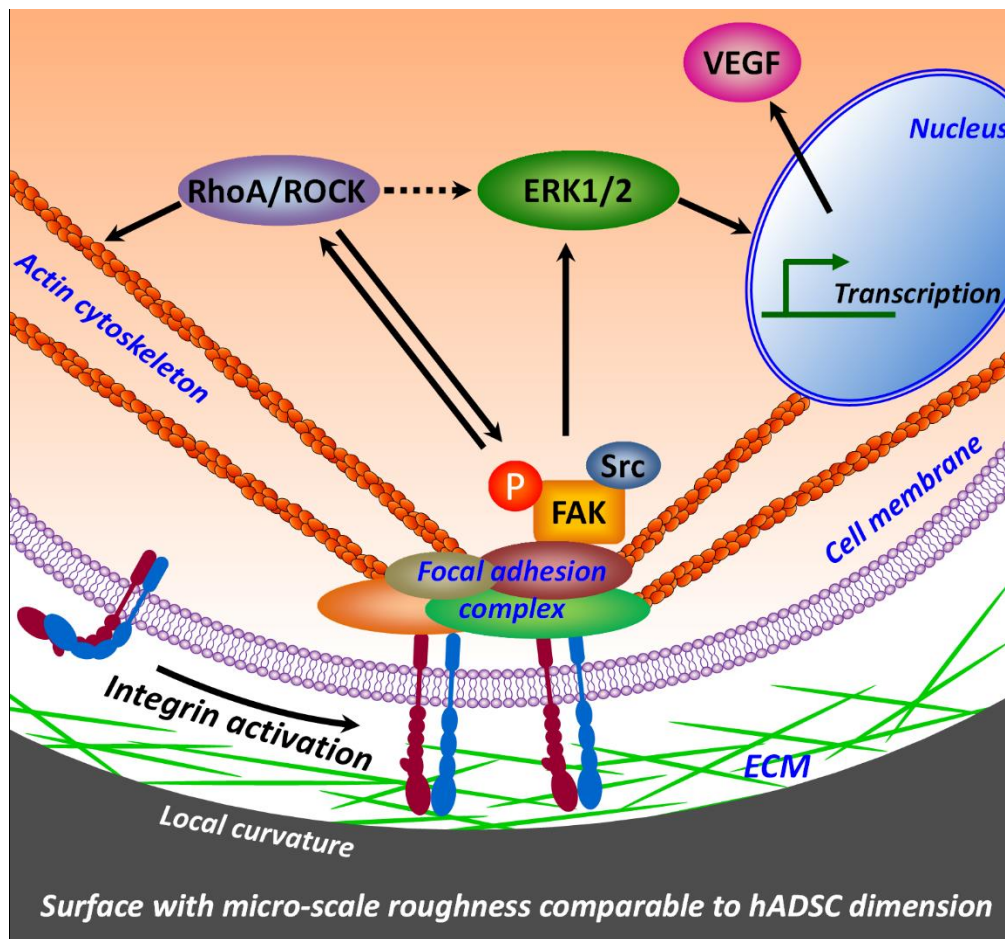


Fig. 6. Proposed model of regulatory effect of micro-scale curvature on hADSCs.

Compared to smooth surface (PS-000) or rougher surface (PS-320), the surface with micro-scale roughness comparable to hADSC dimension (PS-160) could present a larger portion of surface with optimal curvature properties for modulating hADSCs. The cell shape and morphology of hADSCs would be altered on such a surface. This physical cue of local curvature would induce the enhancement of integrin activation on cell surface, and then activate FAK to form a signaling network. The actin cytoskeleton organization would be modulated accordingly with the involvement of ROCK. And the downstream ERK signaling might be activated, leading to the upregulation of VEGF expression.

#### **4 Conclusion**

PS inserts with three different types of culture surface roughness (smooth surface: PS-000; with roughness level comparable to hADSC size: PS-160; with roughness level surpassing hADSC size: PS-320) were fabricated to investigate the effect of micro-scale curvature on hADSCs. The cells exhibited different morphology and actin cytoskeleton on different surfaces, but neither their surface markers nor their proliferation were altered by micro-scale curvature. The conditioned medium derived from the substrate with a roughness comparable to hADSC size had a higher pro-angiogenic potential than that from smooth and rougher substrates, which could improve the tube formation and migration of HUVEC cells and enhance the new vessel formation on the chorioallantoic membrane of hen's eggs. Compared to smooth and rougher substrates, the substrate with a roughness comparable to hADSC size could promote VEGF secretion of hADSCs to a significantly higher level, and this effect was regulated through the increased high-affinity  $\beta 1$  integrin level of hADSCs and downstream FAK signaling with participation of RhoA/ROCK. These findings allow a better mechanistic understanding of MSC response to micro-scale curvature. This knowledge might help to design and develop biomaterials with effective and functional surface structures, which can be potentially utilized as implants or *in vitro* cell culture materials, to modulate MSCs and consequently achieve clinical benefits in regenerative medicine.

#### **Acknowledgements**

The authors acknowledge Robert Jeziorski, Mario Rettschlag for preparation of sterilized PS inserts and Yi Jiang as well as Manuela Keller for technical support. This work was financially supported by the Helmholtz Association of German Research Centers (including Helmholtz Cross Programme Initiative "Technology and Medicine - Adaptive Systems", grant no. VH-VI-423 (Helmholtz Virtual Institute, Multifunctional Biomaterials for Medicine), as well as programme-oriented funding) and the Federal Ministry of Education and Research, Germany, for funding through the Programme Health Research (grant no. 13GW0098, as well as project number 0315696A "Poly4BioBB").

### Conflict of interest

There are no conflicts of interest to declare.

### References

1. H. O. Kim, S. M. Choi and H. S. Kim, *Tissue Eng Regen Med*, 2013, **10**, 93-101.
2. J. Du, X. F. Chen, X. D. Liang, G. Y. Zhang, J. Xu, L. R. He, Q. Y. Zhan, X. Q. Feng, S. Chien and C. Yang, *P Natl Acad Sci USA*, 2011, **108**, 9466-9471.
3. K. Ye, X. Wang, L. P. Cao, S. Y. Li, Z. H. Li, L. Yu and J. D. Ding, *Nano Lett*, 2015, **15**, 4720-4729.
4. X. Xu, W. W. Wang, K. Kratz, L. Fang, Z. D. Li, A. Kurtz, N. Ma and A. Lendlein, *Adv Healthc Mater*, 2014, **3**, 1991-2003.
5. K. Kulangara, Y. Yang, J. Yang and K. W. Leong, *Biomaterials*, 2012, **33**, 4998-5003.
6. G. Abagnale, M. Steger, V. H. Nguyen, N. Hersch, A. Sechi, S. Jousen, B. Denecke, R. Merkel, B. Hoffmann, A. Dreser, U. Schnakenberg, A. Gillner and W. Wagner, *Biomaterials*, 2015, **61**, 316-326.
7. L. G. Xia, K. L. Lin, X. Q. Jiang, B. Fang, Y. J. Xu, J. Q. Liu, D. L. Zeng, M. L. Zhang, X. L. Zhang, J. Chang and Z. Y. Zhang, *Biomaterials*, 2014, **35**, 8514-8527.
8. X. N. Liu, R. L. Liu, B. Cao, K. Ye, S. Y. Li, Y. X. Gu, Z. Pan and J. D. Ding, *Biomaterials*, 2016, **111**, 27-39.
9. B. Y. Xu, G. B. Song, Y. Ju, X. Li, Y. H. Song and S. Watanabe, *J Cell Physiol*, 2012, **227**, 2722-2729.
10. F. Guilak, D. M. Cohen, B. T. Estes, J. M. Gimble, W. Liedtke and C. S. Chen, *Cell Stem Cell*, 2009, **5**, 17-26.
11. J. D. Humphrey, E. R. Dufresne and M. A. Schwartz, *Nat Rev Mol Cell Bio*, 2014, **15**, 802-812.
12. A. B. Faia-Torres, S. Guimond-Lischer, M. Rottmar, M. Charnley, T. Goren, K. Maniura-Weber, N. D. Spencer, R. L. Reis, M. Textor and N. M. Neves, *Biomaterials*, 2014, **35**, 9023-9032.
13. D. S. Harburger and D. A. Calderwood, *J Cell Sci*, 2009, **122**, 159-163.
14. A. Arjonen, J. Alanko, S. Veltel and J. Ivaska, *Traffic*, 2012, **13**, 610-625.
15. S. J. Shattil, C. Kim and M. H. Ginsberg, *Nat Rev Mol Cell Bio*, 2010, **11**, 288-300.
16. D. A. Calderwood, I. D. Campbell and D. R. Critchley, *Nat Rev Mol Cell Bio*, 2013, **14**, 503-517.
17. J. L. Guan, *Iubmb Life*, 2010, **62**, 268-276.
18. T. Roch, A. Kruger, K. Kratz, N. Ma, F. Jung and A. Lendlein, *Clin Hemorheol Micro*, 2012, **52**, 375-389.

19. W. W. Wang, N. Ma, K. Kratz, X. Xu, Z. D. Li, T. Roch, K. Bieback, F. Jung and A. Lendlein, *Clin Hemorheol Micro*, 2012, **52**, 357-373.
20. M. Bigerelle, S. Giljean and K. Anselme, *Acta Biomater*, 2011, **7**, 3302-3311.
21. M. A. Schwartz, *Csh Perspect Biol*, 2010, **2**.
22. K. A. Kilian, B. Bugarija, B. T. Lahn and M. Mrksich, *P Natl Acad Sci USA*, 2010, **107**, 4872-4877.
23. I. Wierzbicka-Patynowski and J. E. Schwarzbauer, *J Cell Sci*, 2003, **116**, 3269-3276.
24. G. L. Lin, D. M. Cohen, R. A. Desai, M. T. Breckenridge, L. Gao, M. J. Humphries and C. S. Chen, *Febs Lett*, 2013, **587**, 763-769.
25. X. Zhao and J. L. Guan, *Adv Drug Deliver Rev*, 2011, **63**, 610-615.
26. C. T. Mierke, *Phys Biol*, 2013, **10**, doi: 10.1088/1478-3975/1010/1086/065005. Epub 062013 Dec 065004.
27. S. K. Mitra and D. D. Schlaepfer, *Curr Opin Cell Biol*, 2006, **18**, 516-523.
28. S. K. Mitra, D. Mikolon, J. E. Molina, D. A. Hsia, D. A. Hanson, A. Chi, S. T. Lim, J. A. Bernard-Trifilo, D. Ilic, D. G. Stupack, D. A. Cheresch and D. D. Schlaepfer, *Oncogene*, 2006, **25**, 5969-5984.
29. A. A. Abdeen, J. Lee, Y. Li and K. A. Kilian, *Regen. Eng. Transl. Med.*, 2017, **3**, 10.
30. R. Meili, A. T. Sasaki and R. A. Firtel, *Nat Cell Biol*, 2005, **7**, 334-335.
31. M. S. Song, L. Salmena and P. P. Pandolfi, *Nat Rev Mol Cell Bio*, 2012, **13**, 283-296.
32. S. Zimmermann and K. Moelling, *Science*, 1999, **286**, 1741-1744.
33. F. G. Teixeira, M. M. Carvalho, N. Sousa and A. J. Salgado, *Cell Mol Life Sci*, 2013, **70**, 3871-3882.
34. S. H. Ranganath, O. Levy, M. S. Inamdar and J. M. Karp, *Cell Stem Cell*, 2012, **10**, 244-258.
35. D. Drago, C. Cossetti, N. Iraci, E. Gaude, G. Musco, A. Bachi and S. Pluchino, *Biochimie*, 2013, **95**, 2271-2285.
36. C. Gallina, V. Turinetto and C. Giachino, *Stem Cells Int*, 2015, **2015**, doi: 10.1155/2015/765846. Epub 762015 May 765845.
37. V. R. Burst, M. Gillis, F. Putsch, R. Herzog, J. H. Fischer, P. Heid, J. Muller-Ehmsen, K. Schenk, J. W. U. Fries, C. A. Baldamus and T. Benzing, *Nephron Exp Nephrol*, 2010, **114**, E107-E116.
38. M. Leiker, G. Suzuki, V. S. Iyer, J. M. Canty and T. Lee, *Cell Transplant*, 2008, **17**, 911-922.
39. E. J. Lee, H. W. Park, H. J. Jeon, H. S. Kim and M. S. Chang, *Regen Med*, 2013, **8**, 283-293.
40. R. A. Boomsma and D. L. Geenen, *Plos One*, 2012, **7**, e35685. doi: 35610.31371/journal.pone.0035685. Epub 0032012 Apr 0035625.
41. A. Hoeben, B. Landuyt, M. S. Highley, H. Wildiers, A. T. Van Oosterom and E. A. De Bruijn, *Pharmacol Rev*, 2004, **56**, 549-580.

## Supporting Information for:

### **Integrin $\beta$ 1 activation by micro-scale curvature promotes pro-angiogenic secretion of human mesenchymal stem cells**

Zhengdong Li, ‡<sup>ab</sup> Weiwei Wang, ‡<sup>a</sup> Xun Xu, ‡<sup>ab</sup> Karl Kratz,<sup>ac</sup> Jie Zou,<sup>ab</sup> Liudmila Lysyakova,<sup>ac</sup> Matthias Heuchel,<sup>a</sup> Andreas Kurtz,<sup>d</sup> Manfred Gossen,<sup>a</sup> Nan Ma<sup>\*abc</sup> and Andreas Lendlein<sup>\*abc</sup>

<sup>a</sup> Institute of Biomaterial Science and Berlin-Brandenburg Center for Regenerative Therapies, Helmholtz-Zentrum Geesthacht, Kantstraße 55, 14513 Teltow, Germany; E-mail: nan.ma@hzg.de, [andreas.lendlein@hzg.de](mailto:andreas.lendlein@hzg.de)

<sup>b</sup> Institute of Chemistry and Biochemistry, Freie Universität Berlin, Takustraße 3, 14195 Berlin, Germany

<sup>c</sup> Helmholtz Virtual Institute „Multifunctional Biomaterials for Medicine“, Kantstraße 55, 14513 Teltow, Germany

<sup>d</sup> Charité – University Medicine Berlin, Augustenburger Platz 1, 13353 Berlin, Germany

‡ These authors contributed equally to this work.

## Supporting methods

### **Supporting method S1: surface microscale roughness characterization via optical profilometry**

The microscale roughness of the insert bottom was determined with an optical profilometer type MicoProf 200 (FRT - Fries Research & Technologie GmbH, Bergisch Gladbach, Germany) equipped with a CWL 300 chromatic white-light sensor. A scan size

7 x 7 mm<sup>2</sup> was investigated for calculation of the arithmetic average roughness ( $R_a$ ). The data were acquired with the software AQUIRE (ver. 1.21) and evaluated with the software MARK III (ver. 3.9). The mean spacing between the peaks ( $S_m$ )-value was measured based on the obtained profilometry images. In brief, a mean line was first created and then the average value of the width of peaks at mean line was calculated. The side-view profile of the material surfaces was smoothed by a median filter to eliminate noise with abnormal amplitude.

### **Supporting method S2: nanotopography and local mechanical analysis by AFM investigations**

Surface nanotopography investigations were carried out using an atomic force microscope (AFM, MFP-3D, Asylum Research, Santa Barbara, CA, USA). AC-mode scanning was conducted with a silicon cantilever type OMCL-AC160TS-R3 (Olympus, Tokyo, Japan) having a spring constant of 9 N/m. For topographical analysis an area with a scan size of 2 x 2  $\mu\text{m}^2$  at three different locations of each sample was investigated in dry state at ambient temperature with a scan rate of 0.5 Hz. The arithmetic average roughness ( $R_a$ ) of each image was obtained by the commercial software Igor Pro 6.22A and the mean  $R_a$  value and the respective standard deviation were calculated from these results.

Nanoindentation measurements were conducted with same instrument (MFP-3D Bio-AFM, Asylum Research, Santa Barbara, CA, USA) in the dry state at ambient conditions. The used indenter, chosen from the NanoIndenter module (Asylum Research, Santa Barbara, CA, USA), was a standard diamond Berkovich-tip with a spring constant  $k = 488$  N/m, Poisson's ratio of  $\nu_{\text{ind}} = 0.2$  and Young's modulus of  $E_{\text{indenter}} = 865$  GPa. For each sample up to 100 single indents were recorded within the whole area of a sample, supported by up to three 64-indent arrays (force maps) in a quadratic area of 90 x 90  $\mu\text{m}^2$  with an indentation/scan rate of 0.1 Hz and a trigger force of 100  $\mu\text{N}$ . The Young's modulus was calculated by the Oliver-Pharr model [1] in a range from 20% to 90% at the force-distance curve. To determine the mean values, statistical distributions of Young's moduli were fitted using a Gaussian function. Correspondingly, the error bars are represented by the distribution half width. For rough samples (PS-160 and PS-320) the

local mechanics were solely analyzed on the “hills” of the microstructures, where an orthogonal indentation can be expected. The calculated mean values of the Young’s modulus are listed in Table S1.

### **Supporting method S3: cell proliferation assay**

$1.0 \times 10^4$  hADSCs were seeded into each insert and the culture medium was changed every 3 days. The number of cells at different time points was determined using a Cell Counting Kit-8 (CCK-8, Dojindo Molecular Technologies, Munich, Germany). In brief, for each insert the old medium was replaced with 300  $\mu$ l of fresh medium, followed by adding 30  $\mu$ l of CCK-8 solution. After 3 h of incubation at 37 °C, 100  $\mu$ l of medium/CCK-8 mixture were transferred from each insert into a transparent 96-well tissue culture plate, and the absorbance was measured at a wavelength of 450 nm and a reference wavelength of 650 nm using a microplate reader (Infinite 200 PRO, Tecan Group Ltd., Männedorf, Switzerland). A standard curve, which was generated by measuring the absorbance of a series of samples with known cell numbers, was used to calculate the number of hADSCs in the inserts.

### **Supporting method S4: cell active integrin and pFAK immunofluorescence staining**

After 4 days and 14 days, the cells were fixed with 4% (w/v) paraformaldehyde for 20 minutes, permeabilized with 0.1% (w/v) Triton X-100 for 10 minutes and blocked with 1% (w/v) BSA for 30 minutes. Active integrin  $\beta$ 1 was stained with monoclonal mouse anti-human integrin beta-1 antibody (HUTS-4, Millipore, Darmstadt, Germany) and Alexa Fluor® 488 labeled IgG antibody (Life Technologies, Darmstadt, Germany). pFAK was stained with rabbit anti human phospho-FAK(Y397) antibody (Cell Signaling Technology, MA, USA) and Alexa Fluor® 488 labeled IgG antibody (Life Technologies, Darmstadt, Germany). F-actin was stained with Alexa Fluor® 555 Phalloidin (Life Technologies, Darmstadt, Germany). The cell nuclei were stained with Hoechst 33342 (NucBlue® Live Reagent, Life Technologies, Darmstadt, Germany). After staining, the samples were scanned with a confocal laser scanning microscope (LSM 780, Carl Zeiss, Jena, Germany) and the images were processed with ZEN 2012 software (Carl Zeiss, Jena, Germany).

### **Supporting method S5: Western blotting**

Cell lysates from the hADSCs at day 4 and day 14 were prepared with RIPA buffer (Sigma-Aldrich, St. Louis, MO, USA) supplemented with phenylmethylsulfonyl fluoride (Life Technologies, Darmstadt, Germany) and Protease Inhibitor Cocktails (Sigma-Aldrich, St. Louis, MO, USA). After centrifugation, the supernatant of cell lysates was stored at -80 °C. To quantify the integrin and FAK expression, the protein solutions were denatured by heating at 95 °C for 5 minutes, separated by electrophoresis on 4–20% Mini-PROTEAN® TGX™ Precast Protein Gels (Bio-Rad, München, Germany) and then transferred onto nitrocellulose membranes (Millipore, Darmstadt, Germany). The blots were probed with monoclonal primary antibodies (mouse anti-human integrin beta-1 antibody (HUTS-4, Millipore, Darmstadt, Germany), rabbit anti human total integrin beta-1 antibody (Abcam, Cambridge, UK) or mouse anti human FAK antibody and rabbit anti human phosphor-FAK(Y397) antibody (Cell Signaling Technology, MA, USA)) and the IRDye 680LT and IRDye 800CW secondary antibodies (Li-Cor, Bad Homburg, Germany). Fluorescent signal were then detected using an Odyssey Imaging scanner and the intensity was analyzed by image studio software (Li-Cor, Bad Homburg, Germany).

### **Supporting method S6: model-based analysis of regulation of micro-roughness on hADSCs**

To investigate the complex relation between surface roughness, local curvature, and cell development, the optical profilometry experiments on the PS surface samples PS-160 and PS-320 were further analyzed. Fig. S6A and S6B show typical examples for 3D height profiles for samples PS-160 and PS-320 over a base area of  $1000 \times 1000 \mu\text{m}^2$ . To determine local surface area values, the base area was divided into  $5 \times 5$  partitions of  $200 \times 200 \mu\text{m}^2$ , indicated by the black grids. The 3D height profile of the central partition of the grid (marked in green) is presented enlarged in Fig. S6C for the PS-160, and in Fig. S6D for the PS-320 sample. Image analysis determines for the PS-160 partition a surface area  $A$  of  $47085 \mu\text{m}^2$  and for the PS-320 partition a significant larger value of  $129400 \mu\text{m}^2$ . These values should be set in ratio to the surface  $A_0$  of the respective base area ( $40000 \mu\text{m}^2$ ). A larger local surface area is a result of extent and spatial distribution of local curvature effects. Therefore, the ratio  $A/A_0$  can be used as a (spatial averaged) estimate



of surface curvature. For the two partitions, values of the surface area ratio  $S_{AR} = A/A_0$  of 1.18 and 3.24 are obtained. Assuming half spherical valleys as local surface structure with  $A = 4\pi r^2/2$  and  $A_0 = \pi r^2$  a ratio of  $S_{AR} = 2.0$  would result as “curvature measure”. On the other side a flat surface would be characterized by  $S_{AR} = 1.0$ . The sample PS-160 with  $S_{AR} = 1.18$  shows in the 3D profile Fig. S6C a hilly and well curved structure and is characterized by maximum roughness depth values of about 35  $\mu\text{m}$ . The rougher PS-320 surface (Fig. S6D) with  $S_{AR} = 3.24$  shows a canyon structure with plateaus and deeply incised valleys (profile depth about 190  $\mu\text{m}$ ). Here the flat walls of both sides of the valleys contribute significantly to the high local surface area, but not to a curvature of the surface. From the presented image analysis, one can conclude that  $S_{AR}$  values between 1.10 and 2.0 should characterize well curved surfaces in the respective surface level. The lower value was chosen to distinguish from “real” flat surfaces, which show always some small roughness. Assuming a diameter of 100  $\mu\text{m}$  for the living cells, the selected base areas with a side length of 200  $\mu\text{m}$  are in the same size level as the cells, because a respective square could accommodate up to 4 or 5 cells. So, finally one can use the  $S_{AR}$  parameter to estimate the extent of surface regions of a sample, where an optimal curvature for cell growing can be expected. Fig. S6E and S6F show for the two polymer samples PS-160 and PS-320 the 2D distribution of  $S_{AR}$  values over the 25 partition of the grid over the 3D height profiles of Fig. S6A and S6B. The PS-160 sample (Fig. S6E) contains extended regions of “optimal”  $S_{AR}$  values, indicated in green. They are surrounded by more or less flat regions with only low surface curvature ( $S_{AR} < 1.1$ ). The PS-320 sample (Fig. S6F) shows a significantly smaller proportion of “green region”, i.e. optimal for cell growth. The surface of the PS-320 sample is dominated through the central canyon region with a high surface area ratio,  $S_{AR} > 2.0$ , indicated in light gray, and two “flat” regions ( $S_{AR} < 1.1$ ), which are also significant in extension.

## Supporting tables, figures and legends

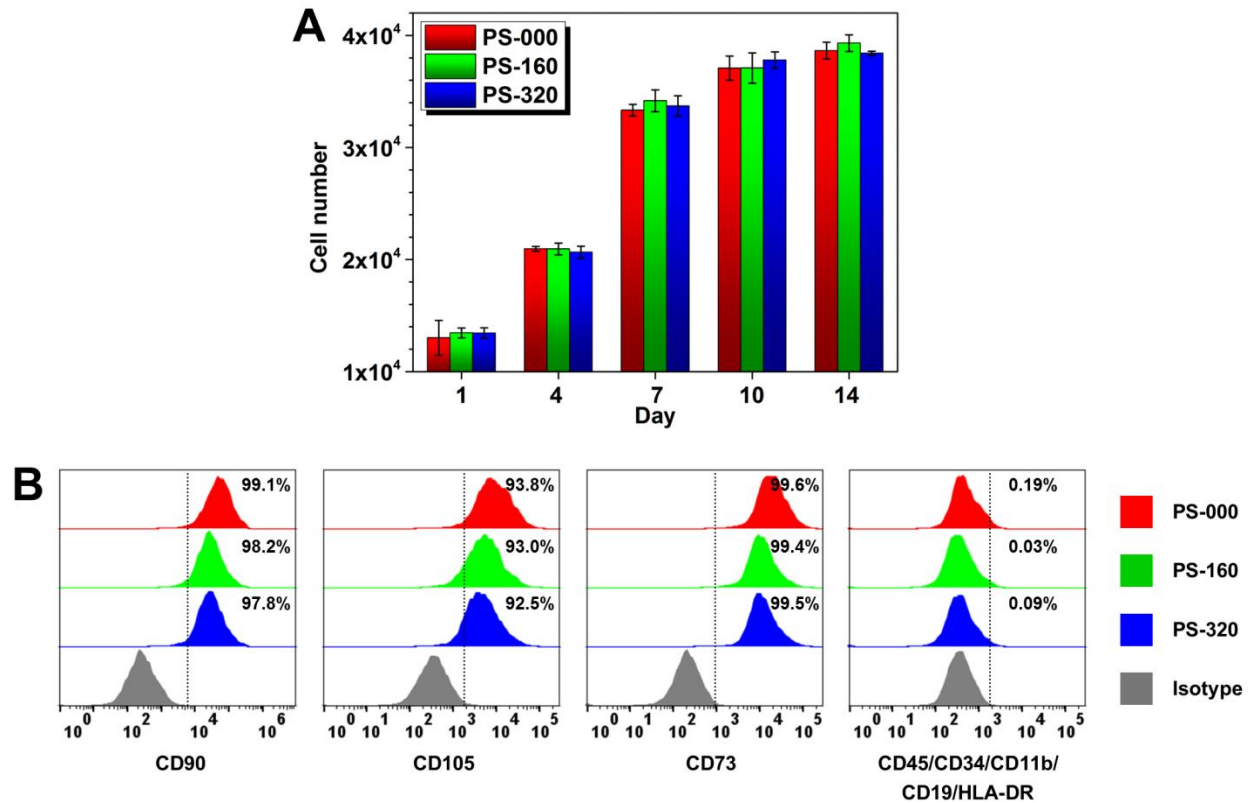
### Supporting Table S1. Surface roughness and local mechanics characterization

Sample ID	Micro-roughness <sup>a)</sup>		Nano-roughness <sup>b)</sup>	Local mechanics <sup>c)</sup>
	R <sub>a</sub> (μm)	S <sub>m</sub> (μm)	R <sub>a</sub> (nm)	Young's modulus (GPa)
PS-000	0.13 ± 0.07	/	2.6 ± 0.8	31 ± 2
PS-160	4.17 ± 0.17	164 ± 16	12.0 ± 4.3	30 ± 5
PS-320	25.4 ± 3.8	316 ± 36	7.2 ± 0.4	29 ± 2

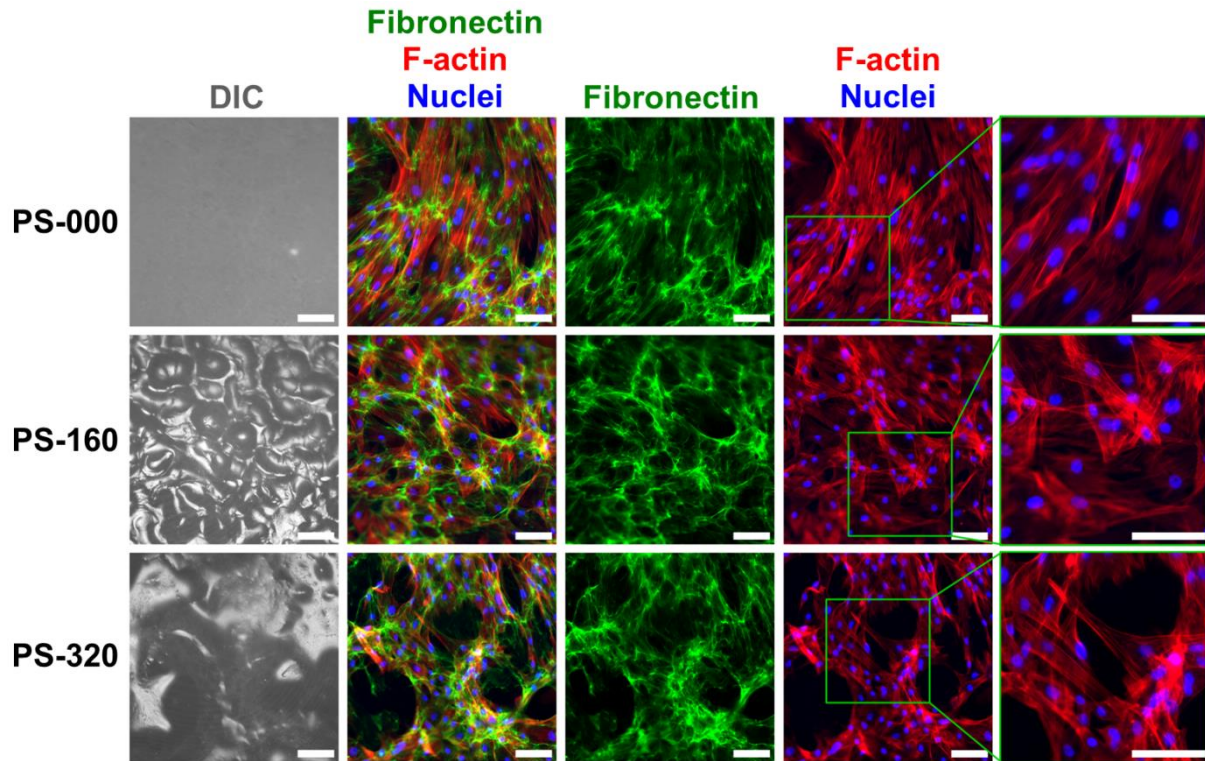
a) Optical profilometry measurement by scanning an area of 7 × 7 mm<sup>2</sup>.

b) Atomic force microscopy experiments with a scan size of 2 × 2 μm<sup>2</sup>.

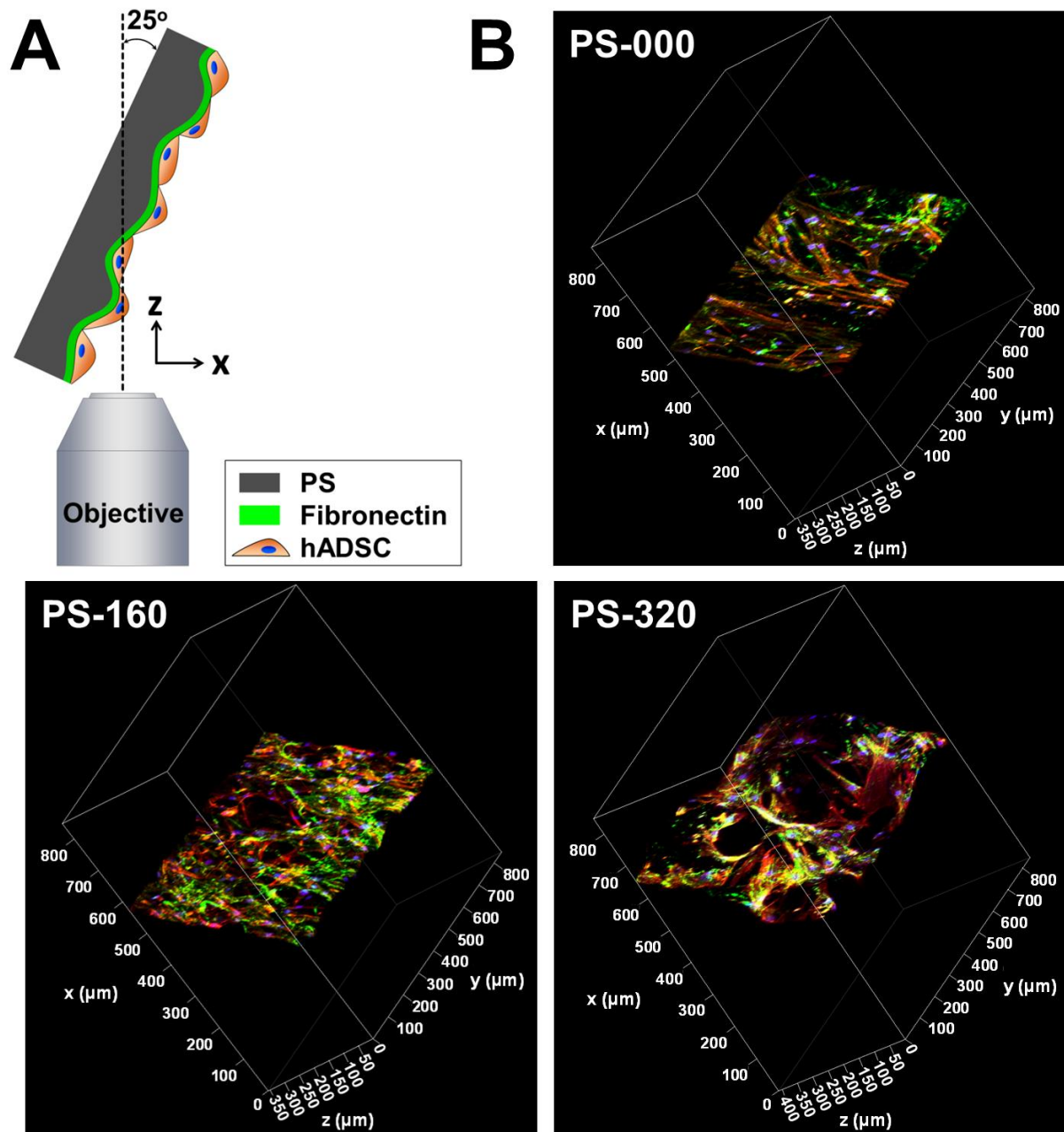
c) AFM nanoindentation experiments.



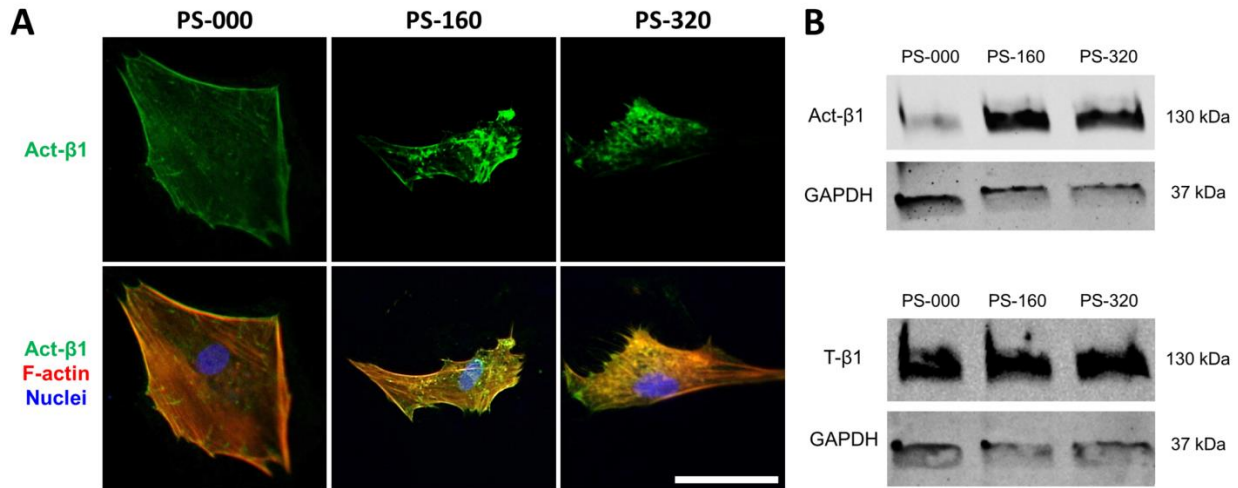
**Supporting Fig. S1.** Micro-scale surface roughness did not alter hADSC surface markers and proliferation. (A) hADSCs growing on different surfaces exhibited the similar proliferation rate ( $n = 3$ ). (B) The phenotypic markers of MSCs (CD90, CD105 and CD73) were preserved, and the non-MSC markers (CD45, CD34, CD11b, CD19 and HLA-DR) were negative after 14 days of culture on different surfaces.



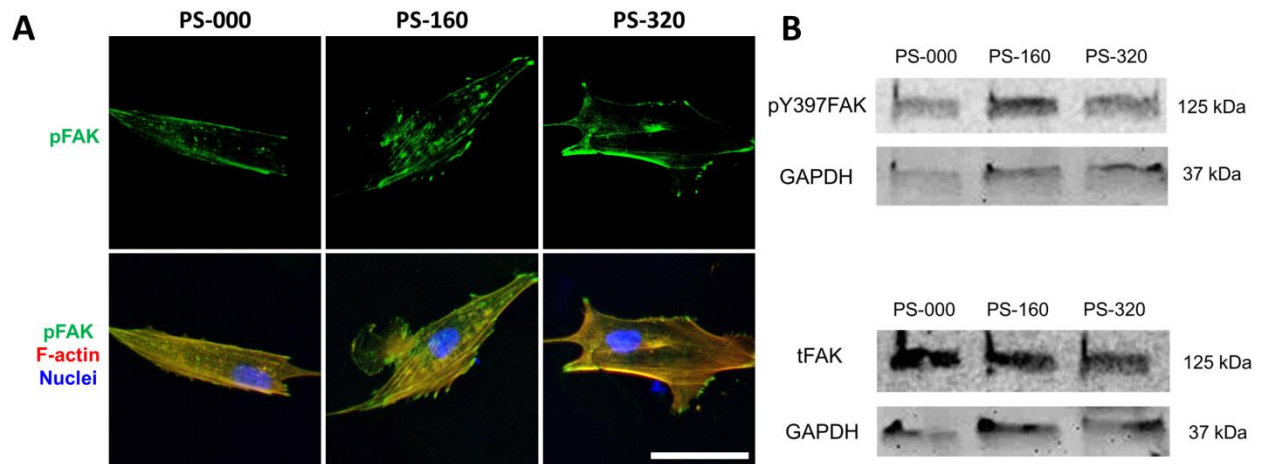
**Supporting Fig. S2.** The morphology of hADSCs and fibronectin remodeling were influenced by micro-scale roughness. The cells were cultured on fibronectin-coated surfaces followed by fluorescence staining after 4 days of culture to detect the actin cytoskeleton (red), nuclei (blue) and fibronectin (green) using a confocal laser scanning microscope (bar = 100  $\mu\text{m}$ ).



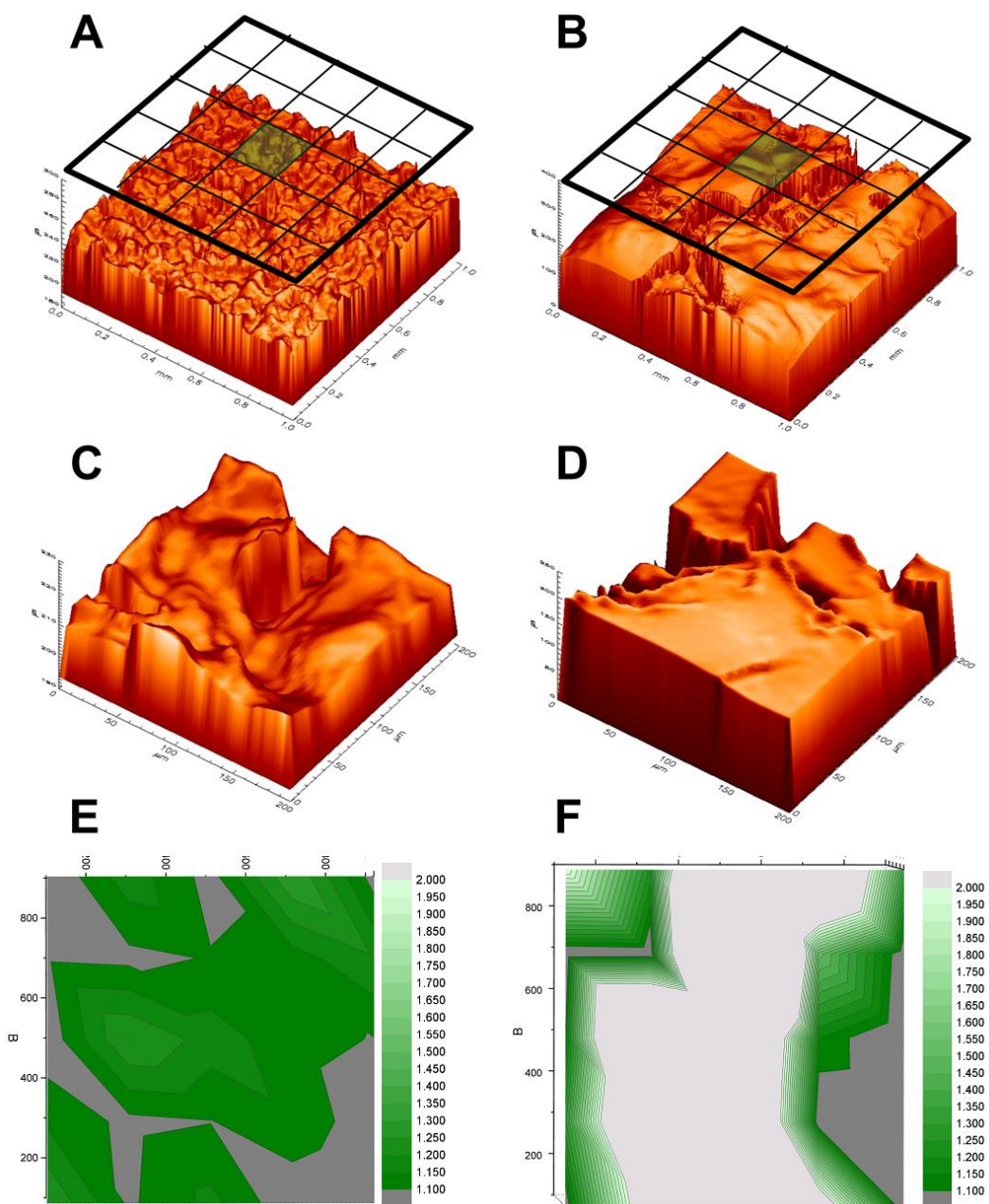
**Supporting Fig. S3.** 3D reconstruction of tilted-view images of hADSCs cultured on surfaces with different micro-roughness. (A) The scanning was performed by tilting the samples to make a 25° angle between the optical axis of the objective and the material surface. (B) The 3D reconstruction images demonstrated the dominant effect of surface roughness on topography of the cell layers (F-actin: red; nuclei: blue; fibronectin: green).



**Supporting Fig. S4.** Activated and total  $\beta$ 1 integrin expression level of hADSCs cultured on different substrates for 4 days: (A) Immunostaining of activated  $\beta$ 1 integrin (green) F-actin (red) and cell nuclei (blue) (bar = 50  $\mu$ m); (B) Representative images of Western blot analysis of activated and total  $\beta$ 1 integrin of hADSCs on different substrates.



**Supporting Fig. S5.** Level of phosphorylated FAK in hADSCs cultured on different substrates for 14 days: (A) Immunostaining of phosphorylated FAK (green) F-actin (red) and cell nuclei (blue) (bar = 50  $\mu$ m); (B) Representative images of Western blot analysis of phosphorylated FAK at Y397 and total FAK.



**Supporting Fig. S6.** Model-based analysis of the optical topography measuring data for the two polymer samples PS-160 (left) and PS-320 (right). 3D height profiles over a base area of  $1000 \times 1000 \mu\text{m}^2$  for samples PS-160 (A) and PS-320 (B). To access local surface area values, the base area was divided into  $5 \times 5$  partitions of  $200 \times 200 \mu\text{m}^2$ , indicated by the black grid. 3D height profile of the central partition of the grid (marked in green) is enlarged for PS-160 (C) and PS-320 (D). The 2D distribution of the surface area ratio

parameter  $S_{AR} = A/A_0$ , calculated for the 25 partitions of the grid over the surface, are presented for samples PS-160 (E) and PS-320 (F).

## **Supporting references**

[1] W.C. Oliver and G.M. Pharr, Measurement of Hardness and Elastic Modulus by Instrumented Indentation: Advances in Understanding and Refinements to Methodology, *Journal of Materials Research* 2004;19:13-20.

[2] Xu X, Wang WW, Kratz K, Fang L, Li ZD, Kurtz A, et al. Controlling Major Cellular Processes of Human Mesenchymal Stem Cells using Microwell Structures. *Adv Healthc Mater.* 2014;3:1991-2003.



## Chapter III

### **Modulation of the mesenchymal stem cell migration capacity via preconditioning with topographic microstructure**

**Clinical Hemorheology and Microcirculation. 2017;67(3-4):267-278.**

<https://doi.org/10.3233/CH-179208>

# **Modulation of the mesenchymal stem cell migration capacity via preconditioning with topographic microstructure**

Zhengdong Li <sup>1,2</sup>, Xun Xu <sup>1,2</sup>, Weiwei Wang <sup>1</sup>, Karl Kratz <sup>1,4</sup>, Xianlei Sun <sup>1,3</sup>, Jie Zou <sup>1,2</sup>, Zijun Deng <sup>1</sup>, Friedrich Jung<sup>1,4</sup>, Manfred Gossen <sup>1,4</sup>, Nan Ma <sup>1,2,4,\*</sup> and Andreas Lendlein <sup>1,2,3,4,\*</sup>

<sup>1</sup> Institute of Biomaterial Science and Berlin-Brandenburg Center for Regenerative Therapies, Helmholtz-Zentrum Geesthacht, Kantstraße 55, 14513 Teltow, Germany

<sup>2</sup> Institute of Chemistry and Biochemistry, Freie Universität Berlin, Takustraße 3, 14195 Berlin, Germany

<sup>3</sup> Institute of Biochemistry and Biology, Universität Potsdam, Am Neuen Palais 10, 14469 Potsdam, Germany

<sup>4</sup> Helmholtz Virtual Institute “Multifunctional Materials in Medicine”, Kantstraße 55, 14513 Teltow, Germany

\* To whom correspondence should be addressed:

Prof. Dr. Nan Ma, Prof. Dr. Andreas Lendlein

Email: nan.ma@hzg.de, andreas.lendlein@hzg.de

Phone: +49 (0)3328 352-235

Fax: +49 (0)3328 352-452

## Abstract

Controlling mesenchymal stem cells (MSCs) behavior is necessary to fully exploit their therapeutic potential. Various approaches are employed to effectively influence the migration capacity of MSCs. Here, topographic microstructures with different microscale roughness were created on polystyrene (PS) culture vessel surfaces as a feasible physical preconditioning strategy to modulate MSC migration. By analyzing trajectories of cells migrating after reseeding, we demonstrated that mobilization velocity of human adipose derived mesenchymal stem cells (hADSCs) could be promoted and persisted by brief preconditioning with the appropriate microtopography. Moreover, the elevated activation levels of focal adhesion kinase (FAK) and mitogen-activated protein kinase (MAPK) in hADSCs were also observed during and after preconditioning process. These findings underline the potential enhancement of *in vivo* therapeutic efficacy in regenerative medicine via transplantation of topographic microstructure preconditioned stem cells.

**Key words:** Mesenchymal stem cells, Precondition, Microstructure, Migration, FAK-MAPK

## 1 Introduction

Mesenchymal stem cells (MSCs) have been considered as a promising cell source for cell transplantation and tissue engineering [1-3]. The improvement of MSCs migration capacity *in vivo* towards the damaged tissue such as the infarcted myocardium is one of the major challenges in stem cell therapy [4-7]. An *in vivo* study with a rat myocardial infarction model revealed that merely 1% of MSCs injected systemically can reach the ischemic myocardial area [8]. Further, since MSCs were also not able to preserve a long lifespan after transplantation [9, 10], the beneficial effects from transplanted MSCs may mainly attribute to the rapid targeting to the site of injury. Thus, cell migration to the lesion site remains the lingering problem in MSCs-based therapies. It is of great benefit to enhance the MSCs migration capacity prior to their transplantation.

Several biochemical approaches have been developed to promote MSC migration. For instance, Short-term exposure of MSCs to hypoxia and pretreating MSCs with cytokines and growth factors such as IL-6 and HGF could upregulate the expression of chemokine receptors and therefore promote the MSC migration [11-13]. Besides, overexpression of chemokine receptors such as CXCR4 on MSC surfaces via genetic engineering can also efficiently enhance the migration capacity and result in an improved recovery of myocardial infarction [14]. However, genetically modified MSCs may not yet be feasible for therapeutic applications in terms of safety issues. Therefore, preconditioning of MSCs with biochemical factors is currently widely applied in regulating cell migration capacity.

It is particularly attractive to induce and modulate MSCs migration without introducing artificial biochemical factors through the physical, especially mechanical properties, of biomaterials. From this point of view, modification of wettability [15] and rigidity [16, 17] of materials has been reported to influence the cell motility. Moreover, it was demonstrated that cells could reach their maximum migration capacity when treated with optimal mechanical cues [18-21]. As a natural topography of extracellular matrix, material surface with nanoscale roughness has been described as a strong modulator in regulating cell migration [22, 23]. Materials with microscale surface roughness were demonstrated in regulating cell adhesion, proliferation and differentiation [24, 25]. One up-to-date study indicated that the proper level of microscale roughness could alter the osteoblast migration speed [26]. Meanwhile, polymeric material with the advantage of tailorable physical and mechanical properties provides broad platform to study the cell-material interactions. Strategies such as surface structures manipulating [27] and protein patterning [28] on polymeric materials were demonstrated to induce specific effects on cells. Thus, it is of great interest to study the influence of polymeric materials with surface microscale structures on the migration capacity of MSCs.

Focusing on the interface between cell and material surface, integrin, as the cell transmembrane receptor, is responsible for sensing and translating external mechanical signal into cellular biochemical information [29, 30]. Intracellularly, integrin interacts with focal adhesion kinase (FAK) via the cytoskeletal protein talin [31]. FAK has been demonstrated to play a key role in cell migration [32, 33]. Furthermore, FAK activation is

connected to mitogen-activated protein kinase (MAPK) cascade [34]. Thus, it is of great interest to study the effects of topographic microstructures on stem cell migration capacity and the activity of FAK and MAPK, which may reveal the underlying mechanism and present a safe and robust approach to increase the therapeutic efficacy of MSCs in regenerative medicine. Here, we hypothesize that microscale surface roughness could influence the stem cell migration capacity through the activities of FAK and MAPK.

To test our hypothesis, polystyrene (PS) cell culture inserts with topographic microstructures defined in three distinct roughness levels (R0, R1 and R2) on the bottom surfaces were fabricated to explore the effects of microstructures on the migration capacity of human adipose-derived mesenchymal stem cells (hADSCs). The morphology and focal adhesion (FA) of hADSCs were observed. The influence of microstructure on migration capacity was evaluated *in vitro* using time-lapse and gap closure assays. Furthermore, the activation of FAK and MAPK in response to topographic microstructures was extensively investigated.

## **2 Materials and methods**

### **2.1 Cell culture surfaces**

As described before [35], polystyrene inserts with different microstructures on the bottom were manufactured by injection moulding. The prepared inserts were sterilized using gas sterilization. The roughness level of the insert bottom with different microstructures was determined as previously described [36]. In brief, optical profilometer (MicoProf 200, FRT - Fries Research & Technologie GmbH, Bergisch Gladbach, Germany) equipped with a CWL 300 chromatic white-light sensor was used to measure the level of root mean square roughness (Rq). The data were acquired with the software AQUIRE (ver. 1.21) and were evaluated with the software MARK III (ver. 3.9). To enhance the cell adhesion, the bottom surfaces of the prepared inserts were coated with 300  $\mu$ l of human fibronectin solution (10 $\mu$ g/ml in PBS, Sigma-Aldrich, St. Louis, MO, USA) was coated and incubated at 37 °C for 1 h.

## 2.2 Cell cultivation

hADSCs isolated from human adipose tissue were positively expressed phenotype markers CD90, CD105 and CD73 [37]. The adipose tissue was obtained by abdominal liposuction from a female donor after informed consent (No.: EA2/127/07; Ethics Committee of the Charité - Universitätsmedizin Berlin, approval from 17.10.2008). The isolated hADSCs were cultured in the human adipose-derived stem cell medium (ADSC™ growth medium, Lonza, Walkersville, MD, USA) at 37 °C in a humidified atmosphere containing 5% CO<sub>2</sub>.

## 2.3 Migration assay

### 2.3.1 Gap closure assay

A 24-well wound healing assay plate (CytoSelect™ 24-Well wound healing assay plate, Cell Biolabs. INC, San Diego, USA) was used to assess cell migration according to manufacturer's instructions (Fig. 1). In brief, hADSCs cultured on surfaces with different microstructures for 2 days to 14 days were collected and then reseeded in the 24-well wound healing assay plate at a density of  $3 \times 10^4$  cells per cm<sup>2</sup>. After overnight adhesion, the gap was created by removing the baffle in the central of the well, images of gaps at each time point were taken with a digital camera connected to a phase-contrast Olympus microscope (IX81 motorized inverted microscope, Olympus, Hamburg, Germany,  $\times 10$  objective). The same visual field was marked and used throughout the experiment. The area of wound gap was measured by Image-Pro Plus software with the wound healing tool (Media Cybernetics, Inc. Rockville, USA). Gap closure (%) =  $[\text{Gap area } (T_0 - T) / \text{Gap area } T_0] \times 100\%$  (where T is the image taking time and T<sub>0</sub> is the time that the gap was initiated).

### 2.3.2 Time-Lapse Microscopy

The migration of surface microstructures preconditioned cells was tracked using the phase contrast time-lapse imaging microscope (IX81 motorized inverted microscope, Olympus, Hamburg, Germany) combined with a bold line cage incubator providing a humidified atmosphere (37 °C, 5% CO<sub>2</sub>) (Fig. 1). Briefly, suspended cells collected from the different surfaces were reseeded in the 24 well TCP at a density of  $3 \times 10^4$  cells per

cm<sup>2</sup>. After overnight adhesion, cells were observed and recorded every 10 minutes for 20 h. The images were processed using ImageJ software (National Institutes of Health, USA) combined with the software plug-ins “manual tracking” and “chemotaxis and migration tool” (ibidi GmbH, Martinsried, Germany) to calculate the migration parameters.

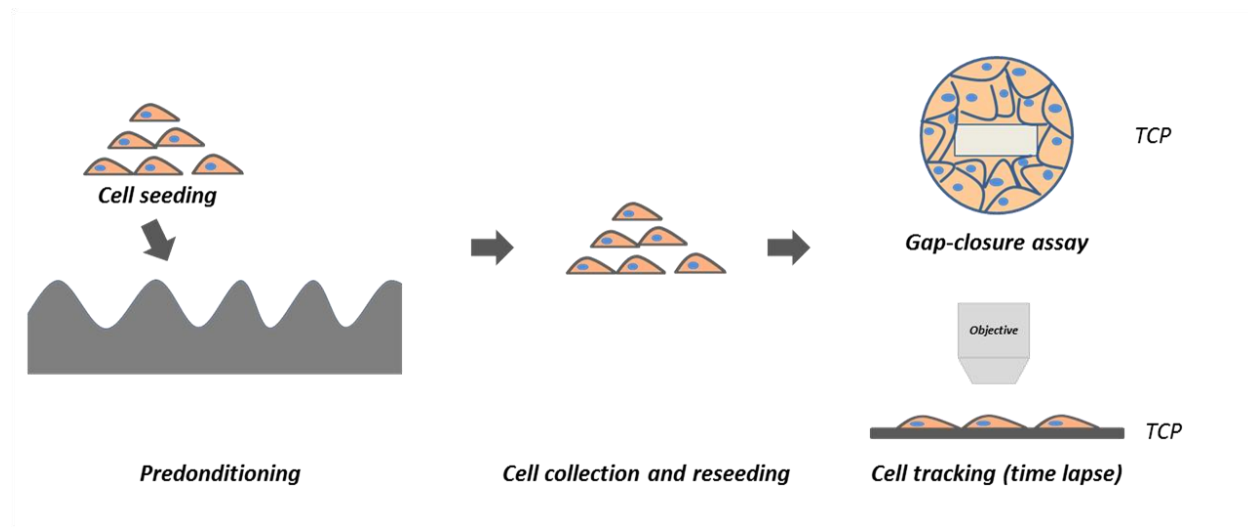


*Fig. 1. Schematic diagram of the methods for investigating migration capacity of microtopography preconditioned hADSCs.*

## 2.4 Immunocytochemistry

The hADSCs cultured on different surfaces or reseeded in TCP for overnight were fixed by adding 4% (w/v) paraformaldehyde (Sigma-Aldrich, St. Louis, MO, USA) for 15 minutes and then permeabilized with 0.1% (w/v) Triton X-100 (Sigma-Aldrich, St. Louis, MO, USA) for 5 minutes. After blocking with 3% (w/v) bovine serum albumin (BSA) (Sigma-Aldrich, St. Louis, MO, USA) solution for 30 minutes, the vinculin was stained with mouse anti-human primary antibodies (mouse anti-human vinculin monoclonal antibody (Merck Millipore, Darmstadt, Germany) and the Alexa Fluor® 488 labeled anti-mouse IgG antibody (Life Technologies, Darmstadt, Germany); F-actin was stained with Alexa Fluor® 555 conjugated Phalloidin (Life Technologies, Darmstadt, Germany); the nuclei were stained with Hoechst 33342 (NucBlue® Live Reagent, Life Technologies, Darmstadt, Germany). After washing with PBS, the samples were scanned with a confocal laser scanning microscope (LSM 780, Carl Zeiss, Jena, Germany).

## **2.5 Protein extraction**

Cell lysates from hADSCs preconditioned on the microstructure for 14 days before and after overnight reseeding were prepared with RIPA buffer (Sigma-Aldrich, St. Louis, MO, USA) supplemented with phenylmethylsulfonyl fluoride (Life Technologies, Darmstadt, Germany) and protease inhibitor cocktails (Sigma-Aldrich, St. Louis, MO, USA). After centrifugation, the supernatant of cell lysates was stored at -80 °C for further analysis.

## **2.6 Enzyme-linked immunosorbent assay (ELISA)**

The expression levels of phosphorylated FAK (pFAK) were quantified by ELISA. The concentration of pFAK in the cell protein solutions were measured using the pFAK (Tyr397) ELISA kits (Life Technologies, Darmstadt, Germany). The total amount of protein in the cell extract was determined using a BCA protein assay kit (Thermo Fisher Scientific, Bonn, Germany), and used to normalize the expression levels of the proteins of interest.

## **2.7 Western blotting**

To quantify the protein expression, the obtained protein solutions were denatured by heating at 95 °C for 5 minutes, separated by electrophoresis on 10% (v/v) SDS-PAGE and then transferred onto nitrocellulose membranes (Millipore, Darmstadt, Germany). The blots were probed with monoclonal primary antibodies (rabbit anti human MAPK, mouse anti human phospho-MAPK (Thr202, Tyr204), Millipore, Darmstadt, Germany) and the IRDye 680LT and IRDye 800CW secondary antibodies (Li-Cor, Bad Homburg, Germany). Fluorescent signal were then detected using an Odyssey Imaging scanner and the intensity was analyzed by image studio software (Li-Cor, Bad Homburg, Germany).

## **2.8 Statistics**

Experiments were repeated more than three times. For each experiment, cells from the female candidate were used between passage 3 to passage 5; 8 polystyrene inserts in



each roughness level (24 inserts in three roughness levels) were used to collect the cell or protein samples. Data are shown as mean  $\pm$  standard deviation. Statistical analysis was performed using the two-tailed independent-samples t-test, and a significance level (Sig.)  $< 0.05$  was considered to be statistically significant.

### **3 Results**

#### **3.1 Surface characterization of polymer substrates**

The topographic microstructures on the insert bottom were determined via optical profilometry. As previously described, R0 has a relatively plane surface with a  $R_q$  value of  $0.12 \pm 0.04 \mu\text{m}$ , while R1 and R2 have rougher surfaces (R1:  $3.52 \pm 0.26 \mu\text{m}$  and R2:  $16.04 \pm 1.24 \mu\text{m}$ ) [35].

#### **3.2 Migration of microtopography preconditioned hADSCs**

The surface microstructures preconditioned cells were reseeded in a wound healing assay plate to perform the gap closure assay. The surface R1 and R2 preconditioned cells could rapidly narrow down the gap when compared to the flat R0 surface preconditioned cells. The gap closure percentage of the cells from R1 surface after 7 days preconditioning was significantly higher than the cells from flat surface R0 (Fig. 2A, B). To further confirm our findings, the time-lapse microscope was used to track the cell migration and quantify the migration velocity. The results strengthened the findings from the gap closure assay. Surface R1 preconditioned cells had a higher velocity than the cells from the other two surfaces. After 4 days preconditioning with different topographic microstructured surfaces, remarkable differences in velocity of hADSCs were observed (Fig. 2C, D).

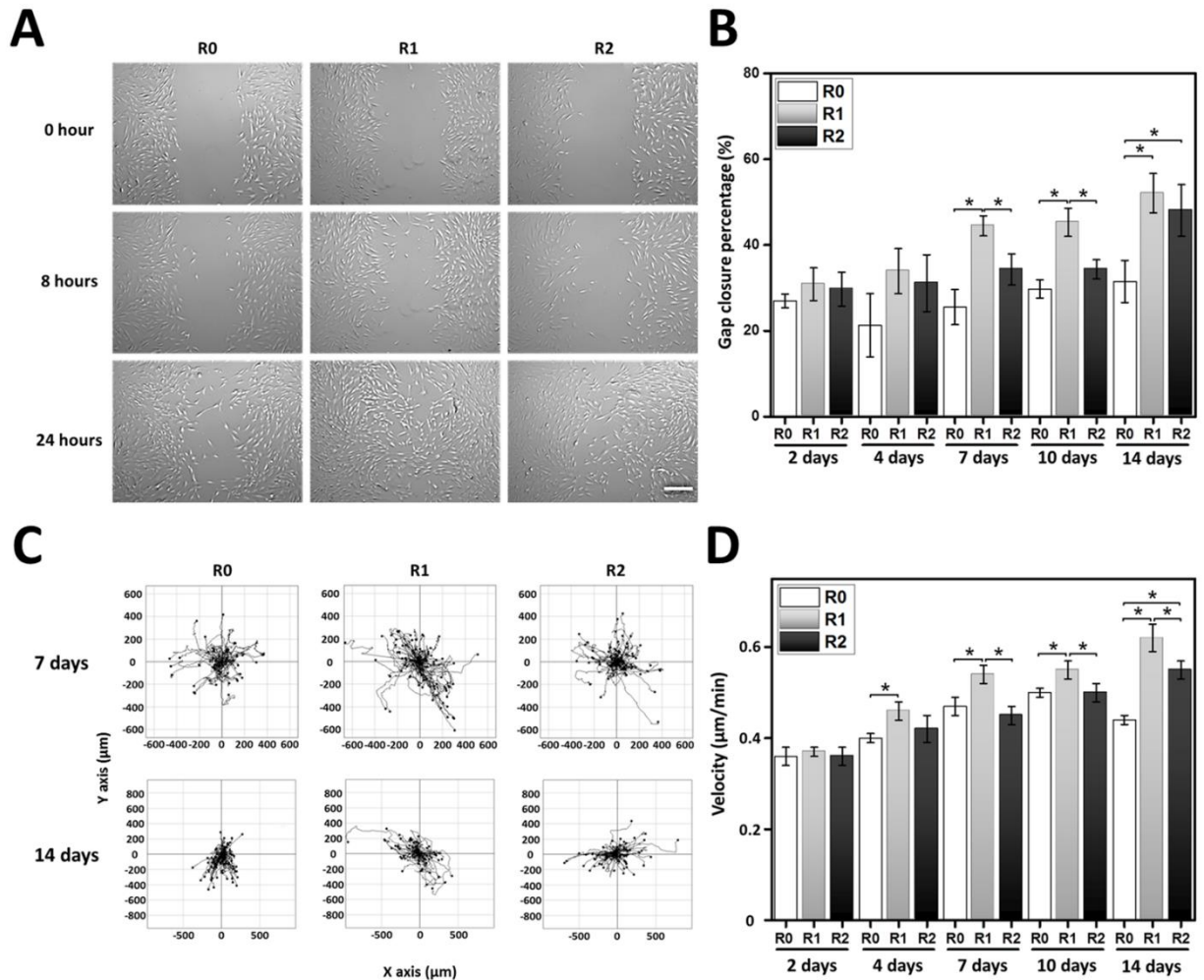


*Fig. 2. Enhanced migration capacity of hADSC via surface microtopography preconditioning. (A) Representative images showed the gap closure of hADSCs preconditioned for 7 days by different surface microstructures (bar = 500 µm). (B) The percentages of gap closure were quantified by Image-Pro Plus software (n = 5; \*Sig < 0.05). The hADSCs, preconditioned on different surfaces were reseeded on tissue culture plates up to 20 h and tracked to generate the migration trajectories (C) and to calculate the migration velocity (D)(n≥50; Mean ± standard error of the mean (SEM); \*Sig < 0.05).*

### 3.3 Focal adhesion of microtopography preconditioned hADSCs

Focal adhesion related components were investigated to study the cell-material interaction. The focal adhesion complex formation was examined by immunofluorescent staining of vinculin and F-actin. After 4 days of cultivation, hADSCs on R1 and R2

surfaces formed smaller and more aggregated focal adhesions than those on flat R0 surface (Fig. 3A). The 4 days preconditioned cells were reseeded on TCP, after overnight adhesion, the cells from R1 and R2 surfaces had more focal adhesions at the edges (Fig. 3B).

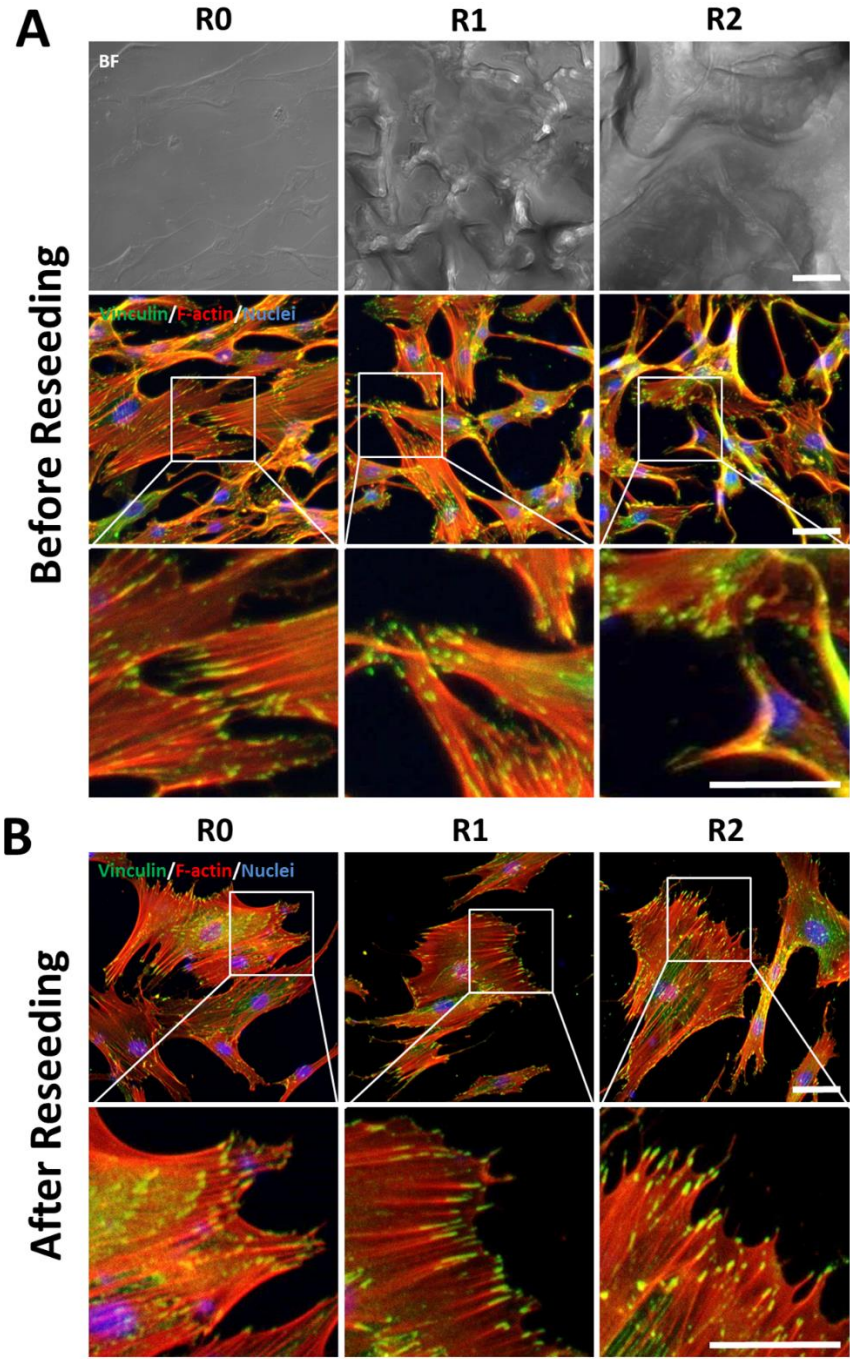


Fig. 3. Focal adhesion alteration in appearance and amount of hADSCs via different topographic microstructures during and after preconditioning (BF: bright field). Representative laser scanning confocal microscopic images are shown: At day 4, the formation of focal adhesion and organization of F-actin cytoskeleton in hADSCs grown on three distinct surfaces (A) and after reseeding on TCP (B) (red: F-actin; green: vinculin; blue: nuclei; bar = 50  $\mu$ m).

### 3.4 FAK activation level of microtopography preconditioned hADSCs

After 4 days precondition, the pTyr397 FAK was significantly higher in R1 group, and this elevated FAK phosphorylation level was maintained for up to 14 days (Fig. 4A). Further, after reseeding on TCP, a significantly increased FAK phosphorylation level of the cells from R1 surface was observed compared to the cells from R0 and R2 surfaces (Fig. 4B).

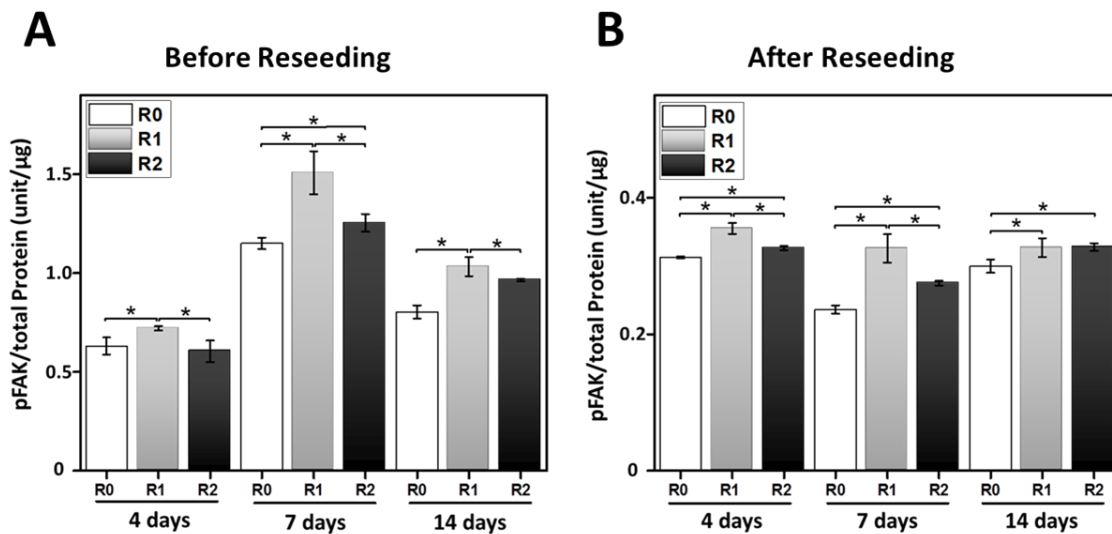


Fig. 4. Activation levels of FAK of hADSCs during and after preconditioning. (B) The normalized FAK phosphorylation levels of hADSCs harvested directly from microscale roughness surfaces at day 4, 7 and 14 (B) and roughness pretreated cells post 24 h reseeding (C) ( $n = 3$ ; \*Sig < 0.05).

### 3.5 MAPK phosphorylation level of microtopography preconditioned hADSCs

Protein blotting was performed to evaluate the expression and activation of MAPK in 14 days surface microtopography preconditioned hADSCs before (Fig. 5A) and after reseeding (Fig. 5B). It was found that the ratio of phosphorylated MAPK to total MAPK was significantly higher in hADSCs grown on microtopographic surfaces R1 and R2 compared to that on flat surface R0 (Fig. 5C). After reseeding of preconditioned cell on TCP, the ratio of phosphorylated MAPK to total MAPK was sustained at a high level from cells preconditioned with R1 surface (Fig. 5C).

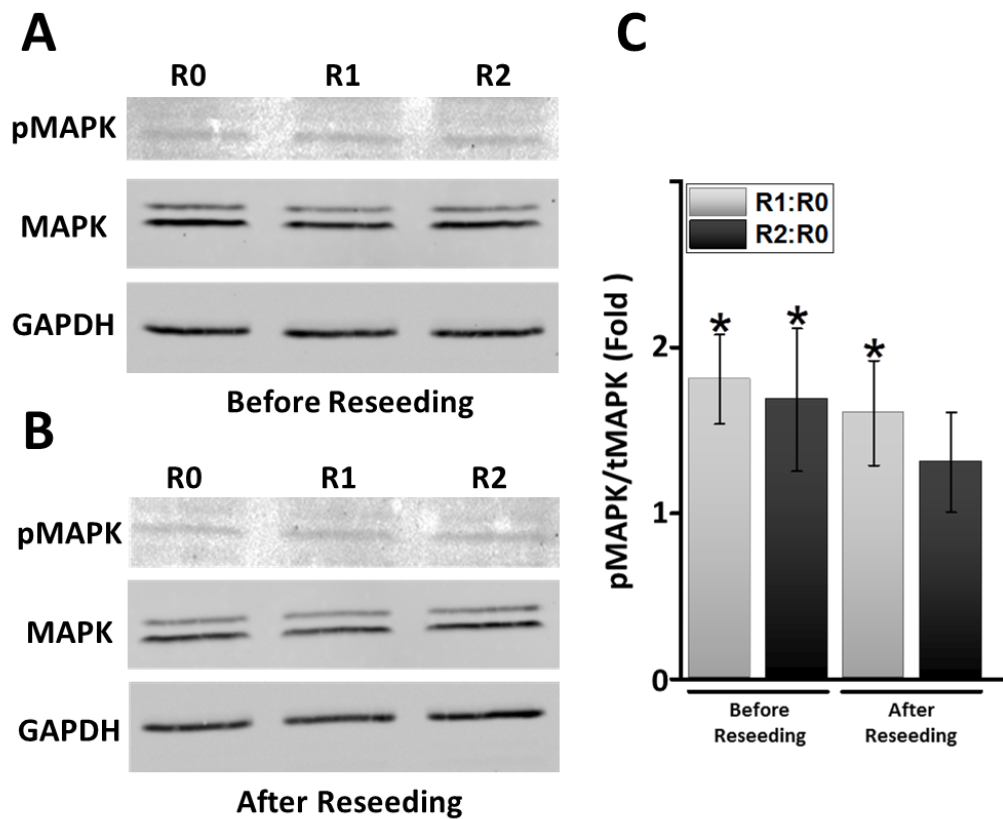


Fig. 5. Surface microtopography enhanced the MAPK phosphorylation. The proteins expression of MAPK and phosphorylated MAPK in 14 days surface microstructure preconditioned cells before (A) and after reseeding on tissue culture plate (B) was

*analyzed via western blot. (C) The statistical analysis of pMAPK/MAPK ratio were presented in a fold change histogram (n = 3, \* Sig. < 0.05 compared with R0).*

## **4 Discussion**

It has been reported that the stem cell behavior can be influenced by preconditioning in micro environments [38]. In this study, the microstructures were applied to precondition the hADSCs, the preconditioned cells were then harvested and reseeded in the same conventional cell culture vessel to compare the migration capacity and activity of potentially migration-associated modulators such as FAK and MAPK. Our results demonstrated that the hADSCs were able to develop different migration capacities induced by preconditioning on different topographic microstructures. Within these microstructures, the cell-material contact surface with intermediate roughness level promoted cell migration. Meanwhile, accompanied with the promoted migration, an elevated FAK and MAPK activation level was observed. These findings indicate that the MSCs are capable of reserving the previously received structural signal. Only the cells preconditioned for 4 days or longer obtained and maintained the enhanced migration capacity, which suggests that the functional alteration of MSC behavior may exhibit only in response to a satisfied dosage of topographic cues. This phenomenon is in consistence with a recent report, which illustrated a clear relationship between the stem cell memory and the precondition dosage of mechanical signals [39].

The formation and turnover of focal adhesion (FA) complexes are crucial dynamics in cells migration [40]. During migration, on one hand, FA forms at the leading edge so as to initially generate the necessary forces to pull the cell body forward. On the other hand, FA turns over at the rear edge to eliminate the resistance force and continue cell movement. Hence continuously synchronized formation and turnover of FA of the cell body are required in migration [41]. Moreover, it has been demonstrated that the size of FA predicted the cell migration speed [42]. In the present study, the distinct appearance in size and density FA of cells during and after microstructures precondition might contribute to the initiation of the different migration.

As one of the most prominent signaling molecules, FAK is involved in both formation and turnover of FAs during cell migration [32, 43]. FAK is composed of an N-terminal FERM domain, a C-terminal FAT and an intermediate kinase domain. The FERM domain of FAK has been demonstrated to interact with integrins and growth factor receptors [44]. These extracellular interactions can elicit the intracellular autophosphorylation of FAK at Tyr397, located at the kinase domain. The phosphorylated FAK at Tyr397, which binds and recruits Src protein, can lead to further phosphorylation of FAK at various tyrosine sites including Tyr576, Tyr577, Tyr861 and Tyr925 [45-47]. In terms of dynamics in FA, on one side, Tyr925 is necessary for the interaction of FAK with Grb2, which helps the recruitment of dynamin to adhesion site to support FA formation [48]. On the other side, FA disassembly requests the dephosphorylation of phosphorylated Tyr397 and FAK after the extension of microtubule to FA [48, 49]. Therefore, activation of FAK is indispensable in formation, turnover of FA, and intracellular transduction of integrin and growth factor receptor mediated external signals. It has been demonstrated that cells with highly activated FAK level exhibited an enhanced migration capacity [50-52]. Here, in agreement with these studies, an increased cell migration speed accompanied with an elevated FAK phosphorylation level at Tyr397 site was detected in hADSCs that have been preconditioned with R1 microstructured PS surface. It is suggested that the enhanced cell migration through microstructure preconditioning might be closely associated with the elevation of FAK activity.

MAPK regulates the cell migration through the FAK and myosin light chain kinase. The activation of MAPK can induce the phosphorylation of myosin light chain, which could enhance the cell migration [53]. Further, the activation of FAK was reported to subsequently activate its downstream effectors including MAPK [54]. Our results demonstrated that the R1 surface microstructure could enhance the migration capacity, elevated the FAK phosphorylation and the MAPK phosphorylation levels. This alteration of subcellular structure and function of cells is in consistence with previous studies [55, 56], in which it was demonstrated that the formation of a paxillin-FAK-MAPK complex regulates the cell migration capacity. Therefore, we assume that topographic microstructures modulate the MSCs migration capacity through the activation of FAK and MAPK.

In summary, the observations presented here indicate that hADSCs migration capacity could be modulated by surface microstructures. The appropriate roughness level promoted migration, which was accompanied with a higher activated FAK-MAPK level. This might be helpful for further understanding the underlying mechanism of microstructure modulated hADSCs migration capacity.

## 5 Conclusion

Effects of surface microtopography on hADSCs migration capacity were investigated in this study. The cells preconditioned with topographic microstructures exhibited distinct morphologies, focal adhesion sizes and migration velocities. The appropriate topographic microstructure significantly enhanced the cell migration capacity, and this effect was accompanied with increased FAK and MAPK activation level. These findings suggest that the cell migration capacity could be modulated by the preconditioning of cells via surface topographic microstructures of culture vessels, which might be helpful for improving the in vivo stem cell therapeutic efficacy by fine-tuning the in vitro physical or mechanical cues prior to stem cell transplantation.

## Acknowledgements

The authors acknowledge Robert Jeziorski, Mario Rettschlag for preparation of sterilized PS inserts and Manuela Keller for technical support. This work was financially supported by the China Scholarship Council (CSC) and the Helmholtz Association through Helmholtz Graduate School for Macromolecular Bioscience (MacroBio), Helmholtz-Portfolio Topic “Technology and Medicine”, Helmholtz Virtual Institute “Multifunctional Materials for Medicine (VH-VI-423), and programme-oriented funding.

## References

1. Wei, X., et al., *Mesenchymal stem cells: a new trend for cell therapy*. *Acta Pharmacologica Sinica*, 2013. **34**(6): p. 747-754.
2. Tuan, R.S., G. Boland, and R. Tuli, *Adult mesenchymal stem cells and cell-based tissue engineering*. *Arthritis Research & Therapy*, 2003. **5**(1): p. 32-45.



3. Stoltz, J.F., et al., *Stem cells and vascular regenerative medicine: A mini review*. Clin Hemorheol Microcirc, 2016. **64**(4): p. 613-633.
4. Schmidt, A., et al., *Basic fibroblast growth factor controls migration in human mesenchymal stem cells*. Stem Cells, 2006. **24**(7): p. 1750-8.
5. Amado, L.C., et al., *Cardiac repair with intramyocardial injection of allogeneic mesenchymal stem cells after myocardial infarction*. Proc Natl Acad Sci U S A, 2005. **102**(32): p. 11474-9.
6. Pittenger, M.F. and B.J. Martin, *Mesenchymal stem cells and their potential as cardiac therapeutics*. Circulation Research, 2004. **95**(1): p. 9-20.
7. Russo, V., et al., *Mesenchymal stem cell delivery strategies to promote cardiac regeneration following ischemic injury*. Biomaterials, 2014. **35**(13): p. 3956-74.
8. Barbash, I.M., et al., *Systemic delivery of bone marrow-derived mesenchymal stem cells to the infarcted myocardium: feasibility, cell migration, and body distribution*. Circulation, 2003. **108**(7): p. 863-8.
9. Liu, X.B., et al., *Angiopoietin-1 preconditioning enhances survival and functional recovery of mesenchymal stem cell transplantation*. J Zhejiang Univ Sci B, 2012. **13**(8): p. 616-23.
10. Eggenhofer, E., et al., *Mesenchymal stem cells are short-lived and do not migrate beyond the lungs after intravenous infusion*. Front Immunol, 2012. **3**: p. 297.
11. Shi, M., et al., *Regulation of CXCR4 expression in human mesenchymal stem cells by cytokine treatment: role in homing efficiency in NOD/SCID mice*. Haematologica, 2007. **92**(7): p. 897-904.
12. Ponte, A.L., et al., *The in vitro migration capacity of human bone marrow mesenchymal stem cells: comparison of chemokine and growth factor chemotactic activities*. Stem Cells, 2007. **25**(7): p. 1737-45.
13. Hung, S.C., et al., *Short-term exposure of multipotent stromal cells to low oxygen increases their expression of CX3CR1 and CXCR4 and their engraftment in vivo*. PLoS One, 2007. **2**(5): p. e416.
14. Cheng, Z., et al., *Targeted migration of mesenchymal stem cells modified with CXCR4 gene to infarcted myocardium improves cardiac performance*. Mol Ther, 2008. **16**(3): p. 571-9.
15. Shen, Y., et al., *Surface wettability of plasma SiO<sub>2</sub>:H nanocoating-induced endothelial cells' migration and the associated FAK-Rho GTPases signalling pathways*. J R Soc Interface, 2012. **9**(67): p. 313-27.
16. Lo, C.M., et al., *Cell movement is guided by the rigidity of the substrate*. Biophysical Journal, 2000. **79**(1): p. 144-152.
17. Pelham, R.J., Jr. and Y. Wang, *Cell locomotion and focal adhesions are regulated by substrate flexibility*. Proc Natl Acad Sci U S A, 1997. **94**(25): p. 13661-5.
18. Dimilla, P.A., et al., *Maximal Migration of Human Smooth-Muscle Cells on Fibronectin and Type-Iv Collagen Occurs at an Intermediate Attachment Strength*. Journal of Cell Biology, 1993. **122**(3): p. 729-737.

19. Hansen, T.D., et al., *Biomaterial arrays with defined adhesion ligand densities and matrix stiffness identify distinct phenotypes for tumorigenic and non-tumorigenic human mesenchymal cell types*. Biomaterials Science, 2014. **2**(5): p. 745-756.
20. Peyton, S.R. and A.J. Putnam, *Extracellular matrix rigidity governs smooth muscle cell motility in a biphasic fashion*. J Cell Physiol, 2005. **204**(1): p. 198-209.
21. Stroka, K.M. and H. Aranda-Espinoza, *Neutrophils Display Biphasic Relationship Between Migration and Substrate Stiffness*. Cell Motility and the Cytoskeleton, 2009. **66**(6): p. 328-341.
22. Han, J.J., et al., *An in vitro study on the collective tumor cell migration on nanoroughened poly(dimethylsiloxane) surfaces*. Journal of Materials Chemistry B, 2015. **3**(8): p. 1565-1572.
23. Chen, W., Y. Sun, and J. Fu, *Microfabricated nanotopological surfaces for study of adhesion-dependent cell mechanosensitivity*. Small, 2013. **9**(1): p. 81-9.
24. Rosa, A.L. and M.M. Beloti, *Effect of cpTi surface roughness on human bone marrow cell attachment, proliferation, and differentiation*. Braz Dent J, 2003. **14**(1): p. 16-21.
25. Gittens, R.A., et al., *The effects of combined micron-/submicron-scale surface roughness and nanoscale features on cell proliferation and differentiation*. Biomaterials, 2011. **32**(13): p. 3395-403.
26. Andrukhov, O., et al., *Proliferation, behavior, and differentiation of osteoblasts on surfaces of different microroughness*. Dent Mater, 2016.
27. Scharnagl, N., et al., *Design principles for polymers as substratum for adherent cells*. Journal of Materials Chemistry, 2010. **20**(40): p. 8789-8802.
28. Ganesan, R., K. Kratz, and A. Lendlein, *Multicomponent protein patterning of material surfaces*. Journal of Materials Chemistry, 2010. **20**(35): p. 7322-7331.
29. Schwartz, M.A., *Integrins and extracellular matrix in mechanotransduction*. Cold Spring Harb Perspect Biol, 2010. **2**(12): p. a005066.
30. Katsumi, A., et al., *Integrins in mechanotransduction*. Journal of Biological Chemistry, 2004. **279**(13): p. 12001-12004.
31. Guan, J.L., *Role of focal adhesion kinase in integrin signaling*. Int J Biochem Cell Biol, 1997. **29**(8-9): p. 1085-96.
32. Mitra, S.K., D.A. Hanson, and D.D. Schlaepfer, *Focal adhesion kinase: in command and control of cell motility*. Nat Rev Mol Cell Biol, 2005. **6**(1): p. 56-68.
33. McLean, G.W., et al., *The role of focal-adhesion kinase in cancer - a new therapeutic opportunity*. Nat Rev Cancer, 2005. **5**(7): p. 505-15.
34. Slack-Davis, J.K., et al., *PAK1 phosphorylation of MEK1 regulates fibronectin-stimulated MAPK activation*. J Cell Biol, 2003. **162**(2): p. 281-91.
35. Roch, T., et al., *Immunological evaluation of polystyrene and poly(ether imide) cell culture inserts with different roughness*. Clin Hemorheol Microcirc, 2012. **52**(2-4): p. 375-89.

36. Hiebl, B., et al., *Cytocompatibility testing of cell culture modules fabricated from specific candidate biomaterials using injection molding*. Journal of Biotechnology, 2010. **148**(1): p. 76-82.
37. Xu, X., et al., *Controlling Major Cellular Processes of Human Mesenchymal Stem Cells using Microwell Structures*. Advanced Healthcare Materials, 2014. **3**(12): p. 1991-2003.
38. Sart, S., T. Ma, and Y. Li, *Preconditioning stem cells for in vivo delivery*. Biores Open Access, 2014. **3**(4): p. 137-49.
39. Yang, C., et al., *Mechanical memory and dosing influence stem cell fate*. Nat Mater, 2014. **13**(6): p. 645-52.
40. Nagano, M., et al., *Turnover of focal adhesions and cancer cell migration*. Int J Cell Biol, 2012. **2012**: p. 310616.
41. Broussard, J.A., D.J. Webb, and I. Kaverina, *Asymmetric focal adhesion disassembly in motile cells*. Curr Opin Cell Biol, 2008. **20**(1): p. 85-90.
42. Kim, D.H. and D. Wirtz, *Focal adhesion size uniquely predicts cell migration*. FASEB J, 2013. **27**(4): p. 1351-61.
43. Ilic, D., et al., *Reduced cell motility and enhanced focal adhesion contact formation in cells from FAK-deficient mice*. Nature, 1995. **377**(6549): p. 539-44.
44. Sieg, D.J., et al., *FAK integrates growth-factor and integrin signals to promote cell migration*. Nat Cell Biol, 2000. **2**(5): p. 249-56.
45. Mitra, S.K. and D.D. Schlaepfer, *Integrin-regulated FAK-Src signaling in normal and cancer cells*. Current Opinion in Cell Biology, 2006. **18**(5): p. 516-523.
46. Westhoff, M.A., et al., *Src-mediated phosphorylation of focal adhesion kinase couples actin and adhesion dynamics to survival signaling*. Molecular and Cellular Biology, 2004. **24**(18): p. 8113-8133.
47. Hamadi, A., et al., *Regulation of focal adhesion dynamics and disassembly by phosphorylation of FAK at tyrosine 397*. Journal of Cell Science, 2005. **118**(19): p. 4415-4425.
48. Ezratty, E.J., M.A. Partridge, and G.G. Gundersen, *Microtubule-induced focal adhesion disassembly is mediated by dynamin and focal adhesion kinase*. Nature Cell Biology, 2005. **7**(6): p. 581-U15.
49. Nagano, M., et al., *ZF21 Protein Regulates Cell Adhesion and Motility*. Journal of Biological Chemistry, 2010. **285**(27): p. 21013-21022.
50. Slack, J.K., et al., *Alterations in the focal adhesion kinase/Src signal transduction pathway correlate with increased migratory capacity of prostate carcinoma cells*. Oncogene, 2001. **20**(10): p. 1152-1163.
51. Sieg, D.J., et al., *FAK integrates growth-factor and integrin signals to promote cell migration*. Nature Cell Biology, 2000. **2**(5): p. 249-256.
52. Sieg, D.J., C.R. Hauck, and D.D. Schlaepfer, *Required role of focal adhesion kinase (FAK) for integrin-stimulated cell migration*. Journal of Cell Science, 1999. **112**(16): p. 2677-2691.

53. Huang, C., K. Jacobson, and M.D. Schaller, *MAP kinases and cell migration*. J Cell Sci, 2004. **117**(Pt 20): p. 4619-28.
54. Zhu, X. and R.K. Assoian, *Integrin-dependent activation of MAP kinase: a link to shape-dependent cell proliferation*. Mol Biol Cell, 1995. **6**(3): p. 273-82.
55. Teranishi, S., K. Kimura, and T. Nishida, *Role of formation of an ERK-FAK-paxillin complex in migration of human corneal epithelial cells during wound closure in vitro*. Invest Ophthalmol Vis Sci, 2009. **50**(12): p. 5646-52.
56. Shi, J., et al., *Activation of ERK-FAK Signaling Pathway and Enhancement of Cell Migration Involved in the Early Interaction Between Oral Keratinocytes and Candida albicans*. Mycopathologia, 2009. **167**(1): p. 1-7.

## **Chapter IV**

### **Influence of surface roughness on neural differentiation of human induced pluripotent stem cells**

**Clinical Hemorheology and Microcirculation 64 (2016) 355–366.**

<https://doi.org/10.3233/CH-168121>

# **Influence of surface roughness on neural differentiation of human induced pluripotent stem cells**

Zhengdong Li <sup>1,2</sup>, Weiwei Wang <sup>1</sup>, Karl Kratz <sup>1,3</sup>, Judit K uchler <sup>1</sup>, Xun Xu <sup>1,2</sup>, Jie Zou <sup>1,2</sup>, Zijun Deng <sup>1</sup>, Xianlei Sun <sup>1</sup>, Manfred Gossen <sup>1,3</sup>, Nan Ma <sup>1,2,3,\*</sup> and Andreas Lendlein <sup>1,2,3,\*</sup>

<sup>1</sup> Institute of Biomaterial Science and Berlin-Brandenburg Center for Regenerative Therapies, Helmholtz-Zentrum Geesthacht, Kantstra e 55, 14513 Teltow, Germany

<sup>2</sup> Institute of Chemistry and Biochemistry, Freie Universit t Berlin, Takustra e 3, 14195 Berlin, Germany

<sup>3</sup> Helmholtz Virtual Institute - Multifunctional Materials in Medicine, Berlin and Teltow, Kantstra e 55, 14513 Teltow, Germany

\* To whom correspondence should be addressed:

Prof. Dr. Nan Ma, Prof. Dr. Andreas Lendlein

Email: nan.ma@hzg.de, andreas.lendlein@hzg.de

Phone: +49 (0)3328 352-450

Fax: +49 (0)3328 352-452

## **Abstract**

Induced pluripotent stem cells (iPSCs) own the capacity to develop into all cell types of the adult body, presenting high potential in regenerative medicine. Regulating and controlling the differentiation of iPSCs using the surface topographic cues of biomaterials is a promising and safe approach to enhance their therapeutic efficacy. In this study, we tested the effects of surface roughness on differentiation of human iPSCs into neural progenitor cells and dopaminergic neuron cells using polystyrene with different roughness (R0: flat surface; R1: rough surface,  $R_q \sim 6 \mu\text{m}$ ; R2: rough surface,  $R_q \sim 38 \mu\text{m}$ ). Neural

differentiation of human iPSCs could be influenced by surface roughness. Up-regulated neuronal markers were found in cells on rough surface, as examined by real-time PCR and immunostaining. Particularly, the R1 surface significantly improved the neuronal marker expression, as compared to R0 and R2 surface. This study demonstrates the significance of surface roughness, depending on the roughness level, in promoting differentiation of human iPSCs towards the neuronal lineage. Our study suggests the potential applications of surface roughness in iPSCs based treatment of neural disorder diseases, and highlights the importance of design and development of biomaterials with effective surface structures to regulate stem cells.

**Key words:** human iPSCs, roughness, neural differentiation, regenerative medicine

## 1 Introduction

Induced pluripotent stem cells (iPSCs), generated from adult cells by introducing transcription factors, hold great promise in regenerative medicine without many of the associated ethical concerns as compared to embryonic stem cells (ESC) [1, 2]. Due to their neural differentiation capacity, iPSCs have been described as scientific breakthrough for treating Parkinson's Disease (PD), which is a common neurodegenerative disorder characterized by a selective loss of dopaminergic neurons. In this area, remarkable progress has been made in the past decade. For example, the dopaminergic neurons as the predominant cell type for treating PD have been effectively generated from iPSCs [3, 4], and functionally integrated into cynomolgus monkey model [5]. These achievements presage a strong immunological, functional and biological rationale to use dopamine neurons derived from iPSCs for cell replacement in PD in the future. However, there are still some challenges that need to be overcome such as inefficient cell derivation, genetic abnormalities during *in vitro* expanding [6]. Most of all, it is of utmost importance to avoid the teratoma or tumor formation caused by inadequate differentiation [7]. It is only of benefit if there is a complete differentiation to generate the cell types of interest. Hence, controlled neural differentiation of iPSCs is critical for treating PD by cell replacement.

Researchers have assembled considerable knowledge on how biochemical factors, signaling pathways and transcriptional networks regulate iPSCs behaviors [8]. Increasing evidences have demonstrated that the biophysical properties of the microenvironment, such as the extracellular matrix (ECM) stiffness and cyclic strain, could effectively control a variety of cell behaviors of iPSCs [9, 10]. Most of the biophysical properties can be readily generated using the appropriate fabrication technologies, such as the topographic features at micro- and nano-scale which have shown effects to induce changes in cell alignment, polarization, elongation, migration, proliferation and gene expression [11-13]. It has been reported recently that the topography of nano- and micro-grating substrates could regulate the expression of neuronal markers in iPSCs [14]. Further, appropriate microscale roughness could affect the differentiation of mesenchymal stem cells [15]. Therefore, topographical cues might hold a great interest in inducing neural dopaminergic differentiation of iPSCs.

In this study, we hypothesized that surface roughness could influence the neural differentiation of human iPSCs. To examine our hypothesis, neural differentiation was induced in a polystyrene based cell culture insert system with different roughness on the bottom. Considering the single cell size of human iPSCs ( $\sim 43.5 \mu\text{m}^2$ ) [16], surfaces with three different roughness levels were used (R0: flat surface; R1: rough surface,  $R_q \sim 6 \mu\text{m}$ ; R2: rough surface,  $R_q \sim 38 \mu\text{m}$ ) to adapt the cell size. Human iPSCs were induced to differentiate into neural progenitor cells and dopaminergic cells on matrigel coated inserts. The expression of neural ectodermal marker genes and neural marker proteins was assessed. Our results indicated that the differentiation of human iPSCs was promoted by the microscale roughness. Cells on R1 presented the highest level of neural differentiation. These results expand the knowledge of improving neural differentiation of iPSCs by topographic cues, which would be benefit for design and fabrication of biomaterials to enhance efficacy of iPSCs based regenerative therapies.



## 2 Materials and methods

### 2.1 Cell culture surfaces

PS inserts fitting the standard 24-well tissue culture plate (TCP) were prepared via injection molding as described before [17, 18]. Three differently structured cylinders were utilized to manufacture the inserts with different types of bottom roughness: a cylinder with a polished contact surface (R0), and two cylinders with micro-structured surfaces according to the standard of German Institute for Standardization (DIN 16747: 1981-05), M30 (R1) and M45 (R2). The prepared inserts were sterilized by gas sterilization (gas phase: 10% ethylene oxide, 54 °C, 65% relative humidity, 1.7 bar, 3 hours of gas exposure time and 21 hours of aeration phase). The roughness of the insert bottom was determined with an optical profilometer (MicoProf 200, FRT - Fries Research & Technologie GmbH, Bergisch Gladbach, Germany) equipped with a CWL 300 chromatic white-light sensor. The data were acquired with the software AQUIRE (ver. 1.21) and were evaluated with the software MARK III (ver. 3.9).

The PS inserts and tissue culture plate were coated with Matrigel™ Basement Membrane Matrix (BD Biosciences; San Jose, USA) to enable the cell attachment. Matrigel was diluted with Dulbecco's Modified Eagle Medium-Nutrient Mixture F-12 (DMEM/F12, Thermo Fisher Scientific, Bonn, Germany) (1:80 v/v). For each well of 6 well TCP or each PS insert, 2000 µl or 200 µl (approximately 200 µl/cm<sup>2</sup>) of diluted matrigel solution was added and incubated at 37 °C for 1 hour, and then was removed before cell cultivation.

### 2.2 Human iPSCs cultivation and neural differentiation

Human iPSCs (IMR90-4 cell line, WiCell, Wisconsin, USA) were cultured in feeder-free medium (mTeSR™, STEMCELL Technologies, Vancouver, Canada) on matrigel coated dishes at 37 °C in a humidified atmosphere containing 5% CO<sub>2</sub>. For cell maintenance, the medium was changed regularly and the cells were passaged every 5 days at ratios of 1:6.

The neuronal differentiation conditions were adapted from Dual SMAD inhibition protocol [19]. Briefly, the iPSCs clusters were dissociated into single cells with cell detachment

solution (Accutase™, STEMCELL Technologies, Vancouver, Canada). Then, the cells were seeded on matrigel coated dishes or PS inserts at a density of  $3 \times 10^4$  cells/cm<sup>2</sup>. Neural differentiation was inducted at day 4 by changing the culture medium to N2B27 medium (Neurobasal® medium (Thermo Fisher Scientific, Bonn, Germany) supplemented with 0.5 mM L-Glutamin (Thermo Fisher Scientific, Bonn, Germany), B-27® Supplement (Thermo Fisher Scientific, Bonn, Germany) and N-2® Supplement (Thermo Fisher Scientific, Bonn, Germany)) containing different compounds (Fig. 3A). From day 4, N2B27 medium containing 10 μM SB431542 (Merck Millipore, Darmstadt, Germany), 200 ng/ml Noggin (R&D Systems, Minneapolis, USA) and Dorsomorphin (Sigma-Aldrich, St Louis, USA) was used. At day 8, the medium was replaced with that containing 200 ng/ml recombinant N-terminal human sonic hedgehog (SHH, R&D Systems, Minneapolis, USA) instead of SB431542. From day 12 the induction medium was changed to N2B27 medium supplemented with 20 ng/ml brain-derived neurotrophic factor (BDNF, Peprotech, Hamburg, Deutschland), 100 ng/mL FGF8 (R&D Systems, Minneapolis, USA), 200 μM ascorbic acid (AA, Sigma-Aldrich, St Louis, USA) and 200 ng/ml SHH. From day 16, N2B27 medium supplemented with 20 ng/ml BDGF, 200 μM ascorbic acid and 20 ng/mL glial cell-derived neurotrophic factor (GDNF, ProSpec-Tany TechnoGene, Rehovot, Israel) was applied. The medium was changed every 2 days during the whole induction process.

### 2.3 Immunocytochemistry

The human iPSCs cultured in TCP or PS inserts were fixed by adding 4% paraformaldehyde (Sigma-Aldrich, St. Louis, MO, USA) for 15 minutes and then permeabilized with 0.1% Triton X-100 (Sigma-Aldrich, St. Louis, MO, USA) for 5 minutes. After blocking with 3% bovine serum albumin (BSA) (Sigma-Aldrich, St. Louis, MO, USA) solution for 30 minutes, the cells were incubated with mouse anti-human primary antibodies (mouse monoclonal anti-neuronal β-III Tubulin, mouse monoclonal anti-Nestin and mouse monoclonal anti-MAP2 (all are from Millipore, Darmstadt, Germany)) at 4 °C overnight. After washing with PBS, the secondary antibodies (Alexa Fluor-488 goat anti-mouse IgG, 1:500; Alexa Fluor-555 goat anti-mouse IgG, 1:500; Life Technologies, Darmstadt, Germany) were added and incubated for 60 minutes. The cell nuclei were

stained with 4',6-diamidino-2-phenylindole (DAPI, Sigma-Aldrich, St. Louis, MO, USA). After 3 times of washing with PBS, the samples were visualized using a fluorescence microscope (AxioSkop, Carl Zeiss, Jena, Germany) or scanned with a confocal laser scanning microscope (LSM 780, Carl Zeiss, Jena, Germany).

For the cell characterization staining, the hiPSCs were stained with the Fluorescent Human ES/iPS Cell Characterization Kit (Millipore, Darmstadt, Germany) following the manufacturer's protocol.

## 2.4 Real-time PCR

Isolation of total RNA was performed using TRI Reagent® (Sigma-Aldrich, St. Louis, MO, USA) following the manufacturer's instruction. The cDNA was synthesized from the isolated RNA using Superscript™ III First-Strand Synthesis System (Life Technologies, Darmstadt, Germany) according to the given protocol. Quantitative RT-PCR was performed on a StepOnePlus™ Real-time PCR Systems (Life Technologies, Darmstadt, Germany) using SYBER® Green Master Mix (Thermo Fisher Scientific, Bonn, Germany) and RT-PCR primers (Table 1). The expression of the genes of interest was determined in triplicate for each cell sample. Glyceraldehyde 3-phosphate dehydrogenase (GAPDH) was used as housekeeping gene. Gene expression level was determined using the method as we described before [20]. The  $\Delta C_T$  values of the target genes was normalized with the  $C_T$  value of GAPDH ( $\Delta C_T = C_T, \text{ target} - C_T, \text{ GAPDH}$ ). The fold change of gene expression levels between two samples was expressed as  $2^{-\Delta\Delta C_T}$  ( $\Delta\Delta C_T = \Delta C_T, \text{ sample 2} - \Delta C_T, \text{ sample 1}$ ).

Table 1. Primer sequence

<b>Gene</b>	<b>Primer (Forward)</b>	<b>Primer (Reverse)</b>
<b><i>GAPDH</i></b>	GTGGACCTGACCTGCCGTCT	GGAGGAGTGGGTGTCGCTGT
<b><i>SOX1</i></b>	AATTTTATTTTCGGCGTTGC	TGGGCTCTGTCTCTTAAATTTGT

---

<b>SOX2</b>	CCCAGCAGACTTCACATGT	CCTCCCATTTCCTCGTTTT
<b>NESTIN</b>	CTGGAGCAGGAGAAACAGG	TGGGAGCAAAGATCCAAGAC
<b>PAX6</b>	ATGTGTGAGTAAAATTCTGGGCA	GCTTACAACCTTCTGGAGTCGCTA
<b>MAP2</b>	GGAGACAGAGATGAGAATTCCT	GAATTGGCTCTGACCTGGT

---

## 2.5 Western blotting

To quantify the neuronal protein expression, cell lysates were prepared with RIPA buffer (Sigma-Aldrich, St. Louis, MO, USA) supplemented with phenylmethylsulfonyl fluoride (Life Technologies, Darmstadt, Germany) and Protease Inhibitor Cocktails (Sigma-Aldrich, St. Louis, MO, USA). The obtained protein solutions were denatured by heating at 95 °C for 5 minutes, separated by electrophoresis on 10% gradient SDS-polyacrylamide gel and then transferred onto PVDF membranes (Millipore, Darmstadt, Germany). The blots were probed with monoclonal primary antibodies and fluorescently labeled secondary antibodies (Li-Cor, Bad Homburg, Germany). Fluorescent signal were then detected using an Odyssey Imaging scanner and the intensitie was analyzed by image studio software (Li-Cor, Bad Homburg, Germany).

## 2.6 Statistics

Data are shown as mean  $\pm$  standard deviation. Statistical analysis was performed using the two-tailed independent-samples t-test, and a significant level (Sig.)  $< 0.05$  was considered to be statistically significant.

## 3 Results

### 3.1 Cell culture surfaces characterization

PS inserts with different types of bottom roughness were prepared via injection molding (Fig. 1A-C). The micro-scale roughness of the insert bottom was first determined via

optical profilometry measurement. R0 has a smooth surface with the root mean squared roughness ( $R_q$ ) value around  $0.3 \mu\text{m}$ , while R1 and R2 have the rougher surfaces with  $R_q$  values around  $6 \mu\text{m}$  and  $38 \mu\text{m}$  respectively. At the nanoscale, all of the surfaces are relatively smooth with the average  $R_q$  values less than  $300 \text{ nm}$  (Table 2). The surfaces were coated with ECM gel prior to cell seeding. The ECM gel coated surfaces for human iPSCs seeding were in the level in  $R_q$  analysis compared with uncoated surfaces (Fig. 1 D, Table. 2).

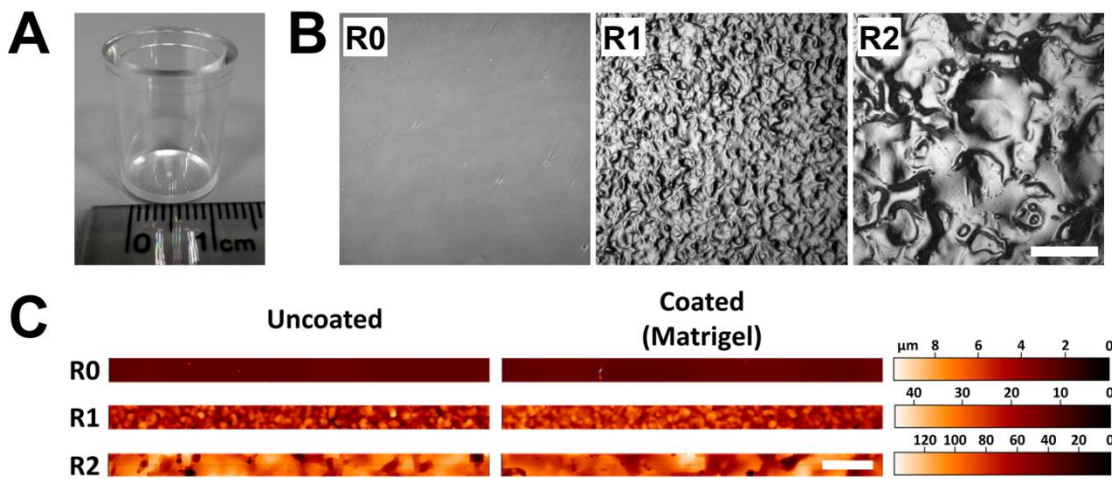


Fig. 1. PS inserts bottom surface characterization. (A) The insert with a suitable size to fit the standard 24-well tissue culture plate. (B) Phase contrast microscope images showed the three types of insert bottom with different roughness (bar =  $500 \mu\text{m}$ ). (C) Representative profilometry scanning images of the surfaces before and after matrigel coating (bar =  $500 \mu\text{m}$ ).

Table 2. Surface roughness

Samples	Uncoated	Matrigel coated
---------	----------	-----------------

	Micro-roughness <sup>a)</sup> R <sub>q</sub> (μm)	Nano-roughness <sup>b)</sup> R <sub>q</sub> (μm)	Nano-roughness <sup>b)</sup> R <sub>q</sub> (μm)
<b>R0</b>	0.31 ± 0.11	0.020 ± 0.010	0.015 ± 0.004
<b>R1</b>	6.01 ± 0.21	0.154 ± 0.044	0.138 ± 0.040
<b>R2</b>	38.15 ± 5.86	0.067 ± 0.021	0.093 ± 0.004

<sup>a)</sup> Optical profilometry measurement by scanning an area of 7×7 mm<sup>2</sup>. <sup>b)</sup> Optical profilometry measurement by scanning an area of 50×50 μm<sup>2</sup>.

### 3.2 Human iPSCs characterization

To characterize the human iPSCs, the alkaline phosphatase (AP) and pluripotent markers (Oct4 and Nanog) were assessed through the immunostaining (Fig. 2). The cultivated human iPSCs showed the typical iPSC colony morphology and a well-defined edge composed of tightly packed cells with round shape and uniform size. The undifferentiated iPSCs positively expressed AP and the iPSC markers Oct4 and Nanog.

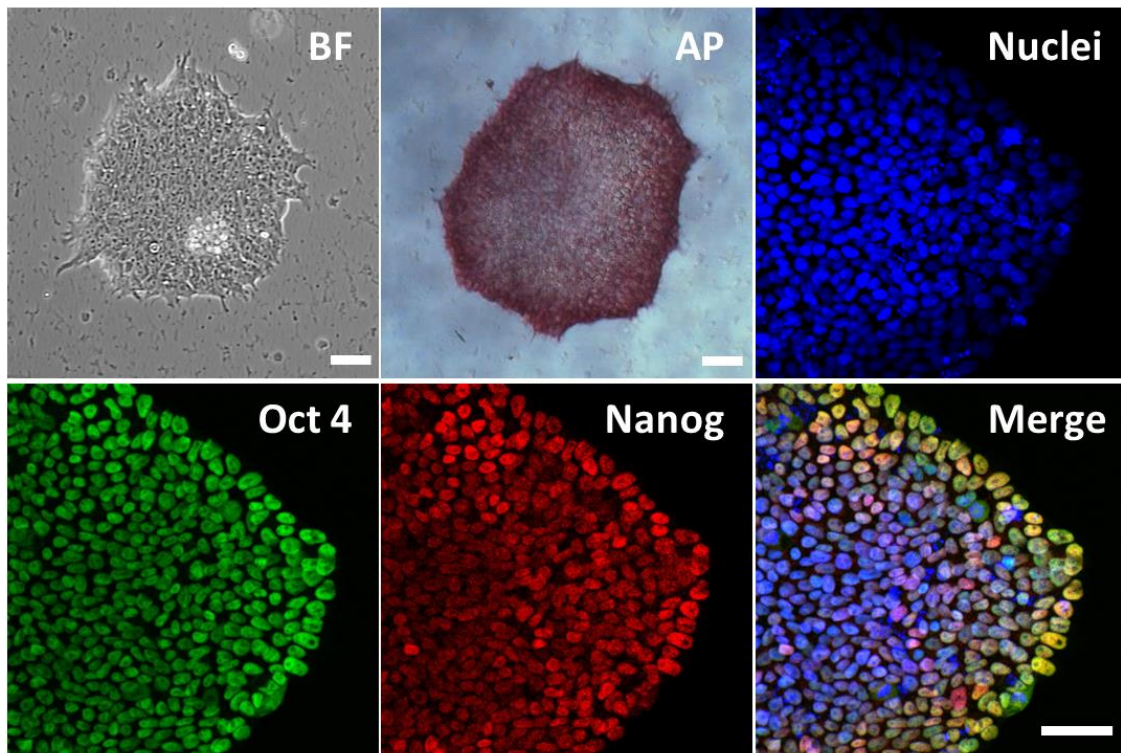


Fig. 2. Human iPSCs characterization. Cultivated iPSCs showed the classic clone morphology and expressed pluripotent markers of Oct4 and Nanog (bar = 50  $\mu$ m).

### 3.3 Neural differentiation on TCP

At first, the neural differentiation of cultivated human iPSCs was performed on the TCP coated with matrigel. Following the dual SMAD pathway inhibition protocol (Fig. 3, A), the iPSCs were rapidly differentiated into neural progenitor cells which was characterized by the immunostaining of Nestin at day 16. The neural progenitor cells derived from iPSCs showed the morphologically identifiable rosette structures (Fig. 3, B upper panel). During this period, the expression of pluripotent gene Oct 4 was downregulated, and the neural progenitor marker genes PAX6, SOX 1 and Nestin were upregulated (Fig. 3, C). With the further induction with BDNF and GDNF, the neural progenitor cells continuously differentiated into neuronal cells. After 42 days of induction, the cells differentiated from iPSCs expressed the mature neural marker  $\beta$ -III Tubulin (Fig. 3, B lower panel).

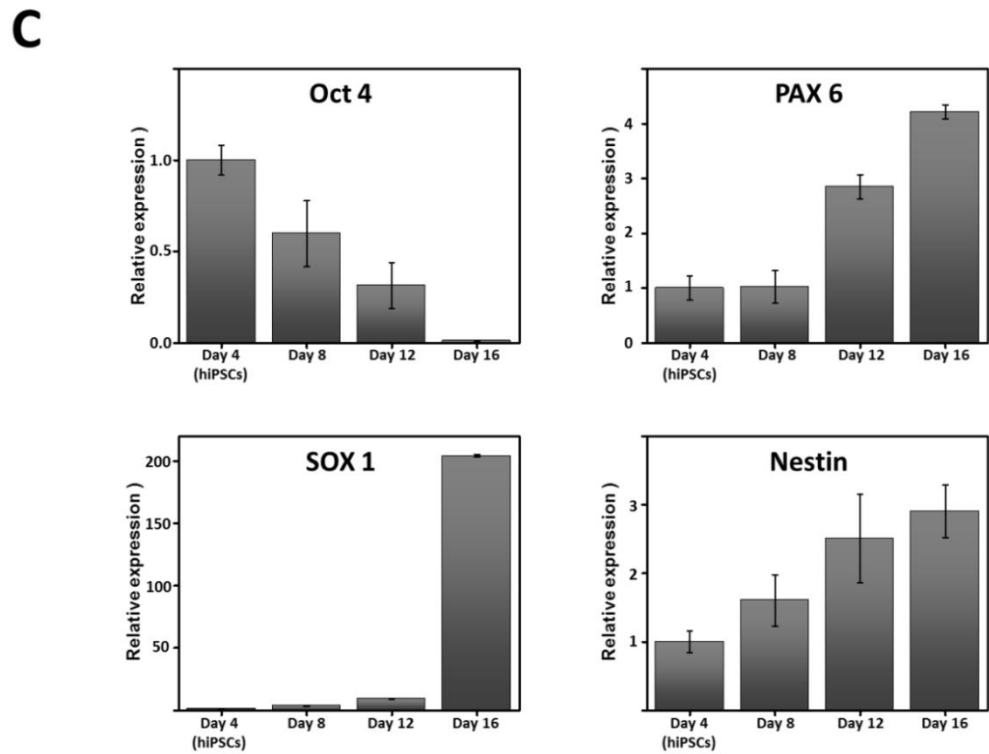
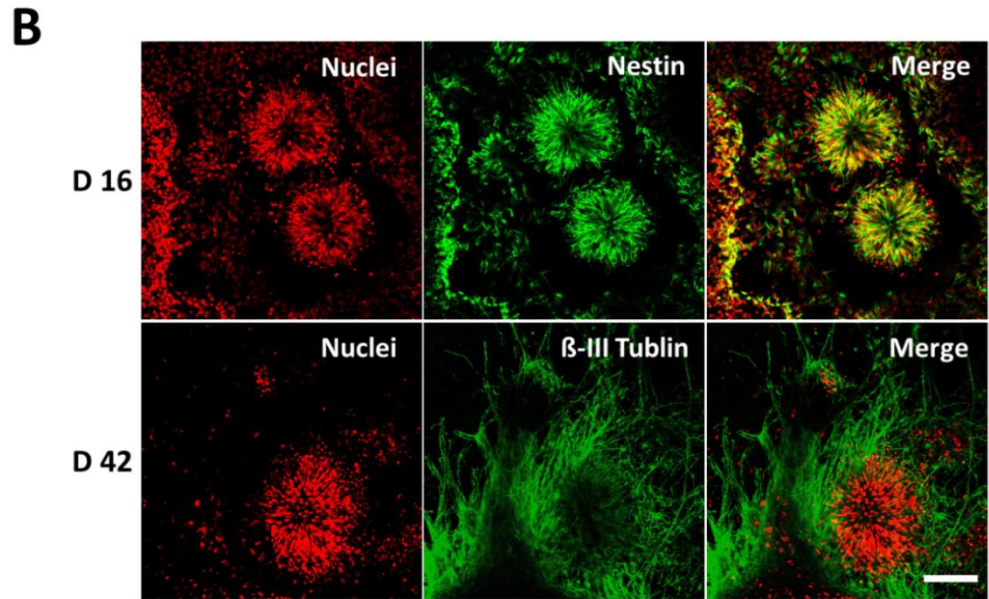
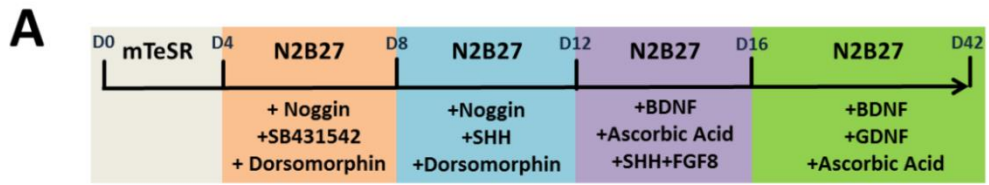




Fig. 3. Human iPSCs neural differentiation on TCP coated with matrigel. (A) The neural differentiation protocol induced by chemicals. (B) Representative images showed that differentiated iPSCs showing identifiable rosette morphology of neural progenitor cells at day 16 (upper panel) and positively expressing the neural marker  $\beta$ -III Tubulin at day 42 (lower panel, bar = 50  $\mu$ m). (C) Pluripotent gene (Oct 4) expression was downregulated while neural genes (PAX 6, SOX 1, Nestin) expression were upregulated during induction process. The undifferentiated human iPSCs were used as control (n = 3).

### 3.4 Neural differentiation on rough surfaces

To study the influence of topographic roughness on neural differentiation of human iPSCs, the neural induction was performed in the PS inserts with different bottom roughness using the same protocol as that on TCP surface (Fig. 3, A). After 42 day of induction, the cells differentiated from human iPSCs showed the neural microtubule structures and positively expressed the neural identifiable proteins MAP2 and  $\beta$ -III Tubulin (Fig. 4).

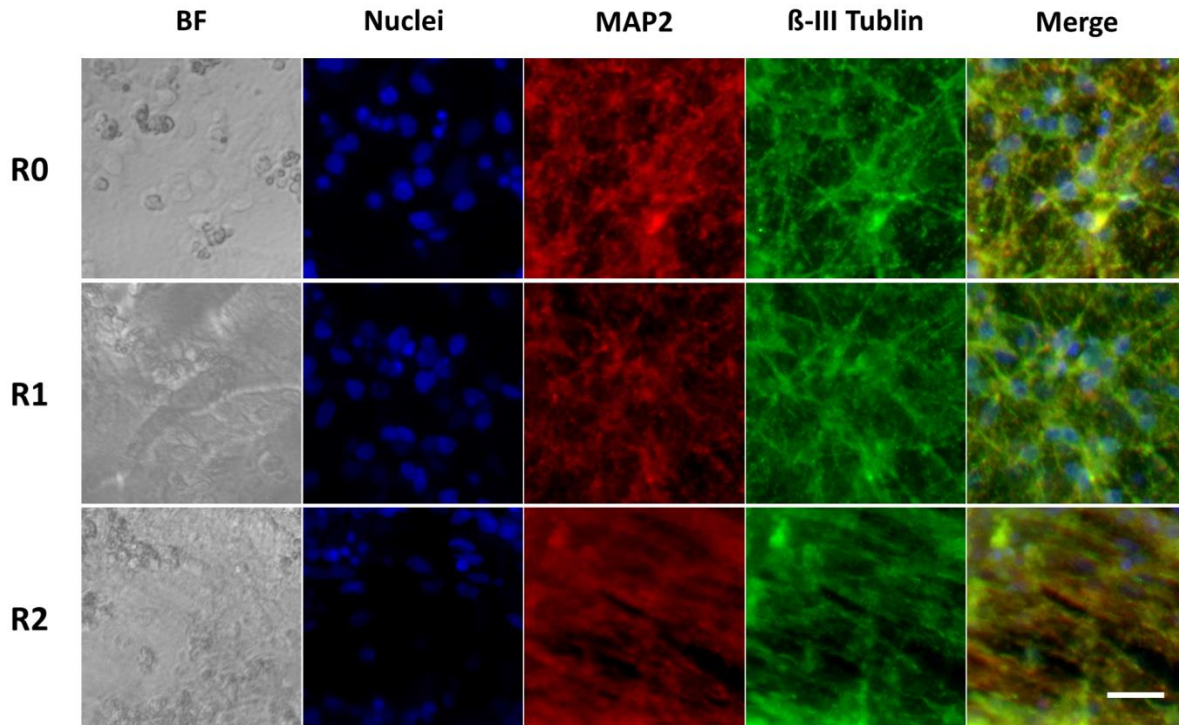


Fig. 4. Neural differentiation of human iPSCs on matrigel coated surfaces with different roughness. After 42 days of induction, human iPSCs differentiated into neural cells on all surfaces, with the expression of the neural identification marker  $\beta$ -III Tubulin and MAP2 (bar = 25  $\mu$ m).

### 3.5 Neural gene and protein expression

To investigate the effects of roughness on neural differentiation of iPSCs, the quantitative real-time PCR was performed to assess the expression of neural genes of the differentiated iPSCs at day 16. Compared with cells on flat surface R0, the neural progenitor cells on rougher surface R1 and R2 exhibited higher expression levels of Nestin and  $\beta$ -III Tubulin. Particularly, these genes expressed significantly higher on R1 surface as compared to those on R0 and R2 (Fig. 5, A). As following, the progenitor cells derived from the human iPSCs were continuously induced to differentiation towards dopaminergic neurons with BDNF, GDNF and AA. After 42 days, the protein expression

was assessed by western blot (Fig. 5, B). The cells on R1 surface expressed higher neural identical proteins compared with the cells on R0 and R2 surfaces. Notably, cells on R1 expressed significantly higher  $\beta$ - III Tubulin than cells on R0 and R2 (Fig. 5, C).

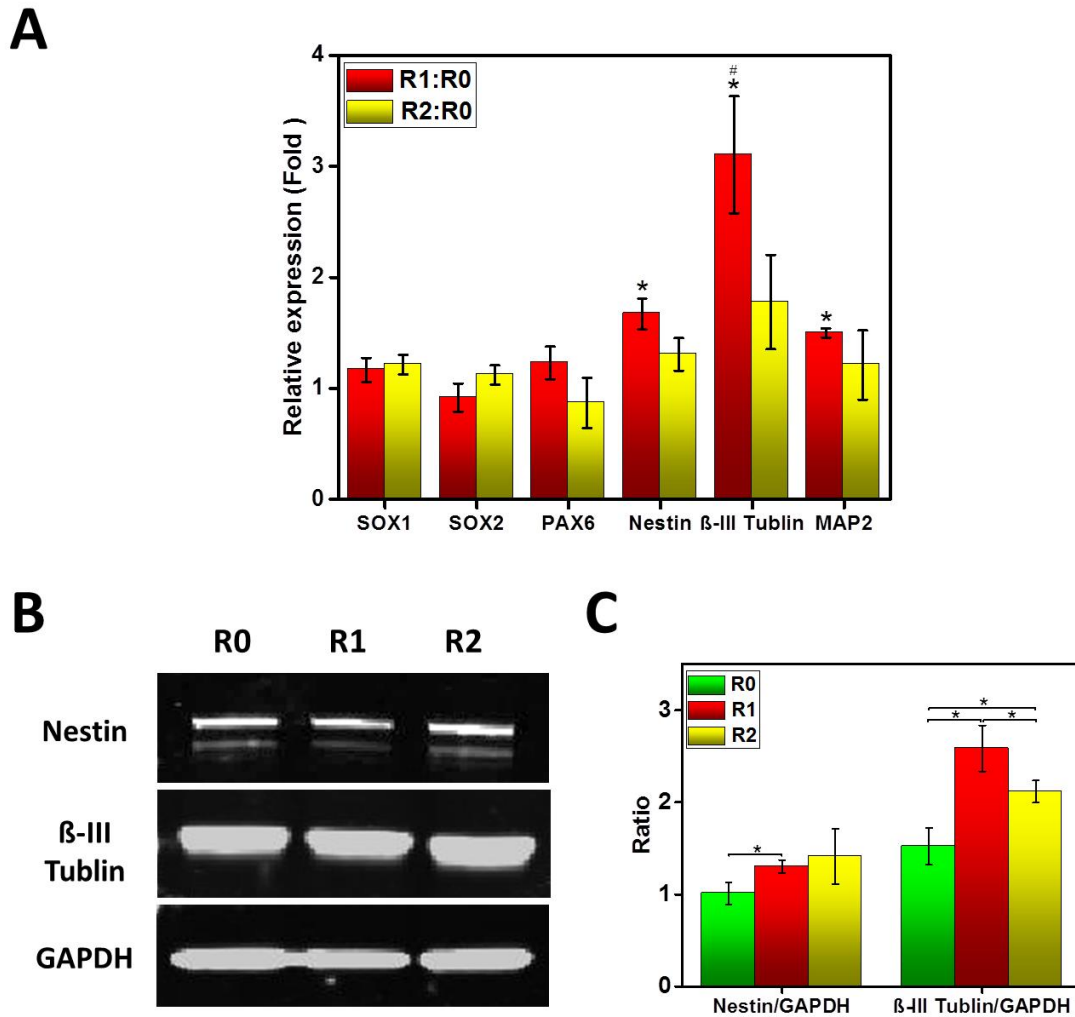


Fig. 5. Expression of neural genes and proteins of iPSCs induced towards neural differentiation on surfaces with different microroughness. (A) After 16 days of induction, the expression of SOX1, SOX2, PAX6, Nestin,  $\beta$ - III Tubulin and MAP2 genes was quantified via RT-PCR and normalized to the expression level on R0 surface (n = 3, \* R1: R0 Sig. < 0.05, # R1: R2 Sig. < 0.05). (B) After 42 days of induction, the expression of Nestin and  $\beta$ - III Tubulin proteins of the cells were analyzed via western blotting. (C) The

statistical analysis of Nestin expression and  $\beta$ - III Tubulin expression (normalized to GAPDH, n = 3, \* Sig. < 0.05).

## 4 Discussion

Neural differentiation of iPSCs represents a promise in neural regenerative medicine. Due to the tumorigenic potential [21], establishment of efficient neural differentiation approach is an essential prerequisite for the further applications. Mechanic cues are increasingly studied to affect the stem cell behaviors. Thus, modulation of neural differentiation of iPSCs with different physical cues is of great interest in regenerative medicine. In our work, designed polymer surface system with different roughness demonstrated that appropriate roughness could promote the dopaminergic neural differentiation of iPSCs in gene and protein expression. Our finding highlights a new approach to enhance the efficiency of dopaminergic neuron derivation of iPSCs.

In current study, highest promotive effects of differentiation were found on the middle ranged R1 surface, which might highly adapt to the iPSCs size. It is reported that nanoscale roughness surfaces tended to induce pluripotent stem cells (PSCs) into spontaneous differentiation while smooth surfaces supported PSCs adhesion, rapid cell proliferation and long-term self-renewal [22]. In our system, higher nanoscale roughness of our designed surfaces was found on R1 and R2 surfaces compared with flat R0 surface. Thus, the elevated neural differentiation on R1 and R2 surface may attributed not only to the microscale roughness, but also to the nanoscale roughness. This finding indicated a optimize roughness condition for the human iPSCs neural differentiation. However, more deep studies are needed to explore the concealed mechanism.

Several approaches can be considered for the induction of iPSCs neural differentiation. Like the early protocol, embryoid bodies generated from the lifting PSCs, are grown in adherent culture condition in N2 and fibroblast growth factor (bFGF) supplemented medium to form neural progenitor cells who are allowed to form the neural rosettes structure [23]. This embryoid body formation way is considered a distinguishing feature of successful neural differentiation induction. Another approach is to use the mouse stromal feeder cells that are known to have the neural inducing effect [24]. However, the

embryoid body formation or feeder cell approaches are not adapted to study influence of the roughness on neural differentiation since the rare directly contact conditions. Recently, a remarkably and robust approach via dual inhibition of SMAD signalling was reported for the neural induction of PSCs [19]. Single cell adherent cultivation of PSCs were stimulated with Noggin (an inhibitor of bone morphogenetic protein 4, BMP4) and SB431542 (an inhibitor of Lefty/Activin/TGF $\beta$  pathways) to achieve neural differentiation. For the feasibility and robustness as well as high efficiency, this approach has resulted in its relative popularity in the neural differentiation induction. In this study, Dorsomorphin (a chemical BMP inhibitor) was added to increase the efficiency and reduce the cost [25]. Additionally, the extracellular matrix has great effects on the efficiency of neural differentiation of PSCs [26, 27]. Matrigel was chosen to coat the surface in current work since its great enrichment of neural differentiation [26].

For the source of the human iPSCs, the IMR90-4 was chose in our study, This cell line was generated from IMR90 fetal lung fibroblasts by viral transduction of a combination of Oct 4, Sox 2, Nanog , and Lin 28 genes. In our cultivation, the cells showed the typical iPSCs colony morphology and a well-defined edge composed of tightly pached round and uniformly sized cells, and an elevated level of AP on the cell membrane. The AP is commonly used to identify the undifferentiated PSCs including ESCs and iPSCs [28, 29]. Additionally, the pluripotent marker Oct 4 and Nanog were characterized in our immunostaining. Further, It has a high efficiency of differentiation towards neural lineage in a cell lines comparable study [30].

In PSCs differentiation, the pluripotent genes and the stage specific lineage genes are programmatically downregulated and upregulated respectively. It is reported that Pax6 gene plays a critical role in neural differentiation and determines the human neuroectoderm cell fate [31], and during PSCs differentiation to neural cells, Oct4 is downregulated before Pax6 becomes highly expressed [32]. Our results showed that the Oct4 gene was sustainably downregulated by induction, and the Pax6 gene was conversely upregulated, which is in accordance with these reports. Besides, the neural marker genes Sox1 and Nestin genes were upregulated during the induction, which is in accordance with previously description [24].

Our results indicated that the neural genes expression of neural progenitor cells was positively expressed after 16 days induction, and among these genes, the Nestin,  $\beta$ -III Tubulin and MAP2 were significantly upregulated by rough surface R1 compared with other flat surface R0 and rougher surface R2, which indicated that the roughness promoted the neural differentiation, and this promotion was dependent on the roughness level. MAP2 as a mature neuron marker was also upregulated on the rough surface, which demonstrated that roughness could enrich the neuron mature from the progenitor stage. As following, the Nestin and  $\beta$ - III Tubulin proteins expression were upregulated after dopaminergic neural induction by the R1 rough surface, which revealed appropriate roughness could increase the neural differentiation of iPSCs. Although the obvious enhancement of neural differentiation was observed, the mechanism of roughness induced differentiation remains unclear. It may attribute to the surface roughness related subtle force which may cause the difference in membrane attachment and in cellular responses to the guidance signals emitted from the substrates [33], the formation and alignment of focal adhesion kinas (FAK) phosphorylation involved focal adhesions induced by the topography which could lead the stem cell differentiation [34, 35]. Further, the cytoskeleton rearrangement and nuclei relocation by the roughness may play a critical role in the mechanical signal transduction to affect the gene expression [36, 37]. In addition, surface roughness formed local curvature may affect the stem cell differentiation [38].

## **5 Conclusion**

In this work, we demonstrated the roughness effects on human iPSCs differentiation towards neuronal lineage. Neural differentiation of human iPSCs was successfully induced on the matrigel coated polymeric roughness. Gene expression profiling by real-time PCR and immunostaining showed significant upregulation of neuronal marker expression on rough surfaces. Notably, middle ranged rough surface induced the highest level of neuronal marker expression. This study demonstrates the significance of microscale roughness in differentiation of human iPSCs towards neuronal lineage. It suggested the potential application of roughness in clinical regenerative medicine.

## Acknowledgements

The authors acknowledge Mr. Robert Jeziorski and Mr. Mario Rettschlag for preparation of sterilized PS inserts, Dr. Harald Stachelscheid for providing cells, Ms. Katrin Michel for technical support. This work was financially supported by the Helmholtz Association of German Research Centers (including Helmholtz-Portfolio Topic “Technology and Medicine”) and the German Federal Ministry of Education and Research (BMBF project number 0315696A “Poly4Bio BB”).

## References

1. Yu, J., et al., *Induced pluripotent stem cell lines derived from human somatic cells*. *Science*, 2007. **318**(5858): p. 1917-20.
2. Bilic, J. and J.C.I. Belmonte, *Concise Review: Induced Pluripotent Stem Cells Versus Embryonic Stem Cells: Close Enough or Yet Too Far Apart?* *Stem Cells*, 2012. **30**(1): p. 33-41.
3. Swistowski, A., et al., *Efficient generation of functional dopaminergic neurons from human induced pluripotent stem cells under defined conditions*. *Stem Cells*, 2010. **28**(10): p. 1893-904.
4. Jiang, H., et al., *Parkin controls dopamine utilization in human midbrain dopaminergic neurons derived from induced pluripotent stem cells*. *Nat Commun*, 2012. **3**: p. 668.
5. Hallett, P.J., et al., *Successful function of autologous iPSC-derived dopamine neurons following transplantation in a non-human primate model of Parkinson's disease*. *Cell Stem Cell*, 2015. **16**(3): p. 269-74.
6. Saha, K. and R. Jaenisch, *Technical Challenges in Using Human Induced Pluripotent Stem Cells to Model Disease*. *Cell Stem Cell*, 2009. **5**(6): p. 584-595.
7. Hong, S.G., et al., *Path to the Clinic: Assessment of iPSC-Based Cell Therapies In Vivo in a Nonhuman Primate Model*. *Cell Reports*, 2014. **7**(4): p. 1298-1309.
8. Engler, A.J., et al., *Matrix elasticity directs stem cell lineage specification*. *Cell*, 2006. **126**(4): p. 677-89.
9. Chowdhury, F., et al., *Soft substrates promote homogeneous self-renewal of embryonic stem cells via downregulating cell-matrix tractions*. *PLoS One*, 2010. **5**(12): p. e15655.
10. Chowdhury, F., et al., *Material properties of the cell dictate stress-induced spreading and differentiation in embryonic stem cells*. *Nat Mater*, 2010. **9**(1): p. 82-8.
11. Flemming, R.G., et al., *Effects of synthetic micro- and nano-structured surfaces on cell behavior*. *Biomaterials*, 1999. **20**(6): p. 573-88.
12. Lim, J.Y. and H.J. Donahue, *Cell sensing and response to micro- and nanostructured surfaces produced by chemical and topographic patterning*. *Tissue Eng*, 2007. **13**(8): p. 1879-91.

13. Kong, H.J. and D.J. Mooney, *Microenvironmental regulation of biomacromolecular therapies*. Nat Rev Drug Discov, 2007. **6**(6): p. 455-63.
14. Pan, F., et al., *Topographic effect on human induced pluripotent stem cells differentiation towards neuronal lineage*. Biomaterials, 2013. **34**(33): p. 8131-9.
15. Faia-Torres, A.B., et al., *Differential regulation of osteogenic differentiation of stem cells on surface roughness gradients*. Biomaterials, 2014. **35**(33): p. 9023-32.
16. Wakao, S., et al., *Morphologic and gene expression criteria for identifying human induced pluripotent stem cells*. PLoS One, 2012. **7**(12): p. e48677.
17. Roch, T., et al., *Immunological evaluation of polystyrene and poly(ether imide) cell culture inserts with different roughness*. Clinical Hemorheology and Microcirculation, 2012. **52**(2-4): p. 375-389.
18. Wang, W.W., et al., *The influence of polymer scaffolds on cellular behaviour of bone marrow derived human mesenchymal stem cells*. Clinical Hemorheology and Microcirculation, 2012. **52**(2-4): p. 357-373.
19. Chambers, S.M., et al., *Highly efficient neural conversion of human ES and iPS cells by dual inhibition of SMAD signaling*. Nat Biotechnol, 2009. **27**(3): p. 275-80.
20. Xu, X., et al., *Controlling major cellular processes of human mesenchymal stem cells using microwell structures*. Adv Healthc Mater, 2014. **3**(12): p. 1991-2003.
21. Cunningham, J.J., et al., *Lessons from human teratomas to guide development of safe stem cell therapies*. Nat Biotechnol, 2012. **30**(9): p. 849-57.
22. Chen, W., et al., *Nanotopography influences adhesion, spreading, and self-renewal of human embryonic stem cells*. ACS Nano, 2012. **6**(5): p. 4094-103.
23. Zhang, Y., et al., *Rapid single-step induction of functional neurons from human pluripotent stem cells*. Neuron, 2013. **78**(5): p. 785-98.
24. Elkabetz, Y., et al., *Human ES cell-derived neural rosettes reveal a functionally distinct early neural stem cell stage*. Genes Dev, 2008. **22**(2): p. 152-65.
25. Kim, D.S., et al., *Robust Enhancement of Neural Differentiation from Human ES and iPS Cells Regardless of their Innate Difference in Differentiation Propensity*. Stem Cell Reviews and Reports, 2010. **6**(2): p. 270-281.
26. Ma, W., et al., *Cell-extracellular matrix interactions regulate neural differentiation of human embryonic stem cells*. BMC Dev Biol, 2008. **8**: p. 90.
27. Li, Y., et al., *Neural differentiation from pluripotent stem cells: The role of natural and synthetic extracellular matrix*. World J Stem Cells, 2014. **6**(1): p. 11-23.
28. Takahashi, K., et al., *Induction of pluripotent stem cells from adult human fibroblasts by defined factors*. Cell, 2007. **131**(5): p. 861-72.
29. Pera, M.F., B. Reubinoff, and A. Trounson, *Human embryonic stem cells*. J Cell Sci, 2000. **113** ( Pt 1): p. 5-10.



30. Hu, B.Y., et al., *Neural differentiation of human induced pluripotent stem cells follows developmental principles but with variable potency*. Proc Natl Acad Sci U S A, 2010. **107**(9): p. 4335-40.
31. Zhang, X.Q., et al., *Pax6 Is a Human Neuroectoderm Cell Fate Determinant*. Cell Stem Cell, 2010. **7**(1): p. 90-100.
32. Pankratz, M.T., et al., *Directed neural differentiation of human embryonic stem cells via an obligated primitive anterior stage*. Stem Cells, 2007. **25**(6): p. 1511-20.
33. Lenhert, S., et al., *Capillary-induced contact guidance*. Langmuir, 2007. **23**(20): p. 10216-23.
34. Chen, Y.C., et al., *Induction and regulation of differentiation in neural stem cells on ultra-nanocrystalline diamond films*. Biomaterials, 2010. **31**(21): p. 5575-87.
35. Yang, K., et al., *Nanotopographical manipulation of focal adhesion formation for enhanced differentiation of human neural stem cells*. ACS Appl Mater Interfaces, 2013. **5**(21): p. 10529-40.
36. Dalby, M.J., et al., *Nanomechanotransduction and interphase nuclear organization influence on genomic control*. J Cell Biochem, 2007. **102**(5): p. 1234-44.
37. Dalby, M.J., et al., *Nanotopographical stimulation of mechanotransduction and changes in interphase centromere positioning*. J Cell Biochem, 2007. **100**(2): p. 326-38.
38. Kilian, K.A., et al., *Geometric cues for directing the differentiation of mesenchymal stem cells*. Proc Natl Acad Sci U S A, 2010. **107**(11): p. 4872-7.

## **Chapter V**

### **Conclusion and discussion**

## Concluding remarks

The present thesis was to better our understanding of the influences of surface topographic microscale structures on the behaviors of stem cells and the undergo mechanisms. As explained in chapter II and III, we investigated the capacities of secretome and migration of the MSCs on the surfaces with different structures; and furtherly, the undergo mechanism in molecular level was studied. Besides, the neural differentiation of human iPSCs on surfaces with different structures was performed and the differentiation efficiency was evaluated in chapter IV. The results in this thesis demonstrated that surface topographic microscale microstructure could affect the stem cell behaviors, the curvature of the structures is a determine factor of the effects, which presents a strong evidence for controlling the stem cell behaviors by manipulating the surface topographic structures of materials.

In chapter II, we found that the VEGF secretion could be improved by the surface structures. The VEGF is a primer factor of vascular growth for its activating the endothelial cells such as increasing the proliferation, migration and forming the tubular network [1-3]. The therapeutic effect of VEGF is dosage dependent. In our study, VEGF level stimulated by surface roughness was within the effective and safe range [4]. Additionally, the secretion stimulated by roughness increased angiogenic potential in our *in vitro* and *ex vivo* assay. This might not only due to the VEGF but also other growth factors since combination of VEGF and other growth factors was much more effective than individual growth factors in angiogenesis [5, 6]. For the underlying mechanism of structures stimulated VEGF secretion, the integrin activation on the surfaces was studied. Integrin as the cell transmembrane receptor receives the micro environment signals and translates them into intracellular biochemical signals [7, 8]. The extracellular environment induced conformation and clustering of integrin result many cellular behaviors such as cell adhesion, cytoskeletal organization, migration, gene expression, cell survival, proliferation and differentiation [9, 10]. The surface structures in our study increased the integrin activation. After the structure and cell size study, it was speculated that the surface structure provided local curvature might be perceived by the cells and regulate the integrin activation. Further, focal adhesion kinase, as the downstream protein of

integrin, was found highly phosphorylated at the domain of Y397 of the cells on surface with curvature. FAK activation can subsequently activate the downstream mitogen-activated protein kinase (MAPK/ERK) pathway. Previously study demonstrated the activation MAPK/ERK by FAK increased the VEGF secretion in tumor cells [11]. In accordance with this report, our work showed an increased VEGF level was statistically correlated with an enhanced FAK level. This result suggested that integrin mediated FAK signaling pathway played a critical role in surface structure stimulated VEGF secretion.

Further, FAK is involved in the formation and turnover of the focal adhesion during cell migration [12, 13]. With the findings that surface roughness modulated the FAK phosphorylation, we hypothesized that the surface structure influenced the cell migration via the activation of FAK and the formation of FAs. In chapter III, the migration of surface structure preconditioned MSCs was studied. The results demonstrated that the migration capacities of MSCs were developed by preconditioning on surface topographic structure. Since the stem cells behaviors could be influenced by the preconditioning in micro environments [14], our findings suggest that surface structure could be an effective precondition factor to modulate the behaviors of stem cells. Furthermore, in our study, the MSCs obtained and maintained the increased migration only after a certain time length of precondition, which indicates that the functional alteration of MSCs behavior may exhibit only in response to a satisfied dosage of topographic stimulation. This phenomenon is in consistence with a recent report, which illustrated a clear relationship between the stem cell memory and the precondition dosage of mechanical signals [15]. Besides, the focal adhesion (FA) is crucial during cell migration. FA formation at the leading edge and turnover at the rear edge are necessary to anchor the cell and pull the cell body forward. Therefore, continuously synchronized formation and turnover of FA of the cell body are required in migration [16]. It has been demonstrated that the size of FA predicted the cell migration speed [17]. The results in our study showed a distinct appearance of FA in size and density at the cells during and after surface roughness preconditioning, which might contribute to the different migration capacities. For the underlying mechanism, the downstream protein of FAK, ERK/MAPK activation could induce the phosphorylation of myosin light chain, which could enhance the cell migration [18]. Our results showed the increased migration capacity was accompanied with

elevated FAK phosphorylation and MAPK phosphorylation levels. This alteration of cells is in consistence with previous studies, which demonstrated that formation of a paxillin-FAK-ERK/MAPK complex regulates the cell migration capacity [19, 20]. Therefore, we infer that surface topographic structure modulates the MSCs migration capacity via the activation of FAK and ERK/MAPK.

To furtherly investigate the influence of surface topographic microscale structure on the other stem cell type (ESCs/iPSCs), in chapter IV, the neural differentiation of human iPSCs was induced on the surface roughness. Neural differentiation of iPSCs represents a promise for neural degenerative diseases. However, the tumorigenic potential of iPSCs limited their application. Controlled and efficient differentiation of iPSCs represents the essential prerequisite before the transplantation. Our results demonstrated that the surface topographic structure could promote the neural differentiation. It highlights a new method to increasing the efficiency of iPSCs differentiation. In our work, the remarkably and robust approach via dual inhibition of SMAD signaling was adopted to induce the neural differentiation of iPSCs. This approach fits the request of the direct contacts between cells and surface structure and was different from the early protocol, which was based on the embryoid body formation from the lifting iPSCs [21]. Meanwhile, the human iPSCs IMR-90 was selected in the work for their high potential of differentiation towards neural lineage [22]. During the differentiation of iPSCs on the structured surface, the neural genes of Nestin,  $\beta$ -III Tubulin and MAP2 were significantly upregulated and the the Nestin and  $\beta$ - III Tubulin proteins expression was consequently enhanced by the surface structures. The promotive effects of surface topographic roughness on iPSCs differentiation might attribute to the roughness induced subtle force, which plays a role in cellular membrane attachment and cellular response to guidance signals from the materials surface [23]. Besides, the FAK phosphorylation induced by the surface topography might lead the stem cell differentiation [24, 25]. Thus, more studies are needed to explore the concealed mechanisms of surface structure enhanced iPSCs differentiation.

## Discussion

It is widely accepted that the cells shape and consequent fate are influenced by the topographical cues from macroscale to nanoscale size in natural environments and the structures of basement membrane such as pores, fibers and ridges play the vital role in these influences [26]. Making use of topographical structure of substrate to improve the regenerative capacity of stem cells after injury attracts the interests of most researchers in area of regenerative medicine. Meanwhile, the developing of patterning techniques such as photolithography, electrospinning, layer by layer microfluidic patterning, three dimensional printing and ion milling make it possible to create the precise controlled geometry, texture, porosity and rigidity on artificial substrates which would contribute to study the controlled cell behaviors *in vitro* [27]. Previous studies have suggested that surface topography of substrates affect the cell shape, size, elongation, position and regulate their interactions [28]. Therefore, addressing the underlying mechanism of effects of topographical pattern to stem cells would be the outstanding prerequisite for the clinical application. Different types of surface topographies including topographical scale (micro or nano), pattern type (ridges, pillar, pit or groove) and distribution (random or regular distributed features) have been generated and investigated for their effect on stem cells behaviors. However, most part of the studies were focused on the topography influenced stem cell differentiations (Table 1). Compared with these studies, current work is dedicated to demonstrate that the improved secretion and migration capacities of stem cells by the topographical structures with appropriate curvature level, which is as important as the differentiation in regeneration. Further, few studies demonstrated the mechanotransduction modulated migration or secretion capacity of stem cells, AJ Engler and his colleagues investigated the migration of human ADSCs on the polyacrylamide hydrogels with stiffness gradients of 0.5, 1.7, 2.9, 4.5, 6.8, and 8.2 kPa/mm, they found that both of the cell-spread area and the nuclear area increased with stiffness; cells exhibited higher y axis velocities with the steep gradient (8.2 kPa/mm) [29]. Proangiogenic effects of MSCs secretion were depended on the stiffness level of substrate, maximum influence was observed when the MSCs cultivated on the 40kPa fibronectin coated hydrogel [30]. Compare with these studies, current work for the first time demonstrated

that local curvature of microstructure directed the cell focal adhesion and consequently affected the secretion and migration.

Table 1: Example of studies, topography influenced the stem cell behaviors

<b>Materials</b>	<b>Stem cell source</b>	<b>Topographical feature</b>	<b>Findings</b>	<b>Ref.</b>
Titanium	UC-MSCs	Pores	Plasmapore promoted osteogenic differentiation	[31]
TiO <sub>2</sub>	hMSC	Nanotubes	70- to 100-nm nanotubes elicited stem cell elongation, and induced differentiation into osteoblast-like cells	[32]
PMMA	hMSCs	square or hexagonal pattern and Nanopits	Disordered square promoted osteogenesis	[33]
PLLA	mESCs	nanotube	Enhanced osteogenesis	[34]
PDMS	hMSC	Grooves	Promoted myogenesis	[35]
Carbon	hMSCs	Grooves	Promoted neurogenesis	[36]
PDMS	hESCs	Grooves	Promoted neural differentiation	[37]
Polystyrene	rMSCs	Grooves	Promoted myogenesis and adipogenesis	[38]
Alumina ceramics	hMSCs	Grooves	Enhanced the adhesion and osteogenesis	[39]
PCL	hMSCs	Nano-pillar, hole and grill	nano-pillar and nano-hole enhanced MSC chondrogenesis and facilitated hyaline cartilage formation	[40]
Polyimide	hiPSCs	groove-ridge structures	Sub-micrometer range structure induced elongation of iPSC colonies, guide the orientation of apical actin fibers, and direct the polarity of cell division	[41]

UC-MSCs: Umbilical cord mesenchymal stem cells; hMSC: Human mesenchymal stem cell; rMSCs: Rat mesenchymal stem cell; hESC: Human embryonic stem cell; mESC: Mouse embryonic stem cell; PMMA: Polymethyl methacrylate; PLLA: Poly(L-lactide); PDMS: Polydimethylsiloxane; PCL: Polycaprolactone; PLL: Poly-L-lysine.

It has been reported that local curvatures play an important role on cells behaviors including the cell adhesion, contractile forces and cytoskeleton deformation [42, 43]. Stem cell osteogenic differentiation can be influenced by the substrate curvature modulated cytoskeletal force and lamin-A expression [44]. Current study indicated that the substrate with surface local curvature as a transitional platform between 2D and 3D system, affected the stem cell behaviors by modulating the activation of integrin and consequently active the downstream signaling pathway.

Considering the dimension of substrate topography, 3D scaffolds represent the promising substrate for regenerative medicine, especially in the reconstruction for the big defects. Surface topography is very important for these 3D substrates. For example, in an electrospun titanium 3D scaffold study, the cell proliferation and differentiation were demonstrated in depending on the microscale roughness level and the fiber diameter [45]. 3D scaffold of electrospun with height alternation has been shown to induce the neural stem cells differentiation into neurons than astrocytes [46]. Concave structure increased the stem cell migration compared to convex structure and flat surface on 3D substrate [44]. In according with the convex study, the insert system with local curvature in current study provided a mimic-convex structure, which promoted not only the cell migration ability but the secretion and differentiation.

Compared with the complexity of three dimensional (3D) native microenvironment, two-dimensional (2D) surfaces represent a convenient platform to evaluate the effects of individual components on cell behaviors. As early as in 1964, the microscale 2D pattern was discussed in regulating the alignment of endothelial, fibroblasts and epithelia [47]. The 2D surface topography of substrate affects the cells by factor of roughness and patterns. Roughness has been well studied in influencing the cell adhesion, migration, proliferation and differentiation [48]. The microscale surface roughness with the average  $R_a$  around 1  $\mu\text{m}$  has the optimal effects to induce the stem cell behaviors [49, 50]. In current study, the topographical microstructures with different curvature levels distinctly directed the secretion, migration and differentiation of stem cells, the roughness level was measured to support current results. In according with this roughness level, the optimal effects to induce stem cell response in this study were observed when the surface with



the roughness level  $Ra\ 4.17\pm 0.17\ \mu\text{m}$  compared with the flat surface with  $Ra\ 0.13\pm 0.07$  and the surface with  $Ra\ 25.4\pm 3.8$ .

The 2D surface pattern can be classified into isotropic and anisotropic ones. Anisotropic pattern is the surface with clear orientation such as ridges and grooves while the isotropic pattern is randomly distributed structure such as pillar, pit, channel, or etc. The anisotropic microscale pattern have been observed to direct the cell alignment, migration and adipogenesis [45, 51]. Further, the anisotropic pattern is conversely reported to improve the osteogenesis than adipogenesis when changing the periodicity [52]. Therefore, more studies need to be carried to explore the underlying mechanism. Compared with the anisotropic pattern, the isotropic pattern conducts collective effects to the cells rather than the cell alignment. The complicated factors of randomly distributed structures make it difficult to in-depth analyze the mechanism of cell responses. For example, the randomly pillared surface has been demonstrated to influence the stem cell differentiation [53], however, the height, shape and distance between pillars can be very varied compared to each other. Studies demonstrated a general trend of cell behaviors on the isotropic surfaces. The pillars or islands usually improve the osteogenic differentiation of MSCs [53-55]. In current work, the surface microscale structures contains randomly distributed ridges and pillars, which provide the average  $160\ \mu\text{m}$  or  $320\ \mu\text{m}$  peak distance respectively and a transitional substrate between 2D and 3D system. The average  $160\ \mu\text{m}$  peak distance provides a stem cell size fit curvature and improved the secretion and migration abilities. This new finding predict that the structure fit for cell size may optimally modulate the cell behaviors. Further, the ridged structures enhanced the human iPSCs neural differentiation which is in consistent to the former study [56].

### **Conclusion and future prospects**

In conclusion, this thesis demonstrates the efficient influences of surface topographic microscale structures on stem cells behaviors including secretion, migration and differentiation, which provides robust evidences of the determinative effects of mechanical cues on stem cells fate. These data are valuable to furtherly study other influences of material surface properties on targeted cells. It highlights the great potential

of controlling stem cell behavior by manipulating the materials surface topographical structures, which would benefit their clinical application in regenerative medicine.

Previous studies have demonstrated valuable insight into the interactions between cell and substrates. However, many challenges in this field need to be addressed, especially in the molecular mechanism area, such as the signal transduction from the cell-substrate adhesion to cell gene expression and consequent behaviors. Further, the determine factor of the topographical pattern on the substrates such as shape, size, depth and curvature would be crucial for the designation of substrates in regeneration. The continuous findings would enhance our knowledge in topographical patterns modulated behaviors of different cell types. Future substrates would contain both chemical and mechanical stimuli, with more degree in biomimetic features. The studies should be more focus on the multi-direction cues to support the application in regenerative medicine. Therefore, topographical 3D pattern need to be further studied to mimic the nature tissue and the associate mechanism should be revealed, which will not only benefit the fundamental biological studies.

## References

1. Hoeben, A., et al., *Vascular endothelial growth factor and angiogenesis. Pharmacological Reviews*, 2004. 56(4): p. 549-580.
2. Yang, S.Y., et al., *Vascular endothelial cell growth factor-driven endothelial tube formation is mediated by vascular endothelial cell growth factor receptor-2, a kinase insert domain-containing receptor. Arteriosclerosis Thrombosis and Vascular Biology*, 2001. 21(12): p. 1934-1940.
3. Morales-Ruiz, M., et al., *Vascular endothelial growth factor-stimulated actin reorganization and migration of endothelial cells is regulated via the serine/threonine kinase Akt. Circulation Research*, 2000. 86(8): p. 892-896.
4. Ozawa, C.R., et al., *Microenvironmental VEGF concentration, not total dose, determines a threshold between normal and aberrant angiogenesis. Journal of Clinical Investigation*, 2004. 113(4): p. 516-527.
5. Asahara, T., et al., *Synergistic Effect of Vascular Endothelial Growth-Factor and Basic Fibroblast Growth-Factor on Angiogenesis in-Vivo. Circulation*, 1995. 92(9): p. 365-371.
6. Castellon, R., et al., *Effects of angiogenic growth factor combinations on retinal endothelial cells. Experimental Eye Research*, 2002. 74(4): p. 523-535.

7. Schwartz, M.A., *Integrins and Extracellular Matrix in Mechanotransduction*. Cold Spring Harbor Perspectives in Biology, 2010. 2(12).
8. Katsumi, A., et al., *Integrins in mechanotransduction*. Journal of Biological Chemistry, 2004. 279(13): p. 12001-12004.
9. Shattil, S.J., C. Kim, and M.H. Ginsberg, *The final steps of integrin activation: the end game*. Nature Reviews Molecular Cell Biology, 2010. 11(4): p. 288-300.
10. Qin, J., O. Vinogradova, and E.F. Plow, *Integrin bidirectional signaling: a molecular view*. Plos Biology, 2004. 2(6): p. 726-729.
11. Mitra, S.K., et al., *Intrinsic FAK activity and Y925 phosphorylation facilitate an angiogenic switch in tumors*. Oncogene, 2006. 25(44): p. 5969-5984.
12. Mitra, S.K., D.A. Hanson, and D.D. Schlaepfer, *Focal adhesion kinase: in command and control of cell motility*. Nat Rev Mol Cell Biol, 2005. 6(1): p. 56-68.
13. Ilic, D., et al., *Reduced cell motility and enhanced focal adhesion contact formation in cells from FAK-deficient mice*. Nature, 1995. 377(6549): p. 539-44.
14. Sart, S., T. Ma, and Y. Li, *Preconditioning stem cells for in vivo delivery*. Biores Open Access, 2014. 3(4): p. 137-49.
15. Yang, C., et al., *Mechanical memory and dosing influence stem cell fate*. Nat Mater, 2014. 13(6): p. 645-52.
16. Broussard, J.A., D.J. Webb, and I. Kaverina, *Asymmetric focal adhesion disassembly in motile cells*. Curr Opin Cell Biol, 2008. 20(1): p. 85-90.
17. Kim, D.H. and D. Wirtz, *Focal adhesion size uniquely predicts cell migration*. FASEB J, 2013. 27(4): p. 1351-61.
18. Huang, C., K. Jacobson, and M.D. Schaller, *MAP kinases and cell migration*. J Cell Sci, 2004. 117(Pt 20): p. 4619-28.
19. Teranishi, S., K. Kimura, and T. Nishida, *Role of formation of an ERK-FAK-paxillin complex in migration of human corneal epithelial cells during wound closure in vitro*. Invest Ophthalmol Vis Sci, 2009. 50(12): p. 5646-52.
20. Shi, J., et al., *Activation of ERK-FAK Signaling Pathway and Enhancement of Cell Migration Involved in the Early Interaction Between Oral Keratinocytes and Candida albicans*. Mycopathologia, 2009. 167(1): p. 1-7.
21. Zhang, Y., et al., *Rapid single-step induction of functional neurons from human pluripotent stem cells*. Neuron, 2013. 78(5): p. 785-98.
22. Hu, B.Y., et al., *Neural differentiation of human induced pluripotent stem cells follows developmental principles but with variable potency*. Proc Natl Acad Sci U S A, 2010. 107(9): p. 4335-40.
23. Lenhert, S., et al., *Capillary-induced contact guidance*. Langmuir, 2007. 23(20): p. 10216-23.

24. Chen, Y.C., et al., *Induction and regulation of differentiation in neural stem cells on ultra-nanocrystalline diamond films. Biomaterials*, 2010. 31(21): p. 5575-87.
25. Yang, K., et al., *Nanotopographical manipulation of focal adhesion formation for enhanced differentiation of human neural stem cells. ACS Appl Mater Interfaces*, 2013. 5(21): p. 10529-40.
26. Abrams, G.A., et al., *Nanoscale topography of the basement membrane underlying the corneal epithelium of the rhesus macaque. Cell Tissue Res*, 2000. 299(1): p. 39-46.
27. Griffin, M.F., et al., *Control of stem cell fate by engineering their micro and nanoenvironment. World Journal of Stem Cells*, 2015. 7(1): p. 37-50.
28. Kshitiz, et al., *Control of stem cell fate and function by engineering physical microenvironments. Integr Biol (Camb)*, 2012. 4(9): p. 1008-18.
29. Hadden, W.J., et al., *Stem cell migration and mechanotransduction on linear stiffness gradient hydrogels. Proc Natl Acad Sci U S A*, 2017. 114(22): p. 5647-5652.
30. Abdeen, A.A., et al., *Matrix composition and mechanics direct proangiogenic signaling from mesenchymal stem cells. Tissue Eng Part A*, 2014. 20(19-20): p. 2737-45.
31. Lauria, I., et al., *Response of umbilical cord mesenchymal stromal cells to varying titanium topographical signals. J Biomed Mater Res A*, 2018. 106(1): p. 180-191.
32. Oh, S., et al., *Stem cell fate dictated solely by altered nanotube dimension. Proc Natl Acad Sci U S A*, 2009. 106(7): p. 2130-5.
33. Dalby, M.J., et al., *The control of human mesenchymal cell differentiation using nanoscale symmetry and disorder. Nature Materials*, 2007. 6(12): p. 997-1003.
34. Smith, L.A., et al., *Enhancing osteogenic differentiation of mouse embryonic stem cells by nanofibers. Tissue Eng Part A*, 2009. 15(7): p. 1855-64.
35. Kurpinski, K., et al., *Anisotropic mechanosensing by mesenchymal stem cells. Proc Natl Acad Sci U S A*, 2006. 103(44): p. 16095-100.
36. D'Angelo, F., et al., *Micropatterned hydrogenated amorphous carbon guides mesenchymal stem cells towards neuronal differentiation. Eur Cell Mater*, 2010. 20: p. 231-44.
37. Lu, D., et al., *Microgrooved Surface Modulates Neuron Differentiation in Human Embryonic Stem Cells. Methods Mol Biol*, 2016. 1307: p. 281-7.
38. Wang, P.Y., et al., *Modulation of osteogenic, adipogenic and myogenic differentiation of mesenchymal stem cells by submicron grooved topography. J Mater Sci Mater Med*, 2012. 23(12): p. 3015-28.
39. Kim, S.Y., et al., *Effect of topographical control by a micro-molding process on the activity of human Mesenchymal Stem Cells on alumina ceramics. Biomater Res*, 2015. 19: p. 23.
40. Wu, Y.N., et al., *Substrate topography determines the fate of chondrogenesis from human mesenchymal stem cells resulting in specific cartilage phenotype formation. Nanomedicine-Nanotechnology Biology and Medicine*, 2014. 10(7): p. 1507-1516.

41. *Abagnale, G., et al., Surface Topography Guides Morphology and Spatial Patterning of Induced Pluripotent Stem Cell Colonies. Stem Cell Reports, 2017. 9(2): p. 654-666.*
42. *Sanz-Herrera, J.A., et al., On the effect of substrate curvature on cell mechanics. Biomaterials, 2009. 30(34): p. 6674-6686.*
43. *Chen, S.S., X.M. Lu, and Q.H. Lu, Effects of concave and convex substrate curvature on cell mechanics and the cytoskeleton. Chinese Chemical Letters, 2017. 28(4): p. 818-826.*
44. *Werner, M., et al., Surface Curvature Differentially Regulates Stem Cell Migration and Differentiation via Altered Attachment Morphology and Nuclear Deformation. Advanced Science, 2017. 4(2).*
45. *Wang, X.K., et al., Effects of structural properties of electrospun TiO<sub>2</sub> nanofiber meshes on their osteogenic potential. Acta Biomaterialia, 2012. 8(2): p. 878-885.*
46. *Xie, J.W., et al., The differentiation of embryonic stem cells seeded on electrospun nanofibers into neural lineages. Biomaterials, 2009. 30(3): p. 354-362.*
47. *Curtis, A.S.G. and M. Varde, Control of Cell Behavior - Topological Factors. Journal of the National Cancer Institute, 1964. 33(1): p. 15-&.*
48. *Metavarayuth, K., et al., Influence of Surface Topographical Cues on the Differentiation of Mesenchymal Stem Cells in Vitro. Acs Biomaterials Science & Engineering, 2016. 2(2): p. 142-151.*
49. *Wennerberg, A. and T. Albrektsson, Effects of titanium surface topography on bone integration: a systematic review. Clinical Oral Implants Research, 2009. 20: p. 172-184.*
50. *Yang, W., et al., Surface topography of hydroxyapatite promotes osteogenic differentiation of human bone marrow mesenchymal stem cells. Mater Sci Eng C Mater Biol Appl, 2016. 60: p. 45-53.*
51. *Matsuzaka, K., et al., The attachment and growth behavior of osteoblast-like cells on microtextured surfaces. Biomaterials, 2003. 24(16): p. 2711-2719.*
52. *Biggs, M.J.P., et al., The use of nanoscale topography to modulate the dynamics of adhesion formation in primary osteoblasts and ERK/MAPK signalling in STRO-1+enriched skeletal stem cells. Biomaterials, 2009. 30(28): p. 5094-5103.*
53. *McNamara, L.E., et al., Skeletal stem cell physiology on functionally distinct titania nanotopographies. Biomaterials, 2011. 32(30): p. 7403-7410.*
54. *Fiedler, J., et al., The effect of substrate surface nanotopography on the behavior of multipotent mesenchymal stromal cells and osteoblasts. Biomaterials, 2013. 34(35): p. 8851-8859.*
55. *Sjostrom, T., et al., Fabrication of pillar-like titania nanostructures on titanium and their interactions with human skeletal stem cells. Acta Biomaterialia, 2009. 5(5): p. 1433-1441.*
56. *Pan, F., et al., Topographic effect on human induced pluripotent stem cells differentiation towards neuronal lineage. Biomaterials, 2013. 34(33): p. 8131-8139.*

## Contribution to publications

1. Zhengdong Li et al. Integrin  $\beta$ 1 activation by micro-scale curvature promotes pro-angiogenic secretion of human mesenchymal stem cells. Journal of Materials Chemistry B. 2017, 5, 7415--7425. <https://doi.org/10.1039/c7tb01232b>
  - 1) Literature study
    - a) Topography and stem cell behaviors
    - b) Effects of stem cells in angiogenesis
    - c) Signaling pathway in stem cell response to mechanical cues
  - 2) Study design (with discussion and advice from co-authors Prof. Nan Ma and Prof. Lendlein)
    - a) Methods of topography characterization
    - b) Methods of stem cell secretion test
    - c) Methods of signaling pathway test
  - 3) Experimental work
    - a) Measurement of VEGF level in stem cell supernatant
    - b) Migration and tube formation test of HUVECs in the supernatant of stem cells
    - c) Blood vessel formation induced by the supernatant of stem cells (HET-CAM assay)
    - d) Signaling pathway test (integrin, FAK, ERK) by ELISA or FACS
  - 4) Analysis and interpretation of experimental data
    - a) The curvature level of materials
    - b) VEGF secretion level of MSCs
    - c) Migration velocity and tube formation level of HUVECs
    - d) Blood vessels induced by MSCs secretome in HET-CAM
    - e) Levels of activated integrin  $\beta$ 1, FAK and ERK
  - 5) Manuscript
    - a) Manuscript structure (discussed with co-authors)
    - b) First manuscript draft
    - c) Revising and finalization of the manuscript according to the comments of Prof. Lendlein and other co-authors.

2. Zhengdong Li *et al.* Modulation of the mesenchymal stem cell migration capacity via preconditioning with topographic microstructure. *Clinical Hemorheology and Microcirculation*. 2017;67(3-4):267-278. <https://doi.org/10.3233/CH-179208>

- 1) Literature study
  - a) Topography and stem cell migration
  - b) Stem cell memory
  - c) Signaling pathway in stem cell migration
- 2) Study design (with discussion and advice from co-authors Dr. Weiwei Wang, Prof. Nan Ma and Prof. Lendlein)
  - a) Methods of migration test
  - b) Methods of precondition
  - c) Methods of signaling pathway test
- 3) Experimental work
  - a) Migration level of preconditioned stem cells
  - b) Focal adhesion staining
  - c) FAK and MAPK expression level by ELISA or Western blot
- 4) Analysis and interpretation of experimental data
  - a) Cell migration velocity
  - b) Focal adhesion
  - c) FAK and MAPK expression level
- 5) Manuscript
  - a) First manuscript draft
  - b) Revising and finalization of the manuscript according to the comments of Prof. Lendlein and other co-authors.

3. Zhengdong Li *et al.* Influence of surface roughness on neural differentiation of human induced pluripotent stem cells. *Clinical Hemorheology and Microcirculation* 64 (2016) 355–366. <https://doi.org/10.3233/CH-168121>

- 1) Literature study
  - a) Human iPSCs neural differentiation
  - b) Topography and neural differentiation of human iPSCs

- 2) Study design (with discussion and advice from co-authors Prof. Nan Ma and Prof. Lendlein)
  - a) Methods of neural differentiation induction
  - b) Methods of evaluation of the differentiation efficiency
- 3) Experimental work
  - a) Human iPSCs characterization
  - b) Neural differentiation induction
  - c) Human iPSCs and neural markers expression (staining and Real-time PCR)
- 4) Analysis and interpretation of experimental data
  - a) Human pluripotent stem cell markers expression level
  - b) Neural markers expression level
- 5) Manuscript
  - a) First manuscript draft
  - b) Revising and finalization of the manuscript according to the comments of Prof. Lendlein and other co-authors.



## List of publications

### First Author

1, Integrin  $\beta$ 1 activation by micro-scale curvature promotes pro-angiogenic secretion of human mesenchymal stem cells. *Journal of Materials Chemistry B*. 2017, 5, 7415--7425. <https://doi.org/10.1039/c7tb01232b>

2, Modulation of the mesenchymal stem cell migration capacity via preconditioning with topographic microstructure. *Clinical Hemorheology and Microcirculation*. 2017;67(3-4):267-278. <https://doi.org/10.3233/CH-179208>

3, Influence of surface roughness on neural differentiation of human induced pluripotent stem cells. *Clinical Hemorheology and Microcirculation* 64 (2016) 355–366. <https://doi.org/10.3233/CH-168121>

### Co-author

1, Wang, WW., K. Kratz, M. Behl, W. Yan, Y. Liu, X. Xu, S. Baudis, **Z. Li**, A. Kurtz, A. Lendlein and N. Ma (2015). "The interaction of adipose-derived human mesenchymal stem cells and polyether ether ketone." *Clinical Hemorheology and Microcirculation* 61(2): 301-321.

2, Wang, WW., X. Xu, **Z. Li**, A. Lendlein and N. Ma (2014). "Genetic engineering of mesenchymal stem cells by non-viral gene delivery." *Clinical Hemorheology and Microcirculation* 58(1): 19-48.

3, Xu, X., W. Wang, K. Kratz, L. Fang, **Z. Li**, A. Kurtz, N. Ma and A. Lendlein (2014). "Controlling Major Cellular Processes of Human Mesenchymal Stem Cells using Microwell Structures." *Advanced Healthcare Materials* 3(12): 1991-2003

4, Xu, X., K. Kratz, WW. Wang, **Z. Li**, T. Roch, F. Jung, A. Lendlein and N. Ma (2013). "Cultivation and spontaneous differentiation of rat bone marrow-derived mesenchymal stem cells on polymeric surfaces." *Clinical Hemorheology and Microcirculation* 55(1): 143-156.

5, Wang, W., N. Ma, K. Kratz, X. Xu, **Z. Li**, T. Roch, K. Bieback, F. Jung and A. Lendlein (2012). "The influence of polymer scaffolds on cellular behaviour of bone marrow derived human mesenchymal stem cells." *Clinical Hemorheology and Microcirculation* 52(2-4): 357-373.

6, Xu, X., K. Kratz, W. Wang, **Z. Li**, T. Roch, F. Jung, A. Lendlein and N. Ma (2013). "Cultivation and spontaneous differentiation of rat bone marrow-derived mesenchymal stem cells on polymeric surfaces." *Clinical Hemorheology and Microcirculation* 55(1): 143-156.

# Curriculum Vitae

## Personal Details

Name and sure name: Zhengdong Li

Birth date: 02. Aug. 1981

Nationality: People's Republic of China (PRC)

Address: Sven-Hedin Straße 41, 14163, Berlin

Telephone number: +49 176 8295 7873

Email: zhengdongli02@hotmail.com

## Education:

10.2011-03.2018: Ph.D candidate, Helmholtz MacroBio Graduate School, Teltow and Freie Universität Berlin.

04.2010 -09.2011: MD candidate, Rudolf-Zenker-Institut für Experimentelle Chirurgie, Universität Rostock.

09.2000-07.2007: Bachelor and master of human medicine, Medical school, Xi'an Jiaotong University (PRC).

## Professional Experience:

01.2017-09.2018: Wissenschaftlicher Mitarbeiter, Helmholtz-Zentrum Geesthacht – Zentrum für Material- und Küstenforschung (Teltow, Germany)

10.2011-12.2016: Doktorand, Helmholtz-Zentrum Geesthacht – Zentrum für Material- und Küstenforschung (Teltow, Germany)

04.2010-09.2011: Wissenschaftliche Hilfskraft, Rudolf-Zenker-Institut für Experimentelle Chirurgie, Universität Rostock.

07.2007-03.2010: Resident physician, Pediatrics and orthopedics, The Third People's Hospital of Chengdu (PRC).

07.2005-06.2007: Resident physician (internship), Orthopedics, The Second Affiliated Hospital of Xi'an Jiaotong University (PRC).

## Language:

1, English: Fluent in reading and scientific writing, good in speaking.

2, Deutsch: Basic level (A2).

3, Mandarin: Mother tongue.

## **Selbständigkeitserklärung**

Ich erkläre, dass ich die vorliegende Dissertation selbständig, ohne unzulässige fremde Hilfe und nur unter Verwendung der angegebenen Literatur und Hilfsmittel angefertigt habe.

I hereby confirm that I have made this work autonomously. I assure that I have read and used only the specified sources claimed in this work.

Berlin, March, 2018

Zhengdong Li